Resistance against oxidative glutamate toxicity: Functional characterization of amino acid antiporter subunit xCT, purinergic ATP receptor P2X3 and mitochondrial fission factor GDAP1

Inaugural Dissertation

submitted to the Faculty of Mathematics and Natural Sciences
of the Heinrich-Heine University Düsseldorf
for the degree of Doctor of Natural Sciences

presented by

Rebecca Noack

Born in Mühlhausen / Thür.

Düsseldorf, March 2011

Publications

Albrecht, P., J. Lewerenz, S. Dittmer, R. Noack, P. Maher, and A. Methner. 2010. Mechanisms of oxidative glutamate toxicity: the glutamate/cystine antiporter system xc- as a neuroprotective drug target. *CNS Neurol Disord Drug Targets*. 9:373-382.

Noack, R., P. Albrecht, T. Dehmel, S. Frede, H. Summer, S. Golz, B. Kieseier, A. Kochanski, J. Lewerenz, G. Maier zur Hörste, A. Pfeiffer, M. Stettner, M. Wiedau-Pazos, and A. Methner. The mitochondrial fission factor GDAP1 protects from oxidative stress by increasing glutathione content and stabilizing the mitochondrial membrane potential
In preparation.

Lewerenz, J., H. Sato, P. Albrecht, N. Henke, R. Noack, A. Methner, and P. Maher. 2012. Mutation of ATF4 mediates resistance of neuronal cell lines against oxidative stress by inducing xCT expression. *Cell death & Differentiation*. 19(5): 847-858.

Declarations

I hereby declare that I have written the submitted dissertation 'Resistance against oxidative glutamate toxicity: Functional characterization of amino acid antiporter subunit xCT, purinergic ATP receptor P2X3 and mitochondrial fission factor GDAP1' myself and in this process have used no other sources or materials than those expressly indicated. I hereby declare that I have not applied to be examined at any other institution, nor have I used the dissertation in this or any other form at any other institution as an examination paper, nor submitted it to any other faculty as a dissertation.

_____   _____
    (Place, Date)   Rebecca Noack

Contents

Abbreviations

$\Delta\Psi$m	Mitochondrial membrane potential
12/15-LOX	12/15-Lipoxygenase
A-317491	({[3-Phenoxybenzyl][(1S)-1,2,3,4-tetrahydro-1-naphthalenyl]amino}arbonyl)-1,2,4-benzenetricarboxylic acid
A-438079	(5-(2,3-Dichlorophenyl)-1H-tetrazol-1-yl) methyl pyridine
AD	Alzheimer's disease
AIF	Apoptosis-inducing factor
ALS	Amyotrophic lateral sclerosis
ARE	Antioxidant response element
BAX	Bcl-2-associated X protein
BCL-2	B-cell lymphoma 2
BID / tBID	BH3-interacting domain death agonist / Truncated BID
BSO	Buthionine sulfoximine
CCCP	Carbonyl cyanide 3-chlorophenyl-hydrazone
cGMP	Cyclic guanosine monophosphate
CMT	Charcot-Marie-Tooth disease
CNS	Central nervous system
CREB	cAMP-response-element binding
CTB	Cell titer blue
ctr	Control
DRG	Dorsal root ganglia
DRP1	Dynamin-related protein 1
EAAT	Excitatory amino acid transporter
EAE	Experimental autoimmune encephalomyelitis
FIS1	Mitochondrial fission protein 1
GDAP1	Ganglioside-induced differentiation protein 1
GFP / eGFP	Green fluorescent protein / Enhanced GFP
GPCR	G-protein-coupled receptor

GSH	Glutathione
GST	Glutathione *S*-transferase
H2DCFDA	2',7'-Dichlorodihydrofluorescein diacetate
HIF-1α	Hypoxia-inducible factor 1α
HK-1/HK-2	Hexokinase 1 / Hexokinase 2
HRE	Hypoxia-responsive element
JC-1	5,5',6,6'-Tetrachloro-1,1',,3,3'-tetraethylbenzimidazolcarbocyanine iodide
LPS	Lipopolysaccharides
MFN1/MFN2	Mitofusin 1 / Mitofusin 2
MOM	Mitochondrial outer membrane
MTT	3-(4,5-Dimethyl-2-thiazolyl)-2,5-diphenyl-2H-tetrazolium bromide (Thiazolyl Blue Tetrazolium Bromide)
NAC	N-Acetyl-L-cysteine
NRF2	Nuclear factor E2-related factor 2
OPA1	Optic atrophy 1
ORF	Open reading frame
OXPHOS	Oxidative phosphorylation
PCR	Polymerase chain reaction
PD	Parkinson's disease
PDH	Pyruvate dehydrogenase
PDK2	Pyruvate dehydrogenase kinase 2
PEDF	Pigment epithelium-derived growth factor
RA	Retinoic acid
ROS	Reactive oxygen species
RT	Room temperature
RT-PCR	Reverse transcription-Polymerase chain reaction
(S)-4-CPG	(S)-4-Carboxyphenylglycine
SAS	Sulfasalazine
shRNA	Small hairpin RNA
siRNA	Small interfering RNA
SRE	Serum response element
TIGR	Transcript increased in glutamate resistance
tMCAO	Transient middle cerebral artery occlusion
TMD	Transmembrane domain
TMRE	Tetramethylrhodamine ethyl ester
VDAC	Voltage-dependent anion channel
VLDLR	Very low density lipoprotein receptor
WT	Wild-type

List of Figures

Summary

Oxidative stress is involved in neurodegenerative diseases. High glutamate concentrations lead to a cell death program distinct from excitotoxicity called oxidative glutamate toxicity. Here, excessive extracellular glutamate blocks the activity of the cystine/glutamate antiporter system X_c^- resulting in depletion of the important antioxidant glutathione (GSH), increased levels of reactive oxygen species (ROS), the activation of 12/15-lipoxygenase (12/15-LOX), and the opening of cyclic guanosine monophosphate (cGMP)-gated Ca^{2+} channels. The hippocampal cell line HT22 is an excellent model to study oxidative glutamate toxicity as it lacks ionotropic glutamate receptors. Furthermore, a glutamate-resistant cell line (HT22R) has been generated providing a useful tool to identify protective proteins and pathways. HT22R cells withstand high glutamate concentrations and exhibit increased GSH and reduced ROS levels. Moreover, they differ from glutamate-sensitive HT22 cells at the transcriptional level. Affymetrix array analysis identified several transcripts, including those for xCT, the functional subunit of X_c^-, the ionotropic P2X receptor P2X3, and the mitochondrial protein Ganglioside-induced differentiation protein 1 (GDAP1), which were further analyzed in this study.

xCT remarkably protected HT22 cells against glutamate toxicity by elevating cellular GSH concentration, which was confirmed by cell death assays with the GSH precursor N-acetyl-L-cysteine. Both xCT silencing and pharmacological inhibition increased the susceptibility of HT22R cells to glutamate and reduced elevated GSH levels indicating that the upregulation of xCT accounts to a large part for the protective phenotype of HT22R cells. Preliminary experiments further indicated a role of xCT in cell differentiation, inflammation, and ischemic stroke.

Despite the high upregulation of P2X receptors P2X3 and P2X7 in HT22R cells, their overexpression did not result in protection against oxidative glutamate toxicity. These factors were therefore not further analyzed.

GDAP1 is a mitochondrial protein and fission factor. Mutations in *GDAP1* cause the hereditary peripheral neuropathy Charcot-Marie-Tooth disease CMT4A. GDAP1 overexpression protected HT22 cells against glutamate toxicity and NSC-34 motor neuron

cells against buthionine sulfoximine (BSO)-induced glutathione depletion. Moreover, GDAP1 rescued HT22 cells from cell death induced by overexpression of 12/15-LOX and truncated Bid. Increased GDAP1 expression caused an increase in the mitochondrial membrane potential ($\Delta\Psi$m) suggesting high respiratory capacities. At the same time, a GDAP1-induced shift in energy metabolism towards glycolysis was observed together with an increase of the expression of hexokinase-2 and its binding to mitochondria - phenotypes that resemble the Warburg effect, namely elevated glycolysis in the presence of oxygen, a main feature of cancer cells. On the other hand, GDAP1 increased the expression and activity of the mitochondrial complex II or succinate dehydrogenase, but the effect on oxidative phosphorylation was not further studied. The disease-associated point mutation R310Q attenuated some of the functions of GDAP1, including mitochondrial fission, protection against glutamate- and BSO-induced cell death, and the increase of $\Delta\Psi$m and complex II activity. Furthermore, fibroblasts derived from two CMT4A patients exhibited reduced $\Delta\Psi$m and complex II activities suggesting that, in addition to the impairment of mitochondrial fission, deficiencies in energy production account for the pathology of CMT4A. Taken together, these results prove the involvement of oxidative stress in the pathogenesis of CMT4A, a hereditary neurodegenerative disease.

Zusammenfassung

Oxidativer Stress spielt bei verschiedenen Krankheiten und auch bei neurodegenerativen Krankheiten eine wichtige Rolle. Hohe Glutamatkonzentrationen führen zu oxidativer Glutamattoxizität, einem Zelltodprogramm, das sich von Exzitotoxizität unterscheidet. Extrazelluläres Glutamat führt hier zu einer Hemmung der Aufnahme der Aminosäure Zystin durch das Glutamat-Zystin-Antiporter-System X_c^-. Zystin wird zur Synthese des wichtigen intrazellulären Antioxidanz Glutathion benötigt. Ein Absinken des Glutathion-Spiegels führt zu einem Anstieg in der Konzentration reaktiver Sauerstoffspezies, der Aktivierung von 12/15-Lipoxygenase (12/15-LOX) sowie dem Öffnen cGMP-gesteuerter Kalziumkanäle. Die hippokampale HT22-Zelllline besitzt keine ionotropen Glutamatrezeptoren und ist daher ein hervorragendes Modell zur Untersuchung von oxidativer Glutamattoxizität. Die glutamat-resistente Zelllinie HT22R stellt ein weiteres Werkzeug zu Identifizierung protektiver Faktoren dar. HT22R-Zellen überleben hohe Glutamatkonzentrationen, besitzen erhöhte Glutathionspiegel sowie verringerte Konzentrationen reaktiver Sauerstoffspezies und unterscheiden sich in ihrem Transkriptom von glutamat-sensitiven HT22-Zellen. Mithilfe einer Arrayanalyse konnten verschiedene Transkripte identifiziert werden, unter anderem die für die regulatorische X_c^--Untereinheit xCT, den P2X-Rezeptor P2X3 und das mitochondriale Protein GDAP1. Ziel dieser Arbeit war, die zelluläre Funktion und insbesondere den Schutz dieser Faktoren vor oxidativem Stress zu untersuchen.

xCT-Überexpression schützte HT22-Zellen erheblich gegen oxidative Glutamattoxizität, während xCT-Knockdown und pharmakologische Inhibierung die Resistenz gegen oxidativen Stress verminderten. Erste Ergebnisse belegten weiterhin eine Rolle für xCT bei der Zelldifferenzierung, während Entzündungsprozessen und beim Schlaganfall.

P2X3 und ein weiterer P2X-Rezeptor, P2X7, waren in HT22R-Zellen stark hochreguliert. Trotzdem konnte ihre Überexpression nicht vor oxidativer Glutamattoxizität schützen. Da hier protektive Faktoren analysiert werden sollten, wurden P2X3 und P2X7 nicht weiter untersucht.

GDAP1 ist ein mitochondriales Protein und spielt eine Rolle bei der Fragmentierung von Mitochondrien. Mutationen im Gen für GDAP1 verursachen die autosomal-rezessive Charcot-Marie-Tooth-Erkrankung 4A. Überexpression von GDAP1 schützte vor Glutamat- und Buthioninsulfoximin (BSO)-induziertem oxidativen Stress sowie vor Zelltod, der durch die Aktivität von 12/15-LOX und tBid verursacht wurde. GDAP1 erhöhte das mitochondriale Membranpotenzial und somit die Kapazität für oxidative Phosphorylierung. Zur gleichen Zeit wurden eine erhöhte Glykolyserate sowie eine erhöhte Expression der Hexokinase-2 sowie deren Bindung an Mitochondrien beobachtet. Dies sind Effekte, die beim Warburg-Effekt (erhöhte Glykolyserate trotz Sauerstoff) in Krebszellen auftreten. Auf der anderen Seite erhöhte GDAP1 die Expression und Aktivität des mitochondrialen Komplexes II, auch Succinat-Dehydrogenase genannt. Die krankheitsverursachende Punktmutation R310Q hob einige der Funktionen von GDAP1 auf, unter anderem die mitochondriale Fragmentierung, den Schutz gegen oxidative Glutamattoxizität, die Erhöhung des mitochondrialen Membranpotenzials sowie die Steigerung der Succinat-Dehydrogenase-Aktivität. Außerdem zeigten Fibroblasten von CMT4A-Patienten verringerte mitochondriale Membranpotenziale und Succinat-Dehydrogenase-Aktivitäten. Dies weist darauf hin, dass neben der Beeinträchtigung der mitochondrialen Fragmentierung auch Defekte in der zellulären Energiegewinnung eine Rolle in der Entstehung der Charcot-Marie-Tooth-Erkrankung spielen.

Zusammenfassend zeigen diese Ergebnisse, das oxidativer Stress eine wichtige Rolle bei neurodegenerativen Erkrankungen spielt.

1.   Introduction

1.1   Oxidative stress is involved in neurological disorders

Oxidative stress is an important feature of neurological disorders and neurodegenerative diseases. It is defined as an imbalance between the production and removal of reactive oxygen species (ROS) (Halliwell, 2001). ROS include superoxides (O_2^-), hydrogen peroxide (H_2O_2) and hydroxyl radicals (Fridovich, 1998). The majority of ROS are derived at the mitochondria along the electron transport chain, namely at complex I (NADH dehydrogenase) and especially at complex III (ubiquinone-cytochrome c reductase). Here, electrons from complex I and II are transferred to ubiquinone or coenzyme Q, which results in the reduced form QH_2. During the regeneration of ubiquinone, the unstable intermediate semiquinone (Q^-) is produced, which leads to the formation of superoxides (reviewed in Finkel and Holbrook, 2000). Moreover, O_2 can be enzymatically reduced to H_2O_2, and there are both enzymatic and spontaneous processes that produce superoxide radicals (Fridovich, 1998). Further intracellular sources contributing to oxidative stress include peroxisomes and enzymes like NADPH oxidases, monoamine oxidases, cyclo-oxygenases, and lipoxygenases (Tan et al., 2001). In addition to endogenous oxidative stress, ROS are produced by exogenous sources such as UV light, toxins or inflammatory cytokines (Finkel and Holbrook, 2000). Cells have evolved different mechanisms to counteract the production of ROS. Superoxide dismutases (SODs), catalases, and glutathione peroxidases are the primary enzymes in the defense against ROS. SODs catalyze the dismutation of superoxide into oxygen and hydrogen peroxide, and catalases and glutathione peroxidases reduce H_2O_2 to water. In addition to these enzymatic ROS scavengers, a number of antioxidant molecules like ascorbate, carotenoids, flavonoids, and most importantly glutathione participate in ROS defense. In case of an imbalance between ROS production and antioxidant defenses, ROS accumulate and damage cell structures including proteins, nucleic acids, lipids and membranes, which finally leads to cell death. Due to the high oxygen consumption and the low regenerative capacity, brain tissue is especially susceptible to oxidative damage (Barnham et al., 2004) and thus, oxidative stress has been

implicated in the pathology of several neurodegenerative diseases (Barnham et al., 2004; Mariani et al., 2005) including Alzheimer's disease (AD) (Mattson, 2004; Su et al., 2008; Zhu et al., 2004), Parkinson's disease (PD) (Olanow, 1990; Shadrina et al., 2010), and amyotrophic lateral sclerosis (ALS) (Barber and Shaw, 2010). AD and PD are characterized by deposits of misfolded proteins, namely the amyloid-β (Aβ) peptide and α-synuclein, both of which were found to be involved in the generation of ROS. In AD, the Aβ peptide coordinates metal ions causing the production of hydrogen peroxide (Huang et al., 1999). In PD, dysfunctional mitochondrial complex I partially accounts for the generation of oxidative stress, and ALS is associated with mutations in SOD, an important enzyme in the detoxification of ROS (reviewed in Barnham et al., 2004, and Mariani et al., 2005).

1.1.1 Oxidative glutamate toxicity

Glutamate is the major excitatory neurotransmitter in the central nervous system. However, excessive glutamate concentrations can lead to oxidative stress and cell death. In several neurological disorders like ischemic stroke or neurodegenerative diseases, high glutamate concentrations cause an overstimulation of ionotropic glutamate receptors leading to increased calcium influx and eventually cell death, a mechanism called excitotoxicity (Choi, 1988). In addition to this process, glutamate induces another oxidative-stress mediated and programmed cell death pathway called oxidative glutamate toxicity (Lewerenz and Methner, 2006; Tan et al., 2001). Here, excessive extracellular glutamate inhibits cystine uptake by the cystine/glutamate antiporter system X_c^-. Once inside the cell, cystine is rapidly reduced to cysteine, which is required for the synthesis of glutathione (GSH). Therefore, excessive extracellular glutamate leads to GSH depletion. GSH is the most important intracellular antioxidant. It consists of the three amino acids glutamate, cysteine and glycine. During the two-step synthesis of GSH, cysteine and glycine are joined by glutamate-cysteine ligase to the dipeptide γ-glutamylcysteine, which is then combined with glycine by glutathione synthetase. Some cells can synthesize cysteine from cystathionine by cystathionine-γ-ligase; neurons, however, do not express this enzyme (Tan et al., 2001). Therefore, and because glutamate and glycine occur at relatively high intracellular concentrations, the uptake of cysteine, respectively cystine, is the rate-limiting step of GSH synthesis. The product of GSH oxidation by glutathione peroxidase is glutathione disulfide (GSSG) that can be converted back to the reduced monomeric GSH by glutathione reductase. Normally, GSH is about 100-fold more abundant than GSSG, and the GSH/GSSG ratio plays an important role in the regulation of the cellular redox status. Decreases in the GSH/GSSG ratio induce the oxidation of thiol groups of proteins leading to interaction with other proteins, DNA, RNA, and lipids (Maher, 2005). GSH inhibits protein oxidation by direct interaction with protein thiol groups. Moreover, GSH is required for the reduction of reactive oxygen species such as hydrogen

peroxide by glutathione peroxidase. It constantly removes ROS that are mainly produced in the mitochondria as by-products of oxidative phoshporylation (Griffith, 1999). In addition, GSH is used for the detoxification of electrophiles and xenobiotics through conjugation by glutathione *S*-transferases (GSTs) (Maher, 2005).

The blockage of X_c^- leads to a depletion of GSH followed by 12/15-LOX activation, the accumulation of ROS levels, and the opening of cGMP-gated channels, which allow calcium influx into the cell (Lewerenz et al., 2006; Tan et al., 2001). In contrast to excitotoxicity, oxidative glutamate toxicity is caused by very high, millimolar glutamate concentrations and the cell death program lasts several hours. Extracellular glutamate concentrations of 500 μM can be observed in ischemia (Maher, 2005). However, the physiological role of this receptor-independent glutamate-induced cell death relies not so much on the glutamate exposure but in the drop in glutathione levels and subsequent oxidative stress that is characteristic of many neurological disorders (Pallast et al., 2009).

1.1.2 HT22 cells as a model for oxidative glutamate toxicity

Glutathione synthesis can also be blocked by buthionine sulfoximine (BSO), which inhibits the first step in GSH synthesis, and oxidative stress can directly be modeled by treatment with H_2O_2. However, glutamate-induced receptor-independent cell death is a cost-effective and very reproducible model for oxidative stress. The mouse hippocampus-derived neuronal cell line HT22 lacks ionotropic glutamate receptors and is therefore used to study oxidative stress in neurons and as a screening tool for neuroprotective reagents (Albrecht et al., 2010; Lewerenz et al., 2009; Lewerenz et al., 2003; van Leyen et al., 2008).

The major events in oxidative glutamate toxicity in HT22 cells are shown in Figure 1. Exposure of HT22 cells to glutamate blocks the antiporter system X_c^- and thus results in a GSH depletion in a time course of approximately eight hours (Tan et al., 1998). GSH levels and cell survival can be restored, however, when GSH is depleted by more than 80% for several hours, cells undergo a programmed cell death (Maher, 2005). The depletion in GSH is paralleled by an increase in ROS. However, during the first six hours of glutamate challenge, when GSH levels are decreased to less than 20%, ROS levels increase very slowly and only to about 10% of maximal values. After that time period, ROS concentrations increase exponentially and are proposed to originate from mitochondria (Maher, 2005; Tan et al., 1998).

The decrease of GSH is tightly coupled to the activation of the lipid-oxidizing enzymes 12/15-lipoxygenases (Li et al., 1997b). Van Leyen and colleagues proposed a role for 12/15-LOX in programmed organelle degradation, in which it integrates into organelle membranes allowing access of proteases, which leads to membrane permeabilization (van Leyen et al., 1998). In this way mitochondrial membranes are directly attacked by 12/15-LOX following their activation by the drop in GSH. Pharmacological inhibition of 12/15-LOX in HT22 cells can not prevent

GSH depletion, but protects mitochondrial membranes and reduces ROS generation. Moreover, incubation of isolated mitochondria with purified 12/15-LOX reproduces the events of oxidative glutamate toxicity including breakdown of the mitochondrial membrane potential, ROS generation, and the release of cytochrome *c* (Pallast et al., 2009). In addition, LOX incorporate molecular oxygen into polyunsaturated fatty acids and thereby produce hydroxyeicosatetraenoic acids (HETE) (Tan et al., 2001). Inhibition of LOX with baicalein prevented production of HETE and blocked glutamate toxicity in HT22 cells (Li et al., 1997b) and protected mice against ischemia (van Leyen et al., 2006). HETE in turn activate soluble guanylate cyclases that produce cGMP. Inhibition of guanylate cyclases prevents glutamate-induced cell death in HT22 cells and moreover, the addition of a cell-permeable cGMP analogue potentiates glutamate toxicity (Li et al., 1997a).

The entry of calcium (Ca^{2+}) into the cells follows the increase in ROS. Ca^{2+} influx can be prevented by inhibition of soluble guanylate cyclases indicating that calcium enters through cGMP-gated Ca^{2+} channels (Li et al., 1997a). Ca^{2+} entry is crucial for the progress of the glutamate-induced cell death program. The prevention of Ca^{2+} influx protects HT22 cells from cell death despite the remarkable increase in ROS (Li et al., 1997b). Furthermore, eight to ten hours after induction of glutamate toxicity, apoptosis-inducing factor (AIF) translocates to the nucleus in a BID (BH3-interacting domain death agonist)-dependent manner and causes nuclear fragmentation followed by cell death within a few minutes (Landshamer et al., 2008). In contrast to apoptosis, the activation of caspases is not required during the cell death program of oxidative glutamate toxicity (Tan et al., 2001; van Leyen et al., 2005).
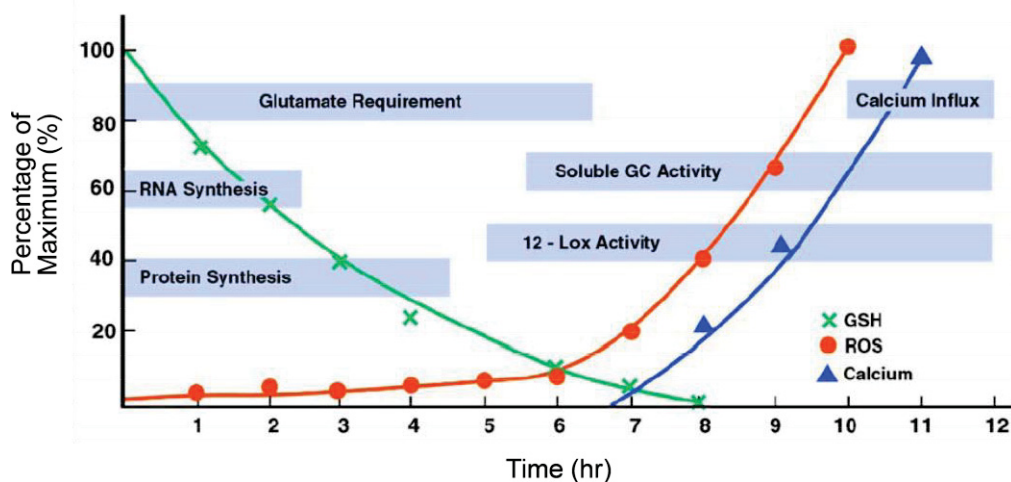
Figure 1 **Schematic diagram of the time course of oxidative glutamate toxicity in HT22 cells.** The lines represent the relative change in GSH, ROS and calcium levels. The blue boxes represent the major events and time points after addition of exogenous glutamate. Adapted from (Maher, 2005).

1.1.3 The glutamate-resistant cell line HT22R

Our group has previously generated a glutamate-resistant HT22 cell line by repeated exposition to glutamate and propagation of the surviving cells (Lewerenz et al., 2006; Sahin et al., 2006). These cells have been named HT22R cells and characterized to exhibit reduced GSH depletion after glutamate treatment and to be resistant against several cell death inducers including glutamate, hydrogen peroxide, tunicamycin, and the direct activation of the caspase cascade by overexpression of Bcl-2-associated X protein (BAX) (Dittmer et al., 2008; Lewerenz et al., 2006; Sahin et al., 2006). The increased resistance to diverse stressors is at least in part caused by changes at the transcriptional level. Northern blot analysis revealed the upregulation of the transcripts for the detoxifying enzyme catalase and, to a more prominent rate, of xCT, the functional subunit of the cystine/glutamate antiporter system X_c^-, and immunoblotting showed an increased expression of the excitatory amino acid transporter EAAT3 in the glutamate-resistant cell line (Lewerenz et al., 2006). Moreover, medium conditioned by glutamate-resistant HT22R cells protects against oxidative glutamate toxicity suggesting the release of cytoprotective factors (Sahin et al., 2006). In addition, HT22R cells display increased phosphorylation of cAMP-response-element binding (CREB) and differ in their G-protein-coupled receptor (GPCR) expression pattern from sensitive HT22 cells. Expression of the GPCR VPAC$_2$ was found to be increased more than 12-fold in HT22R cells, and pharmacological stimulation of VPAC$_2$ and glutamate treatment synergistically induce the expression the antiapoptotic protein B-cell lymphoma 2 (BCL-2), which is accompanied by an increase in GSH levels and the expression of glutamate-cysteine ligase, the rate-limiting enzyme in GSH synthesis (Sahin et al., 2006). Moreover, quantitative PCR revealed the overexpression of the orphan GPCR GPR39 in HT22R cells. GPR39 overexpression protects against glutamate and other cell death stimuli in a RhoA/serum response element (SRE)-dependent manner and by induction of pigment epithelium-derived growth factor (PEDF) and other downstream effectors (Dittmer et al., 2008). Finally, a suppression hybridization approach revealed further transcripts upregulated in the resistant cell line, among them a new protein with a SOD motif, which was named transcript increased in glutamate resistance (TIGR). Overexpression of TIGR protected against glutamate toxicity, colocalized with catalase, and increased SOD activity in Neuro2a cells. However, no direct SOD activity was observed in yeast (Toutzaris et al., 2010).

1.2   The glutamate-cystine antiporter system X$_c^-$

1.2.1   Structure and expression of X$_c^-$

The X$_c^-$ antiporter system has first been described by Watanabe and Bannai as a Na$^+$-independent amino acid transport system in fibroblasts that couples the entry of cystine to the exit of glutamate (Bannai and Kitamura, 1980). As outlined above, cysteine is required for the synthesis of the important antioxidant GSH. Outside the cell, cysteine is rapidly oxidized to cystine, which is thus the predominant form in the extracellular milieu. The system X$_c^-$ exchanges cystine for glutamate with a stochiometry of 1:1 (Bannai, 1986). Once inside the cell, cystine is readily reduced to cysteine (Bannai and Ishii, 1988; Christensen, 1990) that is used for GSH synthesis. Due to the action of glutamate transporters, the extracellular glutamate concentration is much lower than the intracellular concentration (Baker et al., 2003), which provides the driving force for the cystine/glutamate exchange by X$_c^-$ (Bannai and Ishii, 1988).
The transport activity of X$_c^-$ was shown to require the expression of two proteins, namely xCT and 4F2HC (Bassi et al., 2001; Sato et al., 1999; Sato et al., 2000). Thus, X$_c^-$ is a heteromeric amino acid transporter, and its subunits are coupled by a disulfide bridge (Fig. 2). The light-chain subunit xCT contains twelve transmembrane domains with the N and C termini located inside the cell (Gasol et al., 2004) and confers substrate specificity (Sato et al., 1999). The heavy-chain subunit 4F2HC has a single transmembrane domain and is a common component of other transporter families (Wang et al., 2003).
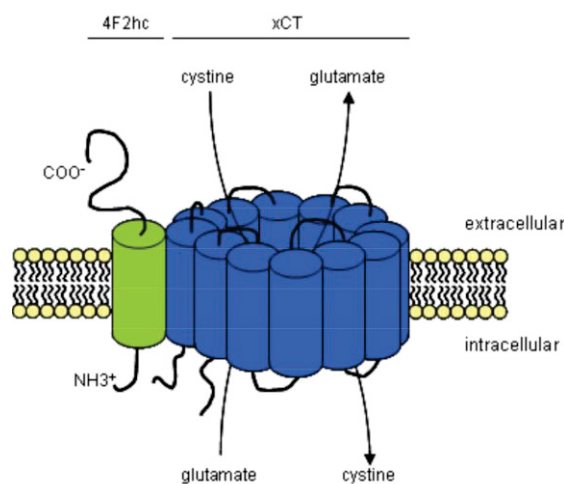
Figure 2 **Schematic diagram of the structure and function of the X$_c^-$ antiporter system.** The heteromeric transporter is composed of two subunits coupled by a disulfide bridge. The heavy subunit 4F2HC is part of several amino acid transporters, has a single transmembrane domain and is involved in trafficking to the plasma membrane. The light subunit xCT consists of twelve transmembrane domains and confers transport and substrate specificity. The transport system X$_c^-$ transports cystine into the cell in exchange to glutamate with a stochiometry of 1:1.

xCT is encoded by the *Slc7a11* gene. It is regulated by the cap'n'collar transcription factor Nuclear factor E2-related factor 2 (NRF2), which binds to the antioxidant response element (ARE) (Shih et al., 2003). The NRF2-ARE signaling pathway coordinates the induction of a variety of cytoprotective genes including phase II detoxification enzymes (van Muiswinkel and Kuiperij, 2005). Shih and colleagues reported a simultaneous upregulation of xCT with other factors involved in GSH metabolism, namely in GSH biosynthesis (glutamate cysteine ligase, GSH synthetase), use (GSTs and GSH reductase) and export (multidrug resistance protein 1) (Shih et al., 2006). Moreover, cystine uptake and expression of both xCT and 4F2HC were stimulated in macrophages by treatment with lipopolysaccharides (LPS) (Sato et al., 1995).

Despite its expression in other organs including kidney, pancreas, colon, spleen, liver, and lung (Bassi et al., 2001; Burdo et al., 2006; Sato et al., 2000; Shih et al., 2006), xCT is prominently expressed in the brain (Sato et al., 1999; Shih et al., 2006). xCT expression was found in several brain regions including cortex, hippocampus, striatum, and cerebellum and in a variety of cultured cells including neurons and astrocytes (Bassi et al., 2001; Burdo et al., 2006; La Bella et al., 2007; Shih et al., 2003). While immature neurons exclusively take up cystine by X_c^-, mature neurons primarily take up cysteine. In a GSH coupling pathway, cystine/cysteine is taken up by astrocytes via X_c^- and other transport mechanisms, used for GSH synthesis, and GSH is exported to the extracellular space. Here, it is degraded to cysteine that can be used for neuronal uptake (Banjac et al., 2008; Shih et al., 2006).

X_c^- has been shown to play a role in diseases of the central nervous system (CNS) and in various cancers (Lo et al., 2008b). In Alzheimer's disease, the release of glutamate by microglia via X_c^- enhances the toxicity of Aβ (Qin et al., 2006). Because of their increased requirement for GSH, the expression of xCT is crucial for tumor growth and has been shown to be upregulated in various cancer cell lines and tissues (Chung et al., 2005; Lo et al., 2008a; Savaskan et al., 2008; Ye et al., 1999). Moreover, pharmacological inhibition and small interfering RNA (siRNA)-mediated silencing of xCT can delay cancer growth *in vivo* (Chung et al., 2005; Savaskan et al., 2008). Therefore, xCT has been proposed as a potential target for therapy of cancer and other diseases (Guan et al., 2009; Lo et al., 2008b).

1.2.2 xCT protects against oxidative glutamate toxicity

Transient transfection of HT22 cells with xCT has been shown to protect against glutamate toxicity and GSH depletion (Lewerenz et al., 2006) showing the crucial role of X_c^- in this model. Moreover, the glutamate transporter EAAT3 protects against glutamate toxicity both, alone and synergistically together with xCT. From these results it has been concluded that glutamate uptake by EAAT3 reduces the glutamate-induced inhibition of cystine uptake by X_c^- and thus prevents GSH depletion and excessive accumulation of ROS in the cell (Lewerenz et

al., 2006). In addition, xCT has been found to be up-regulated in the glutamate-resistant HT22R cell line and in sensitive HT22 cells exposed to glutamate.

1.3 The purinergic ATP receptor P2X3

P2X receptors are nonselective cation channels that open in response to extracellular ATP and are permeable to Ca^{2+}, Na^+ and K^+. They are expressed in excitable and nonexcitable cells including smooth muscle, heart muscle, bone, endothelial and epithelial cells, sensory neurons, dorsal root ganglia, astrocytes, oligodendrocytes, Schwann cells, and microglia (Burnstock, 2006; MacKenzie et al., 1999). P2X receptors mediate various physiological activities like muscle contractility, synaptic transmission and neuroendocrine secretion (Torres et al., 1999). Moreover, they are involved in the transduction of several sensory signals including hearing and tasting, and P2X3 has been associated with the signaling of inflammatory, neuropathic, and visceral pain (Burnstock, 2009; North, 2004). P2X receptors control the influx of sodium ions leading to cell depolarization and the influx of calcium ions for enzyme activation.

In mammals, seven P2X subunits have been identified (Torres et al., 1999). The structure of P2X subunits is shown in Figure 3. All P2X subunits contain two hydrophobic, membrane-spanning domains, TM1 and TM2, that form the ion pore and mediate channel gating. A stretch of 300 amino acids between the TM domains forms an extracellular loop that contains the ATP binding site (Ennion et al., 2000). The N and C termini are localized in the cytosol (Jarvis and Khakh, 2009). P2X receptors are multimers of several subunits.
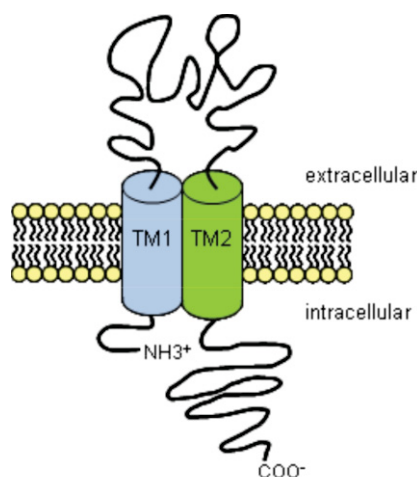
Figure 3 **Schematic diagram of P2X receptors.** P2X subunits contain two hydrophobic, membrane-spanning domains, TM1 and TM2, that form the ion pore and mediate channel gating.

Several studies suggest that either three or six subunits contribute to functional P2X oligomers (North, 2002) that can be of homo-oligomeric or hetero-oligomeric nature. It has been shown by co-immunoprecipitation that all P2X subunits except for P2X6 can form homo-oligomeric complexes (Torres et al., 1999). P2X1, P2X2, P2X5, and P2X6 can hetero-oligomerize with most of the other P2X subunits, whereas P2X7 only forms homomeric assemblies. P2X3 is able to form hetero-oligomers with P2X1, P2X2 and P2X5. Other NTPs can act as P2X agonists, and channel properties vary among the different P2X subtypes. However, ATP is most potent to activate all P2X assemblies (North, 2002).

1.4 Ganglioside-induced differentiation protein 1 (GDAP1)

1.4.1 Structure of GDAP1 gene and protein

GDAP1 is a 358 amino acid protein whose function is not yet known. The corresponding gene is 23,728 base pairs long and contains six exons (Cassereau et al., 2010). Its expression is regulated by the zinc finger transcription factor YY1, which controls the transcription of many nuclear genes encoding mitochondrial proteins (Ratajewski and Pulaski, 2009). *Gdap1* was first described by Liu et al. as one of ten transcripts upregulated after ganglioside differentiation of Neuro2a cells by GD3 synthase overexpression. Moreover, GDAP1 was found to be upregulated in embryonic carcinoma P19 cells after retinoic acid-induced neural differentiation (Liu et al., 1999). From this study it was concluded that GDAP1 may function in a signal transduction pathway responsible for neurite differentiation, however, no further studies indicated the participation of GDAP1 in such a pathway.

Bioinformatic approaches revealed structural similarities to glutathione *S*-transferases and predicted two hydrophobic domains at the C-terminus of GDAP1 (Baxter et al., 2002; Cuesta et al., 2002; Marco et al., 2004; Shield et al., 2006). In addition to the N-terminal thioredoxin fold domain (GST-N) and the C-terminal substrate-binding domain (GST-C) identified by sequence analysis, secondary structure prediction proposed two additional α-helices between the GST domains that are absent in all other GSTs (Marco et al., 2004). No GST activity or GSH binding ability was observed with a recombinant bacterial expressed GDAP1 (Pedrola et al., 2005; Shield et al., 2006). Only recently, both GSH binding and GST activity of GDAP1 has been observed using a truncated GDAP1 expressed by a eukaryotic baculovirus system (Wagner, 2009).

GDAP1 expression was shown in different regions of the CNS, including cortex, cerebellum, olfactory bulb, and spinal cord, as well as in peripheral nerves by RT- and real-time PCR (Pedrola et al., 2005), Western blot analysis (Niemann et al., 2005), and immunohistochemistry

(Pedrola et al., 2008). Niemann et al. found GDAP1 to be expressed in neurons and Schwann cells (Niemann et al., 2005), whereas Pedrola et al. reported GDAP1 expression exclusively in neurons, and did not detect GDAP1 in cultured rat Schwann cells (Pedrola et al., 2005).

1.4.2   Mutations in *GDAP1* are responsible for Charcot-Marie-Tooth 4A

Charcot-Marie-Tooth (CMT) disease is a hereditary peripheral neuropathy. With a prevalence of one in 2,500, it is one of the most common inherited disorders in humans (Berger et al., 2002). Patients suffer from progressive muscle weakness and atrophy, first involving the feet, legs and later the hands, foot deformities, sensory loss, and decreased tendon deficits (Cassereau et al., 2010; Senderek et al., 2003). Being a group of genetically heterogeneous neuropathies, mutations in a variety of genes are responsible for the pathological phenotypes. About thirty genes have been found to be responsible for CMT. Affected proteins include proteins responsible for forming the myelin sheath, like Peripheral myelin protein 22 (PMP22) and Myelin protein zero (MPZ), heat shock proteins (HSP22, HSP27) being involved in correct protein folding, proteins participating in cellular transport including Neurofilament light polypeptide (NEFL), Myotubularin-related protein 2 (MTMR2) and Dynamin 2 (DNM2), and proteins involved in mitochondrial network organisation, namely Mitofusin 2 (Mfn2) and GDAP1 (Patzko and Shy, 2010).

Based on electrophysiological and anatomical pathology findings, CMT syndromes are grouped into two main categories. Type 1 or the demyelinating form is characterized by reduced nerve conduction velocities, due to partial or complete loss of the myelin sheath. Type 2 or the axonal form is characterized by a reduced compound muscle action potential and the formation of onion bulbs, while nerve conduction velocities are normal (Baxter et al., 2002; Berger et al., 2002; Cassereau et al., 2010). Due to their mode of inheritance, CMT forms are grouped into autosomal dominant (CMT1, CMT2), autosomal recessive (CMT3, CMT4) and X-linked (CMT1X) subtypes. While the autosomal dominantly inherited forms CMT1 and CMT2 account for the majority of CMT patients, the autosomal recessive CMT forms CMT3 and CMT4 are very rare. The X-linked dominant form CMT1X is primarily demyelinating and represents the second most common form of CMT (Patzko and Shy, 2010). The classification of CMT into demyelinating and axonal forms is clinically very useful; however, Berger et al. state that phenotypes of myelinopathies and axonopathies are often intermingled (Berger et al., 2002).

CMT4A is the most common among the recessive CMT types (Nelis et al., 2002). It exhibits clinical phenotypes similar to that of CMT1 but is more severe and has a very early age of onset. Baxter and Cuesta independently localized CMT4A-causing mutations to the gene for GDAP1 on 8q21 (Baxter et al., 2002; Cuesta et al., 2002). Although CMT4A has initially been described as a demyelinating form, different *GDAP1* mutations causing axonal,

demyelinating, and intermediate forms have been identified. The *GDAP1* mutations reported by Baxter et al. cause CMT syndromes with a very early onset of age and severe weakness and atrophy of foot and hands. Nerve conduction velocities of both, motor and sensory nerves, have been found to be drastically reduced indicating a demyelinating phenotype (Baxter et al., 2002). Cuesta et al., however, described a typical axonal neuropathy with decreased or completely lost sensory-nerve action potential, but only slightly reduced nerve conduction velocities. Moreover, loss of myelinated fibers and axonal degeneration were observed in nerve biopsies, but no signs of demyelination (Cuesta et al., 2002). In 2003, Senderek and colleagues reported mutations causing truncated proteins and leading to phenotypes combining demyelinating and axonal pathologies (Senderek et al., 2003). To date, more than 40 disease-causing *GDAP1* mutations have been described (Cassereau et al., 2009; Kabzinska et al., 2010), among them missense mutations, several mutations leading to truncated proteins and alterations that affect splice sites in the *GDAP1* transcript.

The 26 missense mutations identified so far are shown in Figure 4 (Ammar et al., 2003; Azzedine et al., 2003; Baxter et al., 2002; Boerkoel et al., 2003; Bouhouche et al., 2007; Cassereau et al., 2009; Chung et al., 2008; Claramunt et al., 2005; Crimella et al., 2010; Di Maria et al., 2004; Kabzinska et al., 2006a; Kabzinska et al., 2006b; Kabzinska et al., 2005; Kabzinska et al., 2007; Kabzinska et al., 2010; Moroni et al., 2009; Nelis et al., 2002; Parman et al., 2004; Sahin-Calapoglu et al., 2009; Xin et al., 2008).
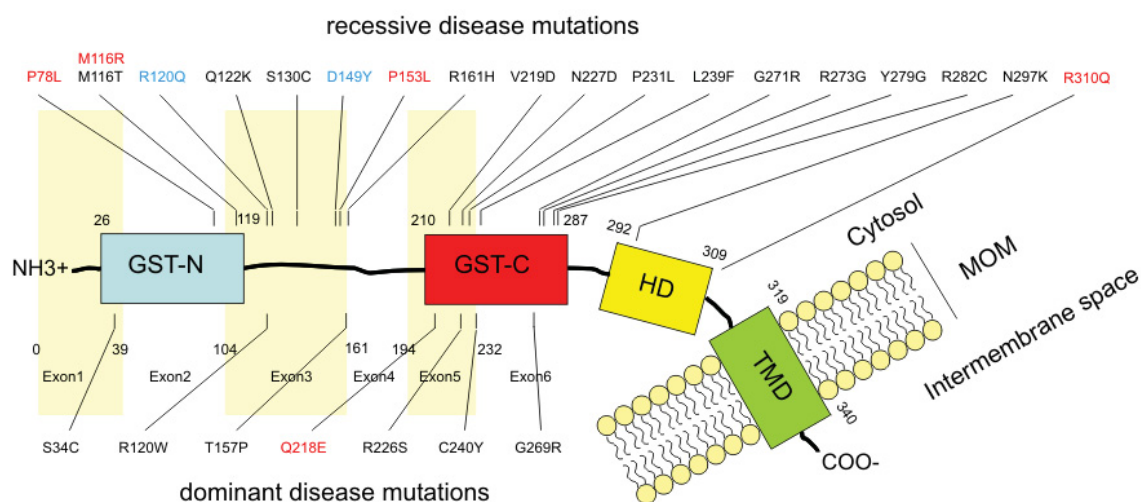
Figure 4 **Schematic representation of the GDAP1 protein** with predicted domains (HD hydrophopic domain, TMD transmembrane domain) and indication of the corresponding exons. CMT-causing mutations and their phenotypes: intermediate, red; demyelinating, blue; axonal, black. Based on figures of Casserau et al. (2010) and Wagner (Dissertation, 2009).

In addition to the varying pathological phenotypes of CMT4A, mutations in *GDAP1* are responsible for other CMT subtypes. Kabzinska and colleagues analyzed the mutation L239F that leads to a relatively mild CMT subtype called CMT4C4 in several families (Kabzinska et al., 2010). In addition, four *GDAP1* mutations are inherited in a dominant mode and have been designated to the subtype CMT2K (Cassereau et al., 2009; Chung et al., 2008; Claramunt et al., 2005). It has been observed that recessive inherited *GDAP1* mutations lead to phenotypes far more severe than those caused by dominant mutations (Cassereau et al., 2010).

1.4.3   GDAP1 is a mitochondrial protein and is involved in mitochondrial fission

GDAP1 is a mitochondrial protein. Proteinase digest studies have revealed that GDAP1 is integrated in the mitochondrial outer membrane (MOM) with the N-terminal part containing the GST domains oriented towards the cytosol (Niemann et al., 2005). The precise topology of GDAP1 and the motifs that are involved in MOM targeting have been studied by Wagner et al. They showed that GDAP1 exhibits a single transmembrane domain whereas the second, N-terminal hydrophobic domain is located in the cytoplasm, identifying GDAP1 as a tail-anchored protein (Wagner et al., 2009). The transmembrane domain (TMD) and the adjacent basic amino acids were found to be crucial for mitochondrial targeting and membrane insertion.

Moreover, GDAP1 is a mitochondrial fission factor. Overexpression of GDAP1 was shown to induce mitochondrial fragmentation in COS-7 cells (Niemann et al., 2005; Pedrola et al., 2008). Mitochondria are highly dynamic organelles, and the mitochondrial network is balanced by the opposing processes of mitochondrial fusion and fission. The role of mitochondrial dynamics is still subject of analysis. The balance of fusion and fission is important for the bioenergetic function of mitochondria since defects in fusion and fission factors are associated with oxidative phosphorylation (OXPHOS) deficiencies (Chan, 2006b). Also a role in mitosis has been suggested. Fusion and fission are probably required to ensure mitochondrial distribution to daughter cells during cytokinesis. Moreover, in several studies impaired mitochondrial dynamics result in developmental defects (Chan, 2006a). For example, mutations in the *Drosophila* fusion factor Fzo lead to developmental defects and sterility (Hales and Fuller, 1997). In mice, the knockout of *Mfn1* or *Mfn2* results in embryonic lethality (Chen et al., 2003). And an infant carrying a mutation in the fission factor Dynamin-related protein 1 (*DRP1*) exhibited elongated mitochondria and died at 37 days (Waterham et al., 2007). The cellular importance of fusion and fission most likely relies on maintaining a healthy mitochondrial population. Through the cooperation of mitochondria, mitochondrial DNA and other components like substrates, metabolites and lipids can be interchanged, and deficiencies of single mitochondria can be restored by fusion (Detmer and Chan, 2007). Finally,

mitochondrial fission is associated with apoptosis and has been shown to regulate the release of apoptotic factors into the cytosol (Cereghetti and Scorrano, 2006; Delivani and Martin, 2006).

The molecular mechanisms of fusion and fission and the involved factors are reviewed in several articles (Chan, 2006b; Detmer and Chan, 2007; Frazier et al., 2006; Westermann, 2008). In mammals, two mitofusins, MFN1 and MFN2, have been identified. These are conserved, large GTPases localized at the MOM. An additional component shown to be involved in mitochondrial fusion is Optic atrophy 1 (OPA1), a dynamin family GTPase that is located in the mitochondrial intermembrane space. During fusion, mitofusins of adjacent mitochondria interact with each other and mediate the fusion of the outer membranes by GTP hydrolysis while OPA1 is thought to facilitate the fusion of the inner membranes. The fission machinery consists of the proteins DRP1 and Mitochondrial fission protein 1 (FIS1). DRP1 is a cytosolic protein and needs to be recruited upon fission. Like dynamin, DRP1 exhibits GTPase function and is thought to assemble into rings that encircle and constrict the mitochondrial tubule. FIS1 that is a receptor-like protein located at the MOM allows for the recruitment of DRP1 to the mitochondria.

GDAP1-induced mitochondrial fragmentation can be counterbalanced by the activity of fusion factors MFN1 and MFN2. In addition, GDAP1-induced fission is dependent on the fission factors DRP1 and FIS1 (Niemann et al., 2009). CMT-causing *GDAP1* mutations were shown to impair the fission activity of GDAP1 (Niemann et al., 2005). Moreover, the fission abilities of CMT-associated GDAP1 mutants differ depending on the mode of inheritance. While recessively inherited *GDAP1* mutations lead to reduced fission activity, dominant GDAP1 forms were shown to interfere with mitochondrial fusion (Niemann et al., 2009). MOM targeting is required for the fission function of GDAP1 although changes in the GDAP1 transmembrane domain do not influence fission activity. However, the TMD-bordering basic amino acids that have been shown to be involved in MOM targeting and the cytosolic hydrophobic domain are required for GDAP1-induced fission (Wagner et al., 2009).

Interestingly, next to *GDAP1*, mutations in other fusion and fission factors were shown to cause neurodegenerative diseases (Chan, 2007). *MFN2* is mutated in CMT2A, and dominant optic atrophy, the most common inherited optic neuropathy, is caused by mutations in *OPA1*. Moreover, a subset of CMT2A patients has optic atrophy as caused by mutations in *OPA1* suggesting that *MFN2* and *OPA1* mutations can lead to overlapping clinical syndromes. This demonstrates that neurons are particularly prone to defects in mitochondrial dynamics. Since effective mitochondrial dynamics are required for energy production, the importance of fusion and fission in neuronal cells can be traced back to their large cell dimensions and their high energy demands (Detmer and Chan, 2007).

1.5   Aim of this study

This study aimed at the identification and characterization of factors involved in protection mechanisms against oxidative stress. The glutamate-resistant HT22R cell line has been generated previously in order to study protection against oxidative glutamate toxicity. HT22R cells have already been compared to glutamate-sensitive cells based on their transcript levels, and Affymetrix array analysis revealed further candidates that might be involved in the protection against glutamate challenge.

In this work, selected candidates, namely xCT, P2X3 and GDAP1 were tested for their protective function.

xCT has already been identified as a key factor in the protection against oxidative glutamate toxicity. It mediates the import of cystine, the limiting precursor for the synthesis of the antioxidant GSH. The role of xCT in diseases that imply oxidative stress was analyzed in preliminary experiments *in vitro* and *in vivo*.

The cellular role of GDAP1 is not yet known. Mutations in *GDAP1* cause the hereditary peripheral neuropathy Charcot-Marie-Tooth disease 4A. Moreover, GDAP1 has been shown to induce mitochondrial fission. This study analyzed the role of GDAP1 in protection against oxidative stress and how its function is affected by a CMT-associated point mutation.

2   Materials and Methods

2.1   Materials

2.1.1   Chemicals and biochemicals

Chemicals	Supplier
2',7'-Dichlorodihydrofluorescein diacetate (H2DCFDA)	Molecular Probes, Invitrogen, Eugene, OR, USA
2-Deoxy-D-glucose	Fluka, Sigma-Aldrich, Steinheim, Germany
2-Propanol	Merck, Darmstadt, Germany
4',6-Diamidino-2-phenylindole dihydrochloride (DAPI)	Sigma-Aldrich, Steinheim, Germany
3-(4,5-Dimethyl-2-thiazolyl)-2,5-diphenyl-2H-tetrazolium bromide (MTT)	Sigma-Aldrich, Steinheim, Germany
3'-[[5-(2,3-Dichlorophenyl)-H-tetrazol-1-yl] methyl]pyridine hydrochloride (A-438079)	Tocris Bioscience, Bristol, UK
5-[[[(3-Phenoxyphenyl)methyl][(1S)-1,2,3,4-tetrahydro-1-naphthalenyl]amino] carbonyl]-1,2,4-benzenetricarboxylic acid sodium salt hydrate (A-317491)	Sigma-Aldrich, Steinheim, Germany
5,5',6,6'-Tetrachloro-1,1',3,3'-tetraethylbenz-imidazolcarbocyanine iodide (JC-1)	Molecular Probes, Invitrogen, Eugene, OR, USA
5',5'-Dithiobis(2-nitrobenzoic acid) (DTNB)	Sigma-Aldrich, Steinheim, Germany
5-Sulfosalicylic acid (SSA)	Fluka, Sigma-Aldrich, Steinheim, Germany
Bovine serum albumin (BSA)	Sigma-Aldrich, Steinheim, Germany
Buthionine sulfoximine (BSO)	Sigma-Aldrich, Steinheim, Germany
Calcium chloride dihydrate	Fluka, Sigma-Aldrich, Steinheim, Germany
Carbonyl cyanide 3-chlorophenyl-hydrazone (CCCP)	Sigma-Aldrich, Steinheim, Germany
D-(+)-Galactose	Sigma-Aldrich, Steinheim, Germany
D-(+)-Glucose	Sigma-Aldrich, Steinheim, Germany
D-(+)-Saccharose	Carl Roth, Karlsruhe, Germany

Dimethyl sulfoxide (DMSO)	Sigma-Aldrich, Steinheim, Germany
Disodium hydrogen phosphate	Sigma-Aldrich, Steinheim, Germany
Ethanol	Merck, Darmstadt, Germany
Ethidium bromide	Sigma-Aldrich, Steinhein, Germany
Ethylenediaminetetraacetic acid (EDTA)	Sigma-Aldrich, Steinheim, Germany
Ethyleneglycoltetraacetic acid (EGTA)	Fluka, Sigma-Aldrich, Steinheim, Germany
Glycerol	Sigma-Aldrich, Steinheim, Germany
L-Glutamic acid	Sigma-Aldrich, Steinheim, Germany
L-Glutathione reduced	Sigma-Aldrich, Steinheim, Germany
Lipopolysaccharides (LPS)	Sigma-Aldrich, Steinheim, Germany
Magnesium chloride hexahydrate	Fluka, Sigma-Aldrich, Steinheim, Germany
Mannitol	Sigma-Aldrich, Steinheim, Germany
N-Acetyl-L-cystine (NAC)	Sigma-Aldrich, Steinheim, Germany
Nicotinamide adenine dinucleotide phosphate (NADPH)	Sigma-Aldrich, Steinheim, Germany
Retinoic acid (RA)	Sigma-Aldrich, Steinheim, Germany
Rhodamine phalloidin	Cytoskeleton, Denver, CO, USA
(S)-4-Carboxyphenylglycine ((S)-4-CPG)	Tocris Bioscience, Bristol, UK
Sodium chloride	Sigma-Aldrich, Steinheim, Germany
Sodium hydroxide	Carl Roth, Karlsruhe, Germany
Sulfasalazine (SAS)	Sigma-Aldrich, Steinheim, Germany
Tetramethylrhodamine ethyl ester (TMRE)	Sigma-Aldrich, Steinheim, Germany
Triethanolamine (TEA)	Fluka, Sigma-Aldrich, Steinheim, Germany
Tris(hydroxymethyl)aminomethane (Tris)	Sigma-Aldrich, Steinheim, Germany
Triton	Sigma-Aldrich, Steinheim, Germany
Tunicamycin	Merck, Darmstadt, Germany
Tween 20	Sigma-Aldrich, Steinheim, Germany

2.1.2   Kits

Kits	Supplier
BC Assay Protein Quantification Kit	Interchim, Montlucon Cedex, France
CellTiter-Blue Cell viability assay	Promega, Karlsruhe, Germany
Complex II Enzyme Activity Microplate Assay Kit	MitoSciences, Eugene, OR, USA
illustra RNAspin Mini Isolation Kit	GE Healthcare, Freiburg, Germany
Nucleobond Xtra Maxi Kit	Macherey & Nagel, Düren, Germany
Qiaprep Spin Miniprep Kit	Qiagen, Hilden, Germany
Qiaquick Gel Extraction Kit	Qiagen, Hilden, Germany
Qiaquick PCR Purification Kit	Qiagen, Hilden, Germany

2.1.3 Buffers and solutions

Standard solutions

Standard buffers and solutions	Supplier
HEPES buffer 1 M	Invitrogen, Karlsruhe, Germany
PBS 10 X	Invitrogen, Karlsruhe, Germany
RIPA buffer	Thermo Scientific, Rockford, IL, USA
TBE 10X	Invitrogen, Karlsruhe, Germany

Assay buffers

Assay buffers	Composition
GSH assay buffer	0.1 M Na_2HPO_4 1 mM EDTA 0.3 mM DTNB 0.4 mM NADPH pH 7.5 5 μl/ml glutathione reductase
Mitochondrial isolation buffer	200 mM mannitol 100 mM sucrose 1 mM EGTA 5 mM $MgCl_2$ pH 7.4 1 Complete Mini Protease Inhibitor cocktail tablet / 15 ml
Immunoblot (IB) blocking buffer	5% BSA 50 mM Tris 150 mM NaCl 0.05 % Tween 20 pH 7.6
Immunocytochemistry (IC) blocking buffer	0.2% BSA 0.2% FCS 0.01% Triton in PBS

2.1.4 Other materials

Materials	Supplier
10X BlueJuice Gel Loading Buffer	Invitrogen, Karlsruhe, Germany
Brain infusion pump 3 – 5 mm	Alzet, Cupertino, CA, USA
Complete Mini Protease Inhibitor cocktail tablets	Roche Diagnostics, Mannheim, Germany
Dounce Homogenizer	Kimble Chase, Vineland, NJ, USA

High performance chemiluminescence film	Amersham, Buckinghamshire, UK
iBlot Transfer Stack, Regular (Nitrocellulose)	Invitrogen, Karlsruhe, Germany
LDS Sample buffer (4X)	Invitrogen, Karlsruhe, Germany
Magic Mark XP Western Protein Standard	Invitrogen, Karlsruhe, Germany
Milk powder	Saliter, Obergünzburg, Germany
NuPAGE Sample Reducing Agent (10X)	Invitrogen, Karlsruhe, Germany
1kb Plus DNA ladder	Invitrogen, Karlsruhe, Germany
Ponceau S solution	Sigma-Aldrich, Steinheim, Germany
8-16% Precise Protein Gels (10 Well)	Thermo Scientific, Rockford, IL, USA
SuperSignal West Pico Chemiluminescent Substrate	Thermo Scientific, Rockford, IL, USA
Trypan Blue stain	Gibco, Sigma-Aldrich, Steinheim, Germany
Universal Probe Library	Roche Diagnostics, Mannheim, Germany

2.1.5   Bacterial culture

Bacteria

The *Escherichia coli* strain DH5α was used for cloning and amplification of plasmid DNA. It has the genotype F' Phi80dlacZ DeltaM15 Delta(lacZYA-argF)U169 deoR recA1 endA1 hsdR17(rK-mK+)phoA supE44 lambda- thi-1.

Media

Media	Supplier
LB Agar, powder	Invitrogen, Karlsruhe, Germany
LB Broth base, powder	Invitrogen, Karlsruhe, Germany
LE Agarose	Biozyme, Oldendorf, Germany
SOC Medium	Invitrogen, Karlsruhe, Germany

Antibiotics

Antibiotics	Supplier
Ampicillin sodium salt	Sigma-Aldrich, Steinheim, Germany
Kanamycin sulfate	Sigma-Aldrich, Steinheim, Germany
Spectinomycin	Sigma-Aldrich, Steinheim, Germany

2.1.6 Cell Culture

Cells and cell lines

The immortalized cell line HT22 was derived from murine hippocampus. It serves as a model for oxidative glutamate toxicity, as it lacks ionotropic glutamate receptors. Glutamate-resistant HT22 cells are a subpopulation of the cell line HT22 that have been generated by repeated exposition to and propagation in 10 mM glutamate. They have been described to protect against oxidative glutamate toxicity and other types of cell death stimuli (Lewerenz et al., 2006). In this study they will be referred to as HT22R cells, whereas the original cells are named HT22 cells.

HT22 cells stably over-expressing wild-type (WT) GDAP1 or the GDAP1 mutant R310Q were generated by the former group member Svenja Frede. HT22 cells were transfected with the vectors pIRES2-EGFP containing the ORFs for mouse *GDAP1*, R310Q or as empty vector.

NSC-34 is a hybrid cell line, which has been generated by fusion of motor neuron enriched, embryonic mouse spinal cord cells with mouse neuroblastoma. NSC-34 cells have been shown to exhibit motor neuron properties like the generation of action potentials, the expression of neurofilament triplet proteins and choline acetyltransferase, as well as the synthesis, storage and release of acetylcholine (Cashman et al., 1992). They were a kind gift of Dr. Jochen Weishaupt, Dept. of Neurology, University of Göttingen who received them from Neil Cashman, Neurology, University of Toronto, Canada.

Two skin biopsies from CMT4A patients could be obtained. One was a gift from Andrzej Kochanski, Neuromuscular Unit, Mossakowski Medical Research Centre, Polish Academy of Sciences, Warsaw, Poland; the second skin biopsy was directly obtained from a German patient seen by Axel Methner. Thomas Dehmel, Neurology, University Clinic Düsseldorf, helped to derive primary fibroblast cell lines from the two skin biopsies. The patient-derived fibroblast cell lines from Andrzej Kochanski and the German patient are here referred to as CMT#1 and CMT#2, respectively. Six different fibroblasts from adult healthy donors were obtained from the Department of Dermatology of the Heinrich-Heine University Düsseldorf.

Cell culture media and solutions

Cell Culture Media and Solutions	Supplier
Dulbecco's Modified Eagle Medium, High Glucose	PAA Laboratories, Pasching, Austria
Dulbecco's Modified Eagle Medium, Without Glucose	PAA Laboratories, Pasching, Austria
Dulbecco's Modified Eagle Medium, F-12	Invitrogen, Karlsruhe, Germany
Dulbecco's PBS without Ca & Mg	PAA Laboratories, Pasching, Austria
Fetal cow serum	Thermo Scientific, Rockford, IL, USA
L-glutamine	Invitrogen, Karlsruhe, Germany
Optimem	Invitrogen, Karlsruhe, Germany
Trypsin	Invitrogen, Karlsruhe, Germany

Antibiotics

Antibiotics	Supplier
Geneticin	Invitrogen, Karlsruhe, Germany
Penicillin / Streptomycin	Invitrogen, Karlsruhe, Germany

Cell transfection reagents

Transfection Reagents	Supplier
Attractene	Qiagen, Hilden, Germany
Lipofectamine 2000	Invitrogen, Karlsruhe, Germany
Dharmafect 2	Dharmacon, Thermo Scientific, UK

2.1.7   Vectors

Expression vector	Backbone	Insert	Supplier
Gdap1:pcDNA	pcDNA3.1/HisB	*Gdap1* cDNA	Axel Niemann, ETH Zurich, Switzerland
Gdap1:pIRES	pIRES2-EGFP2	*Gdap1* cDNA	generated here
Gdap1:pSK	pSK	*Gdap1* cDNA	generated here
Gdap1 M116R:pcDNA	pcDNA3.1/HisB	*Gdap1* mutant M116R cDNA	Axel Niemann, ETH Zurich, Switzerland
Gdap1 R120Q:pcDNA	pcDNA3.1/HisB	*Gdap1* mutant R120Q cDNA	Axel Niemann, ETH Zurich, Switzerland
Gdap1 R310Q:pcDNA	pcDNA3.1/HisB	*Gdap1* mutant R310Q cDNA	Axel Niemann, ETH Zurich, Switzerland
Gdap1 R310Q:pIRES	pIRES2-EGFP2	*Gdap1* mutant R310Q cDNA	generated here
Gdap1 R310Q:pSK	pSK	*Gdap1* mutant R310Q cDNA	generated here
Gdap1 miRNA#1	pcDNA^{TM}6.2-GW/EmGfp-miR	*Gdap1* pre-miRNA ds oligo	generated here
Gdap1 miRNA#2	pcDNA^{TM}6.2-GW/EmGfp-miR	*Gdap1* pre-miRNA ds oligo	generated here
Gdap1 miRNA#3	pcDNA^{TM}6.2-GW/EmGfp-miR	*Gdap1* pre-miRNA ds oligo	generated here
12/15-LOX	pCMV-Sport6	mouse 12/15-LOX cDNA	RZPD, Berlin, Germany
P2X3	pCMV-Sport	P2X3 (*P2rx3*)	RZPD, Berlin, Germany
tBid:pIRES	pIRES2-EGFP	*tBid*, active form 322-732 bp	Carsten Culmsee, University of Marburg, Germany
xCT-GFP:Gw1	Gw1	mouse *Slc7a11* (xCT)-GFP	Andy Shih, University of British Columbia, Vancouver, Canada

xCT miRNA#1	pcDNA™6.2-GW/EmGfp-miR	xCT pre-miRNA ds oligo	generated here
xCT miRNA#2	pcDNA™6.2-GW/EmGfp-miR	xCT pre-miRNA ds oligo	generated here
xCT miRNA#3	pcDNA™6.2-GW/EmGfp-miR	xCT pre-miRNA ds oligo	generated here
Control vectors	**Backbone**	**Insert**	**Supplier**
pcDNA3.1/HisB	empty vector		
pcDNA™6.2-GW/EmGfp-miR-neg control plasmid	pcDNA™6.2-GW/EmGfp-miR	negative control pre-miRNA	Invitrogen, Karlsruhe, Germany
pIRES2-EGFP	empty vector		Clontech
Cloning vectors	**Backbone**	**Insert**	**Supplier**
pcDNA™6.2-GW/EmGfp-miR	empty vector		Invitrogen, Karlsruhe, Germany
pBluescript II SK (+) (pSK)	empty vector		Stratagene, La Jolla, CA, USA

2.1.8 siRNA and miRNA sequences

siRNA sequences

siRNAs were ordered from Dharmacon, Thermo Scientific, UK.

siRNA	Species	Sequence of sense sequence (5' → 3')
xCT si#1	mouse	UAAUUAGCUGUAUAACUCCUU
xCT si#2	mouse	UAUGCUUGUACCUAAUUCUUU
xCT si#3	mouse	UCAUAGAGAGGAUUUCCGGUU
xCT si#4	mouse	UAGCUCCAGGGCGUAUUACUU
xCT pool	mouse	pool of xCT siRNAs si#1 – si#4

shRNA sequences

shRNAs were ordered as unmodified oligos from Eurofins MWG (Ebersberg, Germany).

shRNA	Species	Start	Sequence of RNAi target sequence (5' → 3')
xCT miRNA sh#1	mouse	1082	TATGCATATGCTGGCTGGTTT
xCT miRNA sh#2	mouse	1442	ACTCCTCTGCCAGCTGTTATT
xCT miRNA sh#3	mouse	1501	AGACCTCTATAGTCTTCTAAA
Gdap1 miRNA sh#1	mouse	1901	AACCTATGCACTGCATAGAAA
Gdap1 miRNA sh#2	mouse	2077	GTGAGGTGCTCATCCTGTATA
Gdap1 miRNA sh#3	mouse	2444	CCATATGGAAGAGACGGTTCA

2.1.9   Primers

All primers were purchased from Eurofins MWG (Ebersberg, Germany).

Primers for RT-PCR, sequencing and cloning

Primer	Sequence (5' → 3')	for
EmGFP forward sequencing primer	GGCATGGACGAGCTGTACAA	sequencing *Gdap1*- and xCT-directed shRNA oligos in Block-iT Pol II miR RNAi expression vectors
*Gdap1*_754_for	GCTGTCACATTGCATCGACT	cloning and sequencing cDNA from stable HT22 cells to verify R310Q mutation
*Gdap1*_995_rev	ACTCCTGCAAGCAAACCAAC	
*Gdap1*_433_for	CCCACGGGTACAACATTACC	cloning and sequencing cDNA (from exon 2 to end) to check mutations in patient-derived fibroblasts
*Gdap1*_1177_rev	CACGACAAGATCCCAACAAA	

Primers for qPCR

Primer	Species	Sequence (5' → 3')	UPL probe
β-ACTIN	human	forward ATTGGCAATGAGCGGTTC reverse GGATGCCACAGGACTCCA	11
β- Actin	rat	forward CTAAGGCCAACCGTGAAAAG reverse TACATGGCTGGGGTGTTGA	115
GDAP1	human	forward TGCAAAGAAGAAATGAAGAAACC reverse GTCTGCCAGGGTGAAGGAT	21
Gdap1	mouse, rat	forward AAGAAGAAATGAGGAAACTCCAGA reverse ACATCTGCCAGTGTAAAGGATTC	21
Hk-1	mouse	forward GTGGACGGGACGCTCTAC reverse TTCACTGTTTGGTGCATGATT	58
Hk-2	mouse	forward CAACTCCGGATGGGACAG reverse CACACGGAAGTTGGTTCCTC	21
HPRT	human	forward TGACCTTGATTTATTTTGCATACC reverse CGAGCAAGACGTTCAGTCCT	73
Hprt	rat	forward GACCGGTTCTGTCATGTCG reverse ACCTGGTTCATCATCACTAATCAC	95
Kv1.5	mouse	forward TTTAAAAAGTATCGCATTCCATGA reverse CATCTTACAGTGAATGCTCACCA	92
P2rx2	mouse	forward ATGGGATTCGAATTGACGTT reverse GATGGTGGGAATGAGACTGAA	96
P2rx3	mouse	forward CATCCGTTTCCCTCTCTTCA reverse TTTATGTCCTTGTCGGTGAGG	12
P2rx4	mouse	forward CCAACACTTCTCAGCTTGGAT reverse TGGTCATGATGAAGAGGGAGT	33
P2rx5	mouse	forward GCGAGTTTTACCGAGACAAGA reverse TTGGCCTCAACCTCAACATT	69

P2rx7	mouse	forward TGTGAAGTCTCTGCCTGGTG	63
		reverse GCTCCTCAAGAGTGCAGGTC	
Pdk2	mouse	forward CTGGACCGCTTCTACCTCAG	58
		reverse GCCATCAAAGATGAGGGTGT	
β-Tub3	rat	forward CAGAGCCATTCTGGTGGAC	116
		reverse GCCAGCACCACTCTGACC	
xCT	mouse	forward TGGGTGGAACTGCTCGTAAT	1
		reverse AGGATGTAGCGTCCAAATGC	

Moreover, a human Glycerinaldehyd-3-phosphat-dehydrogenase (*GAPDH*) Primer-Probe-Assay (Applied Biosystems) was used as a further endogenous control.

2.2.10 Enzymes

Restriction enzymes

Enzymes	Supplier
*Bam*HI	New England Biolabs, Frankfurt, Germany
*Bgl*II	New England Biolabs, Frankfurt, Germany
*Sac*II	New England Biolabs, Frankfurt, Germany
*Xba*I	New England Biolabs, Frankfurt, Germany

Other enzymes and enzyme mixes

Enzymes	Supplier
FAST qPCR MasterMix	Eurogentec, Seraing, Belgium
Glutathione reductase	Sigma-Aldrich, Steinheim, Germany
Platinum PCR Supermix	Invitrogen, Karlsruhe, Germany
Reverse Transcriptase	Invitrogen, Karlsruhe, Germany
TaqMan Gene Expression Master Mix	Applied Biosystems, Foster City, CA, USA
T4 DNA Ligase and 1X T4 DNA Ligase Reaction Buffer	New England Biolabs, Frankfurt, Germany

2.1.11 Antibodies

Primary Antibodies	Host/Immunogen	Dilution	Supplier
Anti-ACTIN mAb	mouse	1:2000	Chemicon / Millipore, Temecula, CA, USA
	β-ACTIN, Clone C4, near aa 50-70		
Anti-GDAP1 pAb	rabbit	1:5000	Axel Niemann, ETH Zürich, Switzerland
	aa 1-14 MARRQDEARAGVPL		

Anti-HEXOKINASE 1 mAb	rabbit	1:200	Cell Signalling Technology, Danvers, MA
	synthetic peptide derived from human HEXOKINASE 1		
Anti-HEXOKINASE 2 mAb	rabbit	1:200	Cell Signalling Technology, Danvers, MA
	synthetic peptide derived from human HEXOKINASE 2		
Anti-MITOCHONDRIAL HEAT SHOCK PROTEIN 70 mAb	mouse	1:1000	Affinity Bioreagents, Golden, CO, USA
	synthetic peptide derived from aa 615-633 of mouse mtHSP70 SGSSGTGEQKEDQKEEKQ		
MitoProfile Total OXPHOS Rodent WB Antibody Cocktail:	mouse	1:250	MitoSciences, Eugene, OR, USA
	Anti BOVINE COMPLEX I C-I-20, Clone 20E9DH10C12 Anti BOVINE HEART COMPLEX II C-II-30, Clone 21A11AE7 Anti BOVINE HEART COMPLEX II, III C-III-Core 2, Clone 13G12AF12BB11 Anti HUMAN COMPLEX IV SUBUNIT I C-IV-I, Clone 1D6E1A8 Anti BOVINE COMPLEX V C-V-α, Clone 15H4C4		
Secondary Antibodies	**Host/Immunogen**	**Dilution**	**Supplier**
Goat Anti-Rabbit IgG:HRP	goat	1:5,000	AbD Serotec / Morphosys, Martinsried/Planegg, Germany
IRDye® 680 Conjugated Goat (polyclonal) Anti-Mouse IgG	goat	1:30,000	LI-COR Biosciences, Königstein, Germany
IRDye® 800 Conjugated Goat (polyclonal) Anti-Mouse IgG	goat	1:40,000	LI-COR Biosciences, Königstein, Germany
IRDye® 680 Conjugated Goat (polyclonal) Anti-Rabbit IgG	goat	1:30,000	LI-COR Biosciences, Königstein, Germany

2.1.12   Instruments

Instrument	Supplier
7500 Real Time PCR System	AppliedBiosystems, Darmstadt, Germany
Biofuge Strato	Heraeus, Osterode, Germany
BX51 Flourescence Microscope	Olympus, Hamburg, Germany
Captair Bio PCR Hood	Erlab, Cologne, Germany
Curix 60 Developer	Agfa, Cologne, Germany
FACS Calibur	Beckton Dickinson, Heidelberg, Germany
FluoroGenios Pro	Tecan, Männedorf, Germany
GDS-Gel Imaging System	Intas, Göttingen, Germany
Heracell 150 Incubator	Kendro, Schwerte, Germany
Herasafe Sterile Hood	Kendro, Schwerte, Germany

iBlot Dry Blotting Device	Invitrogen, Karlsruhe, Germany
IX81-Flourescence Microscope	Olympus, Hamburg, Germany
Odyssey Infrared Imaging System	Licor, Bad Homburg, Germany
P25 Powerpack	Biometra, Göttingen, Germany
S2100 Diode Array Spectrophotometer	Biochrom, Cambridge, UK
Subcell GT Powerpack	Biorad, Munich, Germany
Tabletop Centrifuge 5415R	Eppendorf, Hamburg, Germany
T Gradient PCR Cycler	Biometra, Göttingen, Germany
Thermomixer compact	Eppendorf, Hamburg, Germany
Xcell Sure Lock System	Invitrogen, Karlsruhe, Germany

2.2   Methods

2.2.1   Cell culture and transfection

Cell culture

HT22 cells were cultured in DMEM High Glucose with 5% FCS. HT22R cells were additionally maintained in 10 mM glutamate and the medium of stably over-expressing HT22 cells was supplemented with 2 mg/ml geneticin. NSC34 cells, N2a neuroblastoma and BV2 microglial cells were maintained in DMEM High Glucose with 10% FCS. All media were supplemented with 100 U/ml penicillin and 100 g/ml streptomycin (1% Pen/Strep). Cells were grown at 37°C under an atmosphere of 95% air and 5% CO_2. Cells were typically maintained in 10-cm dishes.

To obtain primary fibroblasts from a human skin biopsy, it was transferred onto a cell culture dish, cut into small fragments, and scratched into the plastic to ensure attachment. The biopsy fragments were covered with MEM media supplemented with 20% FCS, 2 mM L-glutamine, and 1% Pen/Strep. It took approximately three weeks for fibroblasts to grow in single cell layers; in this time, medium was changes three times per week. Finally, fibroblasts were detached with trypsin and transferred to a new culture dish. Later, human fibroblast cell lines were grown in DMEM/F-12 containing 10% FCS and 2 mM L-glutamine.

At high confluences, cells were washed, detached with 1 ml trypsin and collected with 10 ml culture medium. Depending on the cell line, cells were split 1:10 or 1:5 every two to three days, whereas human fibroblasts grew at slower growth rates and were split approximately every week. To count cells, a Neubauer improved counting chamber was applied. Trypan blue was used to stain nonviable cells, and only unstained cells were counted.

For storage, cells were frozen and maintained in liquid nitrogen. Therefore, cells were washed with PBS, harvested by trypsination and centrifuged. Pellets were washed twice in PBS and finally resuspended in freezing medium containing 90% FCS and 10% DMSO. Cells were transferred to cryotubes and cooled down to -80°C before they were stored in liquid nitrogen. To thaw cells, cryotube stocks were thawed in a 37°C water bath and resuspended in pre-warmed medium in a cell dish. After 2 – 3 h, when cells have attached to the bottom of the dish, the culture medium was changed in order to remove DMSO.

Transfection of cells

Cells were transfected with plasmid DNA using the transfection reagent attractene, which is suitable for adherent cells. The active component is a nonliposomal lipid that forms complexes with the negatively charged DNA, which in turn enter the target cells. Transfections were performed according to the recommendations of the manufacturer and were usually carried out in 6-well plates. Depending on the cell type, cells were seeded at densities of 20,000 to 32,000 cells/cm² one day prior to transfection to gain 90% confluency at transfection time. For transfection in 6-well plates, 4 µg DNA and 4.5 µl attractene were diluted in 100 µl Optimem per well and mixed by vortexing. Complexes were formed during the incubation time of 15 min. After adding the solution to the cells and swirling the plate, cells were incubated at normal growth conditions.

For transfection with siRNA, Dharmafect 2 was used. Cells in 6-well plates were transfected with 100 pmol siRNA. siRNA and Dharmafect 2 in a ratio of 1:25 were diluted separately in Optimem, combined after 5 min incubation time and incubated for another 10 min to allow complex formation. The solution was diluted 1:5 in antibiotic-free medium and exchanged for the growth medium.

Cells were monitored for gene expression and used for further experiments 48 h post-transfection.

BV2 macrophage activation

BV2 microglia cells were plated onto 6-well plates and macrophage activation was induced 24 h later by treatment with 10 ng/ml LPS, and LPS was added again another 48 h later. RNA was isolated every 12 h in a time course from 24 h to 72 h after first LPS induction.

Neurite outgrowth in N2a neuroblastoma cells

The effect of xCT overexpression and silencing on neurite outgrowth was analyzed in N2a neuroblastoma cells. Briefly, N2a cells were transfected with xCT or vectors encoding xCT-directed shRNAs, and differentiation was induced by treatment with 1 µM RA and FCS privation. After 7 days differentiation, the lengths of cell dendrites were analyzed. Therefore,

six cell categories were defined according to the dendrite length: cells without dendrites, cells with dendrites of the size of the cell body, and cells with approximately 25 nm, 50 nm, 100 nm and larger dendrites. Cells were analyzed using an IX81 fluorescence microscope (Olympus), and at least 100 cells were counted per treatment and experiment.

2.2.2 Microscopy

Fluorescence microscopy

To visualize mitochondria, a vector encoding mitochondria-targeted GFP was transfected into cells prior to plating cells onto cover slips. For staining F-Actin with rhodamine phalloidin, cells were fixed with 3.7% PFA for 15 min at RT and permeabilized with IC blocking buffer for another 10 min. After washing with PBS, cells were incubated in 100 nM rhodamine phalloidin for 30 min at RT and washed again several times with PBS. Cell nuclei were stained with 0.5 µg/ml DAPI. Images were taken using a BX51 Fluorescence microscope (Olympus).

Quantification of mitochondrial morphology

To analyze the mitochondrial morphology in dependence of GDAP1 overexpression, cells were co-transfected with mitoGFP. For quantification, four categories of mitochondrial morphologies were defined: tubular, mixed, vesicular, and fragmented structures. At least 70 cells were analyzed per condition and experiment using the BX51 Fluorescence microscope.

2.2.3 Cell viability assay

For cell viability assays, 5000 HT22 cells/well or 8000 NSC34 cells/well were seeded into 96-well plates. To analyze susceptibility of cells to glutamate, BSO, H_2O_2, or tunicamycin, toxics were added 24 h after cell seeding, and cell viability was assayed another 24 h later. To analyze toxicity in vector or siRNA-transfected cells, cells were plated into 6-well plates, transfected after 24 h, and 24 h later plated into 96-well plates. To evaluate the effect of inhibitors or other compounds, including SAS, (S)-4-CPG, NAC, A-317491, and A-438079, on glutamate toxicity, compounds were added together with different concentrations of glutamate. For growth studies, cells were plated in glucose-free medium (DMEM without Glucose, PAA) supplemented with indicated concentrations of glucose, galactose or deoxyglucose. Cell viability was assessed 24 h or 48 h after the start of the respective treatment using Cell Titer Blue (CTB) and recording absorbance at 562 nm with a reference at 612 nm with the GENios Pro microplate reader or using Thiazolyl Blue tetrazolium bromide (MTT) and measuring absorbance at 562 nm. For cell death experiments with overexpressed 12/15-LOX and truncated BH3-interacting domain death agonist (tBID), HT22 cells were plated into

6-well plates, transfected with 12/15-LOX and *tBid* vectors, and medium was changed 24 h later. 48 h after transfection, 200 µl CTB were added to the medium, and after 4 h incubation, 3 x 100 µl CTB-containing medium, respectively, were transferred to 96-well plates and measured with the microplate reader.

2.2.4   Whole protein isolation and subcellular fractionation

Protein isolation

For western blot analysis, cells were lysed with RIPA lysis buffer supplemented with one Complete Mini Protease Inhibitor cocktail tablet per 15 ml. Lysates were centrifuged at 16,000 g for 30 min at 4°C and supernatants were stored at –80°C. Protein concentrations were determined using the BC Assay Protein Quantification Kit.

Mitochondrial fragmentation

Mitochondrial and cytosolic fractions were obtained by differential centrifugation. HT22 and human fibroblast cell lines were grown in 175 cm² flasks. Cells were washed with PBS, harvested by trypsination and centrifuged at 1,000 g for 6 min. Cell pellets were resuspended in 200 µl mitochondria isolation buffer containing a protease inhibitor cocktail tablet per 15 ml, and cells were disrupted by 50 strokes of a Dounce homogenizer. The homogenates were centrifuged at 1,000 g for 10 min in order to remove nuclei and unbroken cells, and the post-nuclear supernatants were centrifuged at 16,000 g for 30 min to obtain mitochondria-enriched pellets. All steps were performed at 4°C and fractions were stored at –80°C.

2.2.5   Immunoblot analysis

Protein samples were denatured by adding 10X sample reducing agent and 4X LDS and heating to 99°C for 5 min. Equal protein amounts were loaded per lane. Following SDS-PAGE, proteins were transferred onto a nitrocellulose membrane using the iBlot Dry Blotting System (Invitrogen). The protein transfer was verified by staining the blots with Ponceau S solution. After this, the membrane was washed and incubated in IB blocking buffer for 1 h at RT in order to block unspecific binding sites. Blots were probed with primary antibodies at 4°C overnight. After washing with TBS containing 0.05% Tween, membranes were incubated in IB blocking buffer containing the secondary antibody. The membranes were washed again in TBS-Tween. IRDye-conjugates were detected with the Odyssey Infrared Imaging System; horseradish peroxidase conjugates were detected with enhanced chemiluminescent (ECL) substrates on chemiluminescence films.

2.2.6 Enzymatic assays

GSH assay

48 h after transfection, cells were washed twice with ice-cold PBS, resuspended in 200 µl PBS and transferred to a microcentrifuge tube containing 100 µl 10% SSA. Samples were vortexed, incubated on ice for 10 min and centrifuged at 16000 g for 10 min. Supernatants were transferred into a second microcentrifuge tube containing 24 µl TEA. GSH was then enzymatically converted by glutathione reductase in an assay buffer (100 mM Na_2PO_4, 1 mM EDTA, pH 7.5) containing 0.6 mM DTNB (5,5'-Dithiobis-(2-nitro-benzoic acid)) and 0.8 mM NADPH, and NADPH consumption was monitored at 390 nm with the GENios Pro microplate reader (Tecan). All steps were performed at 4°C.

Complex II activity assay

The activity of the mitochondrial complex II, also called succinate-coenzyme Q reductase, was measured with the Complex II enzyme activity microplate assay kit from MitoSciences. The 96-wells of the assay plate are coated with an anti-Complex II monoclonal antibody. The kit measures the decrease in absorbance of the dye DCPIP (2,6-dichlorophenolindophenol) at 600 nm whose reduction is coupled to the enzymatic production of ubiquinol. Detergent, buffers and substrates were contained in the kit and the assay was performed following the instructions of the manufacturer. To prepare cell samples, cells were washed with PBS, trypsinized, collected in PBS, centrifuged at 800 rpm for 5 min and resuspended in 100 µl PBS. 10 µl were added to the suspension, followed by 20-minute incubation on ice. Cell debris were removed by a second incubation step at 21,000 g and 4°C for 40 min. The supernatants were collected, and protein concentrations determined using the BCA assay. Samples were diluted to equal protein concentrations (10 µg/µl) and mixed 1:1 with incubation buffer. 50 µl of the suspension were added per well and incubated for 2 h at RT to immobilize the enzyme. Wells were washed twice with 300 µl buffer solution and incubated with 40 µl lipid solution for 30 min. Finally, 200 µl of activity solution containing ubiquinone, the substrate succinate, and DCPIP were added to the wells, and the absorbance of the dye at 600 nm was monitored in the GENios Pro microplate reader (Tecan) every 30 s for 90 min. The rate of absorbance reduction was calculated in time intervals in that the decrease in absorbance was linear.

Extracellular glucose and lactate concentrations

For determination of extracellular glucose and lactate concentrations, medium was changed 24 h after transfection and the growth medium collected 24 h later into blood sample collection tubes (BD Biosciences). Glucose and lactate concentrations were determined in the central diagnostic laboratory of the University Clinic Düsseldorf.

2.2.7   Flow cytometry assays

Detection of reactive oxygen species

2',7'-Dichlorodihydrofluorescein diacetate (H2DCFDA) is a fluorogen dye that is an indicator for ROS concentrations. It is nonfluorescent until oxidation occurs within the cells. Moreover, cleavage of lipophilic blocking acetate groups by intracellular esterases leads to a charged form of the dye that is well retained by the cells. Oxidation of the dye results in an increase in fluorescence intensity at 519 nm that can be measured by flow cytometry. Cells were washed with PBS, detached with trypsin, resuspended with PBS and centrifuged at 1000 rpm for 5 min. Pellets were resuspended in 1 ml PBS containing 10 μM H2DCFDA. After 20 min incubation at 37°C, cell suspensions were washed twice by centrifugation and resuspension in PBS. Fluorescence was measured with a FACS Calibur flow cytometer (Beckton Dickinson).

Detection of the mitochondrial membrane potential

The mitochondrial membrane potential was investigated using 5,5',6,6'-Tetrachloro-1,1',,3,3'-tetraethylbenzimidazolcarbocyanine iodide (JC-1) and Tetramethylrhodamine ethyl ester (TMRE). 48 h after transfection or 8 h after glutamate treatment, cells were washed and resuspended in PBS and treated with 2 μM JC-1 or 40 μM TMRE, respectively. Preincubation with 200 μM Carbonyl cyanide 3-chlorophenylhydrazone (CCCP), an ionophore and uncoupler of oxidative phosphorylation in mitochondria, served as control for the breakdown of the mitochondrial membrane potential. Fluorescence was analyzed using a FACS Calibur flow cytometer and quantified using CellQuest3.3 software. The JC-1 ratio was calculated as the ratio of the fluorescences at 590 nm to that at 530 nm. TMRE fluorescence was monitored at 590 nm.

2.2.8   RNA isolation and reverse transcription

RNA Isolation

To isolate total RNA from cells or tissues, the illustra RNAspin Mini isolation Kit (GE Healthcare) was used according to the manufacturer's instructions. Briefly, cell pellets or pellets of homogenized tissue samples were resuspended in 350 μl lysis buffer that inactivates RNases and creates appropriate binding conditions. To remove cell debris, lysates were applied to filters and centrifuged. 350 μl 70% ethanol were added to the filtrates in order to adjust binding conditions. The lysates were then loaded onto silica membranes followed by centrifugation at 8,000 g for 30 s. The DNase digest requires a salt removal by applying 350 μl desalting buffer to the column followed by another centrifugation step. Subsequently, 95 μl of a DNase I reaction mixture were applied to the column and incubated for 15 min. Columns

were then washed three times to inactivate the DNase and to remove salts and macromolecular cell components. Finally, RNA was eluted in 40 µl RNase-free water.

Reverse transcription

First strand cDNA synthesis was performed with Superscript II Reverse transcriptase from Invitrogen, following the manufacturer's instructions. Shortly, 1 µl random hexamer primers, 1 µl 10mM dNTPs and 2 µl RNase-free water were added to 8 µl RNA, the mixture was heated to 65°C for 5 min and quick chilled on ice. 4 µl 5X First-Strand Buffer, 2 µl DTT and 2 µl RNase-free water were added and the reaction was incubated 2 min at RT. After addition of 0.2 µl reverse transcriptase, the reaction was incubated for 10 min at RT and 50 min at 42°C. Finally, the reaction was inactivated at 70°C for 15 min.

2.2.9 Primer design and quantitative RT-PCR

Quantitative real-time reverse transcription-polymerase chain reaction (RT-PCR) was performed with a 7500 real time PCR system (Applied Biosystems) using TaqMan Gene Expression Master Mix (Roche) and 5'-FAM-labelled probes of the Universal Probe Library (Roche). The initial polymerase activation step for 10 min at 95°C was followed by 40 cycles of denaturing for 15 s at 95°C and annealing and elongation for 1 min at 60°C. PCR primers were designed using the Universal Probe Library Assay Design Tool (Roche). Expression levels were normalized by expression of the housekeeping genes hypoxanthine phosphoribosyltransferase (*Hprt*), glyceraldehyde 3-phosphate dehydrogenase (*Gapdh*), and β-Actin.

2.2.10 Molecular biology methods

Preparation of chemically competent bacteria

Bacteria were grown in antibiotic-free medium. At an OD of 0.5, bacterial cells were centrifuged at 5000 rpm and 4°C for 15 min and resuspended in ice-cold 100 mM $MgCl_2$. After a second centrifugation step, the pellet was resuspended in 10 mM $CaCl_2$ containing 15% glycerol. All steps were performed on ice, and 100 µL aliquots were stored at -80°C.

Transformation of competent bacteria

To transfer plasmid DNA into bacteria, 100 µl competent bacteria were thawed on ice, mixed with the DNA and incubated on ice for 20 min. During the following 90-second incubation step at 42°C, cell membranes become permeable, which allows the uptake of plasmid DNA. Cells were then quick-chilled on ice, incubated in 350 µl SOC medium for 1 h in a heated

shaker at 37°C, plated onto LB agar plates containing 0.1 µg/ml of the appropriate antibiotic (ampicillin, kanamycin), and grown overnight at 37°C. In order to prepare DNA in a small scale, colonies were picked and grown in 2 ml LB medium containing the respective antibiotic overnight at 37°C on a shaker. For large scale DNA isolation, 1 ml of bacterial suspension were incubated in 300 ml antibiotic-containing medium overnight.

Preparation of DNA

Plasmid DNA was purified with the help of silica membranes. For small scale plasmid DNA purification, the Qiaprep Spin Miniprep Kit was used according to the manufacturer's instructions. Shortly, 1 ml bacteria suspension was centrifuged, resuspended and lysed by alkaline lysis. After neutralization, precipitated compounds were removed by centrifugation, and the lysate was applied to a spin column where the DNA was bound to the silica membrane at high salt concentrations. Following washing steps, DNA was eluted with 40 µl dH_2O.

The Nucleobond Xtra Maxi Kit (Macherey & Nagel) was used to isolate plasmid DNA in a larger scale according to the protocol of the manufacturer. Briefly, 300 ml of bacteria suspension were centrifuged, resuspended, and lysed. After equilibrating the column, the cleared lysate was loaded to bind plasmid DNA to the anion-exchange resin. Following subsequent washing steps, plasmid DNA was eluted in a high-salt buffer, precipitated with isopropanol, centrifuged and washed with 70% ethanol. After centrifugation, DNA pellets were air-dried and reconstituted in dH_2O.

DNA concentrations were measured with a spectrophotometer (Biochrom).

Restriction digest and ligation

To analyze vectors and to clone DNA, plasmids were restricted with DNA endonucleases. With plasmids isolated by small scale preparation, 5 µl of plasmid were incubated with 5 U of the restriction enzymes, the appropriate enzyme buffer and, if required, BSA, in a 10 µl reaction at 37°C for 2 h. For plasmids obtained from large scale DNA purification, 1 µl DNA was used in a 20 µl reaction volume.

T4 DNA ligase was used to ligate DNA fragments. Therefore, different ratios of DNA fragments and linearized vectors were incubated with 1 µl T4 DNA ligase, 1 µl 10X ligase buffer and dH_2O in a total reaction volume of 10 µl either for 1 h at RT or at 4°C overnight.

PCR

Standard PCR was performed in a thermocycler using Platinum PCR Supermix (Invitrogen). Briefly, 1 µl of diluted template DNA and 1 µl, respectively, of forward and reverse primers in concentrations of 10 nmol/ml, were mixed with 22 µl PCR mix containing dNTPS, $MgCl_2$, and

Taq DNA polymerase. After initial DNA denaturing at 95°C, several PCR cycles of denaturing at 95°C for 30 s, primer annealing for 30 s, and polymerization at 72°C for 1 min/kb template were preformed followed by a final 10 min elongation step at 72°C. Annealing temperatures depended on the basepair composition of applied primers and were typically between 50°C and 70°C.

Agarose gel electrophoresis

To analyze PCR products and restricted plasmids, DNA was separated by agarose gel electrophoresis. Therefore, DNA was mixed with BlueJuice sample buffer, loaded onto an agarose gel containing 0.6 µg/ml ethidium bromide, and separated at 120 V in a horizontal chamber containing TBE buffer. Typically, 1% agarose gels were used. Fragments smaller than 100 bp were analyzed on 2% agarose gels. The 1 kb Plus DNA ladder (Invitrogen) served as a size standard.

Generation of miRNA-encoding vectors

The BlockiT™ Pol II miR RNAi Expression vector kit (Invitrogen) served as a tool for vector-based expression of shRNA. Invitrogen's RNAi Designer was used for the selection of RNAi target sequences and the design of pre-miRNAs. The most important features of RNAi target sequences are the length of 21 nucleotides, GC contents between 30% and 50% and the absence of more than three same nucleotides in sequence. The top oligo sequence contained a 5'TGCTG sequence, the reverse complement of the 21-nucleotide sense target sequence, the GTTTTGGCCACTGACTGAC terminal loop sequence, followed by the nucleotides 1 – 8 and 11 – 21 (5'→3') of the sense target sequence. The bottom oligo sequence was designed by removing the 5' TGCT from the top oligo sequence, reversing and complementing the resulting sequence and adding the sequence CCTG to the 5' end. Appropriate oligos were ordered from Eurofins MWG Operon (Ebersberg, Germany). Top and bottom oligos were annealed to generate a ds oligo with 4-nucleotide overhangs and cloned into the pcDNA™6.2-GW/EmGFP-miR expression vector according to the manufacturer's instructions (Invitrogen). The presence and correct orientation of the ds oligo was checked by sequencing with the EmGFP forward sequencing primer.

Cloning of GDAP1 and R310Q pIRES constructs

Wild-type and mutant *Gdap1* ORFs were cloned by restriction digest of the pcDNA vectors with the restriction endonucleases *Bam*HI and *Xba*I and ligation of the *Gdap1* fragment with the *Bam*HI/*Xba*I-linearized pSK cloning vector. The *Gdap1* fragments were further cloned from the pSK vector into the pIRES-EGFP vector using the enzymes *Bgl*II and *Sac*II.

2.1.11   *In vivo* experiments

Pharmacological inhibition of xCT in tMCAO-induced rats

Transient middle cerebral artery occlusion (tMCAO) serves as a model for ischemic stroke. Strokes were induced in female Wistar rats by 45 min occlusion, and starting at day 2 after stroke induction, xCT was inhibited permanently in the brain with 400 µM (S)-4-CPG. Intrathecal application of the drug was delivered with osmotic pumps that allow a constant flow of 0.5 µl/h. Animals were sacrificed 6 days after tMCAO, brains were isolated, and sliced into coronal sections to prepare cryoslices in 200 µm intervals. To visualize stroke lesions, slices were histologically stained with cresyl violet. Induction of tMCAO, implantation of the pumps, and preparation and staining of the cryoslices were performed by Sabine Hamm.

To evaluate lesion sizes, the area of the affected region was determined for all slices with the AxioVision program from Zeiss. The volume was given by the sum of the products of respective lesion areas and the distance between analyzed slices, namely 200 µm. The same was done with the areas of entire hemispheres, and lesion sizes were displayed as percentages of ischemic volume to the overall volume of the ipsilateral hemispheres.

Expression analysis in peritoneal macrophages of EAE-induced mice

Experimental autoimmune encephalomyelitis (EAE) is a mouse model of multiple sclerosis. To observe xCT expression during disease progression, EAE was induced in C57BL/6 mice and peritoneal macrophages were isolated after 6 and 15 days. Animal experiments were carried out by Patrick Vollmar who provided peritoneal macrophage cDNA from one animal per treatment, respectively. To induce EAE, 100 µg myelin oligodendrocyte glycoprotein (MOG) 35-55 peptide and 250 µg complete Freud's adjuvant (CFA) were injected subcutaneously into the flanks. In addition, animals received intraperitoneal injections of 200 ng pertussis toxin on day 0 and 2 of EAE induction. Peritoneal macrophages were isolated and directly used for RNA isolation and cDNA synthesis. Quantitative PCR was performed as described above.

2.1.12   Statistical analysis

Data was summarized as mean ± S.E.M. and the statistical significance assessed using two-tailed *t*-tests or analysis of variance (ANOVA) with Bonferroni's or Dunnett's Multiple Comparison Tests with GraphPad Prism 5 software.

3.   Results

3.1   Glutamate toxicity in HT22 cells as a model for oxidative stress

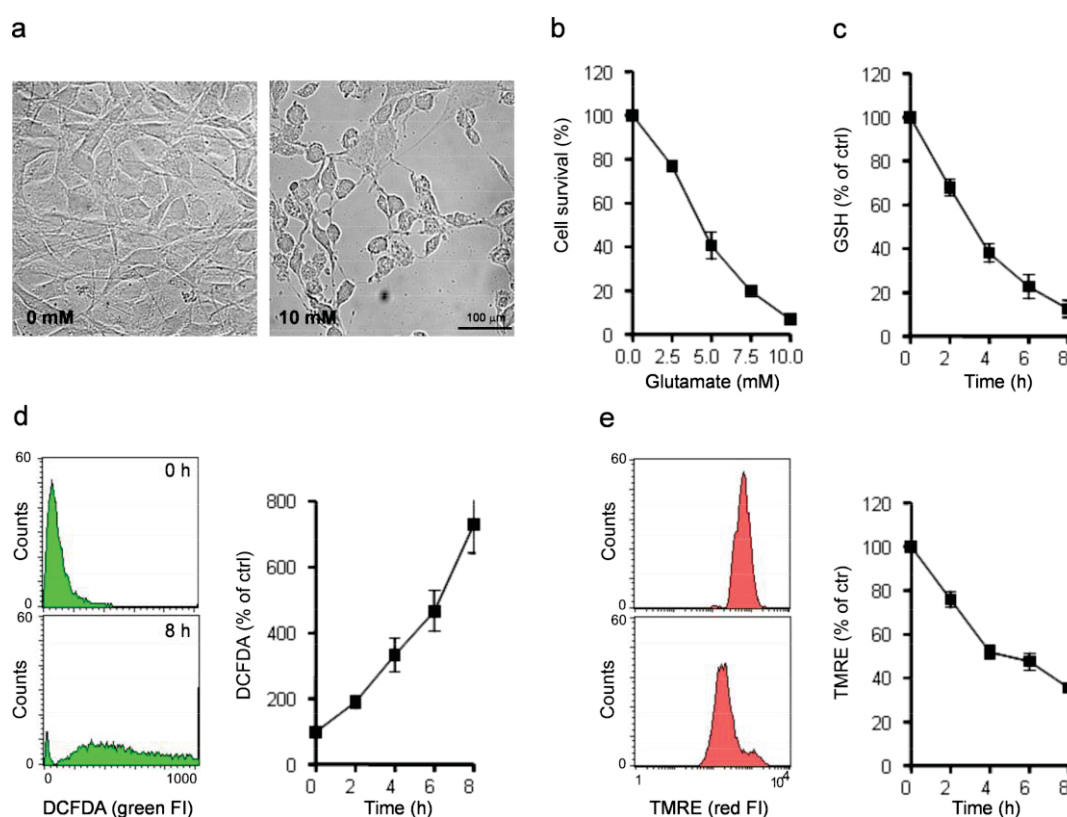### 3.1.1   Oxidative glutamate toxicity in HT22 cells

Applying millimolar concentrations of glutamate to HT22 cells leads to a prolonged cell death by oxidative stress called oxidative glutamate toxicity (Tan, 2001). It is important to repeat that HT22 cells lack ionotropic glutamate receptors. Thus, glutamate toxicity in these cells is not mediated by excitotoxicity but is due to oxidative stress as described before.

To evaluate the model of oxidative glutamate toxicity, HT22 cells were exposed to glutamate that blocks the cystine import by the antiporter system X_c^- and leads to a drop in glutathione levels. HT22 cells died after 12 h exposure to 10 mM glutamate (Fig. 5 a). In a cell viability assay, HT22 cells were seeded into 96-well plates, treated 24 h later with various concentrations of glutamate, and cultured for another day. Cell viability was measured using the MTT assay (Fig. 5 b). 2.5 mM glutamate induced 20% cell death, and more than 50% of cells died at 5 mM glutamate. Complete cell death was achieved by treatment with 10 mM glutamate for 24 h.

In a time course experiment GSH levels of HT22 cells exposed to 10 mM glutamate were measured enzymatically every other hour in a time interval of 8 h (Fig. 5 c). After 2 h of glutamate exposure GSH was decreased to 67.9%, and after 4 h only 37.9% GSH remained. Glutamate exposure led to an almost complete depletion of GSH after 8 h. The GSH decrease followed very much the curve given in the diagram by Tan et al. (2001) and depicted in Fig. 1. Differences in GSH levels may be due to different glutamate concentrations used in this study. The increase of ROS after glutamate exposure was measured with the fluorescent dye H2DCFDA by FACS analysis (Fig. 5 d). In contrast to the findings of Tan and colleagues, the initial linear increase in ROS concentrations was not detected. Instead, ROS levels increased exponentially directly after beginning of glutamate exposure and reached values 7.3 times higher than ROS levels of unchallenged cells. This indicated that the increase of ROS due to

GSH depletion and that due to mitochondrial damage are not such distinct events as proposed by Tan et al. and coincided with the finding that the mitochondrial membrane potential ($\Delta\Psi$m) was impaired quite early after glutamate treatment (Fig. 5 e). $\Delta\Psi$m was measured with the fluorescent dye TMRE. TMRE fluorescence intensity (FI) decreased to 75.8% after 2 h and to 51.8% after 4 h exposure to 10 mM glutamate. After 8 h glutamate exposure, FI values equaled those of cells treated with the ionophore CCCP (data not shown).

Despite the differences between this study and the results of Tan and colleagues, glutamate toxicity in HT22 cells was found to be a very reproducible model to study oxidative stress.

Figure 5 **Glutamate toxicity in HT22 cells is a model for oxidative stress-mediated cell death.** (a) Phase contrast microscopy of HT22 cells after 12 h exposure to vehicle or 10 mM glutamate. (b) HT22 cells die in response to glutamate in a very reproducible manner. 5000 HT22 cells per well were seeded into 96-well plates and grown for 24 h before being exposed to indicated concentrations of glutamate for 24 h. Cell viability was quantified 24 h after glutamate exposition by MTT assay. Data points correspond to means ± S.E.M. of n = 4 independent experiments done in quintuplicates. (c – e) Oxidative glutamate toxicity induces glutathione depletion, increase in ROS and breakdown of the mitochondrial membrane potential. HT22 cells were treated with 10 mM glutamate for indicated time periods. (c) Intracellular GSH concentration was detected by DTNB absorbance after enzymatic reduction of GSH. Results were normalized to protein concentrations and data is represented as means ± S.E.M of two independent experiments done in quadruplicates. (d) Increase in ROS levels after glutamate exposure was detected with DCFDA (10 µM, 20 min). A typical set of histograms showing cell counts versus DCFDA fluorescence intensity (FI) is presented. Quantification of DCFDA FI of n = 3 independent experiments done in duplicate. (e) Mitochondrial membrane potential was assayed by

FACS analysis with TMRE (20 µM, 20 min) and CCCP as positive control to induce a fast breakdown of ∆Ψm. Typical histogram plots and quantification of TMRE FI of n = 2 independent experiments in duplicate shown as means ± S.E.M.

3.1.2 Glutamate resistance and upregulation of several transcripts in glutamate-resistant HT22R cells

Lewerenz et al. (2006) have previously generated a glutamate-resistant HT22 cell line by repeated exposition to glutamate and propagation of the surviving cells. These HT22R cells are resistant to glutamate concentrations as high as 40 mM and are maintained in 10 mM glutamate. xCT, the functional subunit of the cystine/glutamate antiporter system X_c^-, has been found to be up-regulated in HT22R cells (Lewerenz et al., 2006).

To study oxidative glutamate toxicity in both glutamate-sensitive and resistant cell lines, HT22 and HT22R cells were seeded into 96-well plates, treated 24 h later with indicated concentrations of glutamate, and cultured for another day. HT22R cells could withstand high glutamate concentrations. 24 h exposure to 40 mM glutamate resulted in only 50% decrease in cell viability. In contrast, 80% of sensitive HT22 cells died after exposure to 7.5 mM glutamate, and cells were virtually dead at higher glutamate concentrations (Fig. 6 a). GSH and ROS levels were examined in HT22 and HT22R cells. Unchallenged glutamate-resistant HT22R cells contained 1.6 times more GSH than sensitive HT22 cells (Fig. 6 b) indicating that the upregulation of xCT increases the uptake of cystine that is directly used for the synthesis of GSH. Consistent with the increased GSH levels, the concentration of ROS in HT22R cells was 3.4 times lower than in the sensitive HT22 cell line (Fig. 6 c).

It has been assumed that glutamate-resistant HT22R cells have adapted to their high glutamate environment by changing their transcript and protein composition. Indeed, several proteins were found to be upregulated in HT22R cells and to protect against oxidative stress (Dittmer et al., 2008; Lewerenz et al., 2006; Sahin et al., 2006; Toutzaris et al., 2010). In order to find further factors that are involved in the protection against oxidative glutamate toxicity, an Affymetrix assay was conducted. Several transcripts were found to be up-regulated in HT22R cells (Fig. 6 d). The highest increase in transcription level was found for the ionotropic ATP receptor P2X3 that was upregulated almost 700-fold followed by the transcription factor DACHSHUND2 and GDAP1 with more than 100-fold and about 45-fold up-regulation in HT22R cells, respectively. xCT had already been shown by Northern blot analysis to be higher expressed in HT22R cells (Lewerenz et al., 2006), a finding that could be confirmed by the Affymetrix assay. It was assumed that the proteins upregulated in the resistant cell line play a role in the protection against oxidative glutamate toxicity. Therefore, selected transcripts, namely xCT, P2X3, and GDAP1, and their influence on oxidative glutamate toxicity and other cellular functions were examined in this study.
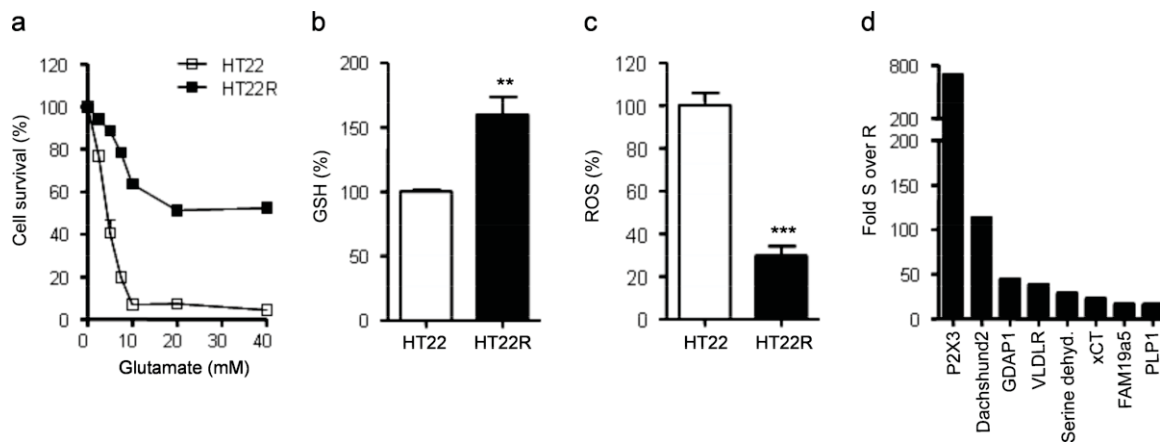
Figure 6 HT22R cells are resistant to oxidative glutamate toxicity and differ from glutamate-sensitive HT22 cells in their transcriptome. (a) HT22R cells can withstand high glutamate concentrations. Cell viability was assayed with MTT 24 h after exposure to indicated glutamate concentrations in four independent experiments. (b) Increased glutathione content in HT22R cells was measured enzymatically in three independent experiments done in duplicate. (c) FACS analysis with DCFDA revealed a significantly reduced ROS content in HT22R cells. Results are from two independent experiments in triplicate. (a - c) Data are shown as means ± S.E.M. ** *P*<0.005, *** *P*<0.0001 as determined by unpaired student's t-test. (d) Transcriptional changes in HT22R cells were analyzed by an Affymetrix array.

3.2   xCT

3.2.1   xCT is upregulated in HT22R cells and protects against oxidative glutamate toxicity

The upregulation of xCT in HT22R cells was reproduced by quantitative RT-PCR (Fig. 7 a). Here, xCT was found to be upregulated about 18-fold, a finding quite consistent with the Affymetrix array analysis, where the xCT transcript was found to be 23-times more abundant in HT22R cells. xCT was also upregulated in glutamate-sensitive HT22 cells after short-time exposure to glutamate (Fig. 7 b). After 24 h exposure to 1 mM and 2.5 mM glutamate, xCT was upregulated 1.9-fold and 2.2-fold, respectively.

When xCT was transiently overexpressed in glutamate-sensitive HT22 cells, these cells were protected against glutamate toxicity (Fig. 7 c). xCT-transfected HT22 cells survived by 95.0% and 48.2% when treated with 2.5 mM or 20 mM glutamate and thus resembled protection rates of glutamate-resistant HT22R cells. At 10 mM glutamate, all control-transfected cells were dead, whereas 84% of xCT-transfected cells survived. These results indicated the crucial role of xCT in the protection against oxidative glutamate toxicity.
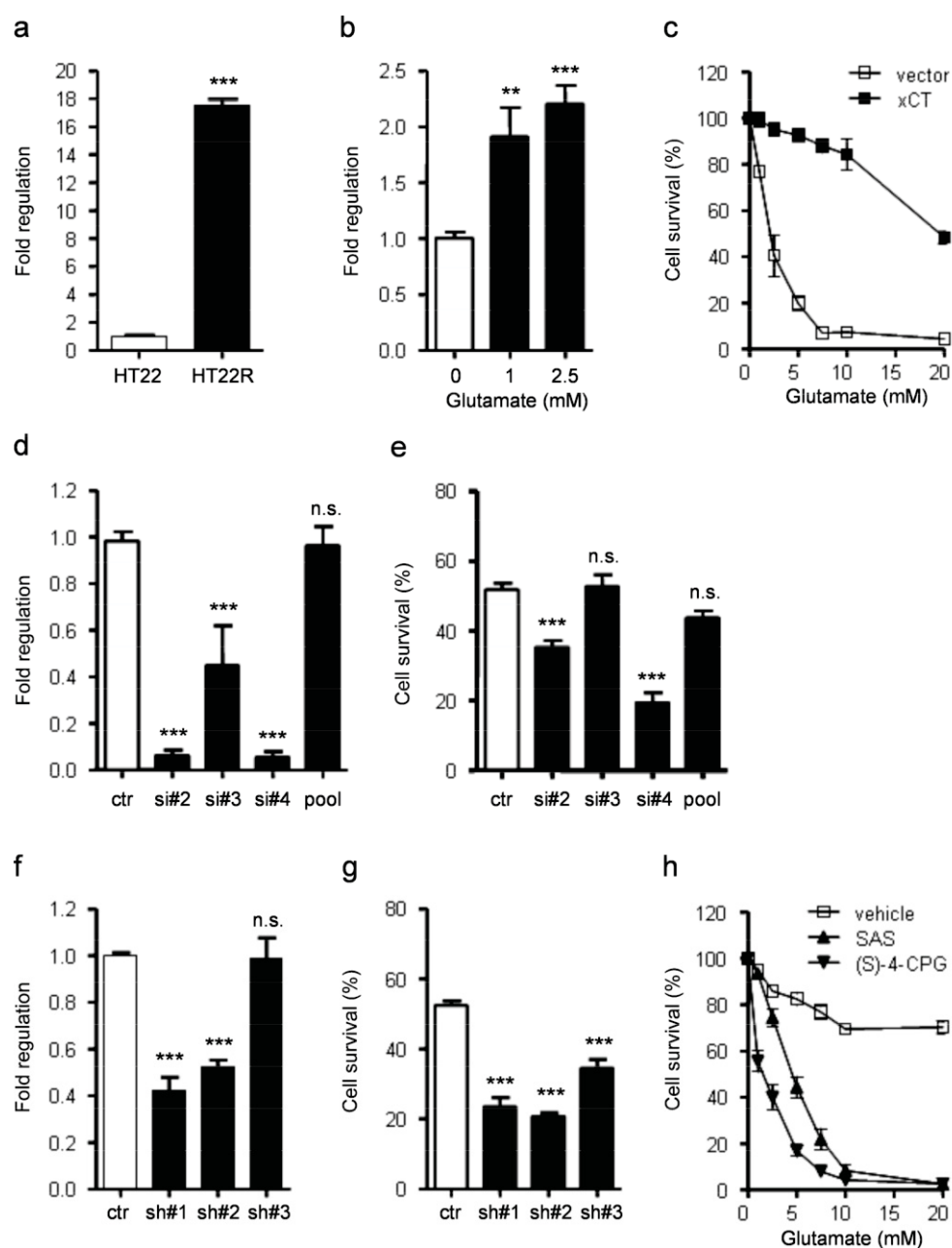
Figure 7 **xCT is upregulated in HT22R cells and protects from oxidative glutamate toxicity.** Quantification of xCT mRNA by real-time RT-PCR and normalization to the housekeeping gene GAPDH and cell viability determined by MTT assay. (a) Upregulation of xCT in HT22R cells. Results from two independent experiments are shown as means ± S.E.M. *** $P<0.0001$ compared with HT22 cells by unpaired student's t-test. (b) xCT upregulation after short-term exposure of glutamate-sensitive HT22 cells to glutamate. Total RNA was isolated after 24 h exposure to 1 mM and 2.5 mM glutamate. Data is shown as means ± S.E.M. from two independent experiments in triplicates. ** $P<0.005$, *** $P<0.0001$ compared with untreated HT22 cells by one-way ANOVA (Dunnett's multiple comparison test). (c) xCT overexpression protects sensitive HT22 cells from glutamate toxicity. HT22 cells were transiently transfected with xCT and treated for 24 h with indicated concentrations of glutamate (n = 10). (d, f) xCT mRNA can be downregulated with different siRNAs

and shRNA constructs. (d) HT22R cells were transfected with 100 pmol of three different siRNAs and a pool of four siRNAs directed against xCT as well as with non-targeting siRNA, respectively (n = 6), and (f) with three different shRNA vector constructs (n = 12). xCT mRNA was quantified 48 h later by real-time RT-PCR. (e) Two siRNAs and (g) all shRNA constructs can abrogate the protection of HT22R cells from glutamate toxicity. Cells were exposed to glutamate 48 h after transfection and cell viability was assayed 24 h later. Bars represent cell viability at 40 mM glutamate as means ± S.E.M. of (e) two or (g) six independent experiments in quintuplicate. (h) Pharmacological inhibition of xCT with SAS and (S)-4-CPG abolishes glutamate resistance of HT22R cells. HT22R cells were exposed to glutamate and to 50 μM SAS or 25 μM (S)-4-CPG, respectively, for 24 h. Data as means ± S.E.M. (n = 3). (d, e, f, g) Data represent means ± S.E.M. *** *P*<0.0001 compared with HT22 cells transfected with control siRNA or empty vector by one-way ANOVA (Dunnett's).

To evaluate the role of xCT for the glutamate-resistance of HT22R cells, siRNAs and vector-encoding small hairpin RNAs (shRNAs) were used to knockdown xCT. siRNAs si#2, si#3 and si#4 were able to reduce xCT transcript abundance 16.3-fold, 2.2-fold and 18.6-fold, respectively, whereas a pool of four xCT-directed siRNAs did not significantly reduce xCT expression (Fig. 7 d). Cell survival of siRNA-transfected HT22R cells was analyzed by CTB assay (Fig. 7 e). siRNAs si#2 and si#4 significantly reduced the glutamate resistance of HT22R cells, which was consistent with their efficiency to knockdown xCT. The cell survival of HT22R cells transfected with si#2 and si#4 and exposed to 40 mM glutamate was reduced to 78.5% and 58.0% compared to cells transfected with a non-targeting siRNA, respectively, while si#3 and the siRNA pool did not alter cell survival.

Moreover, two of three shRNAs were able to decrease xCT transcript abundance (Fig. 7 f). Expression of xCT was reduced 2.4-fold compared to control when transfected with vector encoding shRNA sh#1, and 1.9-fold with sh#2. xCT expression was not altered with sh#3. All applied xCT-directed shRNAs were able to reduce cell survival of HT22R cells treated with 40 mM glutamate (Fig. 7 g). However, the decrease in cell survival was most prominent with sh#1 and sh#2, which also showed the best knockdown efficiencies.

(S)-4-carboxyphenylglycine ((S)-4-CPG) and sulfasalazine (SAS) are specific inhibitors of xCT (Gout et al., 2001; Patel et al., 2004). As for the knockdown of xCT it was supposed that pharmacological xCT inhibition abolishes the glutamate resistance of HT22R cells. Therefore, HT22R cells were treated with 25 μM (S)-4-CPG) or 50 μM SAS, concentrations that did not impair cell survival, exposed to various concentrations of glutamate, and cell survival was measured with CTB. Treatment with both inhibitors resulted in a considerable reduction of HT22R cell survival (Fig. 7 h). At 10 mM glutamate, both xCT inhibitors reduced the cell survival to less than 10%, whereas almost 70% of vehicle-treated cells survived.

In summary, both, xCT knockdown and inhibition partly abolished the resistance of HT22R cells against glutamate stress.

3.2.2   xCT protects from oxidative stress by supplying cystine for GSH synthesis

Glutathione concentrations were measured in xCT-overexpressing cells (Fig. 8 a). As in HT22R cells, GSH levels were increased in glutamate-sensitive xCT-transfected HT22 cells. Moreover, decreasing xCT activity in HT22R by either xCT knockdown or inhibition resulted in reduced GSH levels. Treatment of HT22R with 50 μM SAS or 25 μM (S)-4-CPG led to 27.9% or 44.6% reduction of the GSH concentration compared to unchallenged cells (Fig. 8 b), and knockdown of xCT with shRNAs sh#1 and sh#2 reduced GSH levels to 84.7% and 93.8%, respectively (Fig. 8 c).
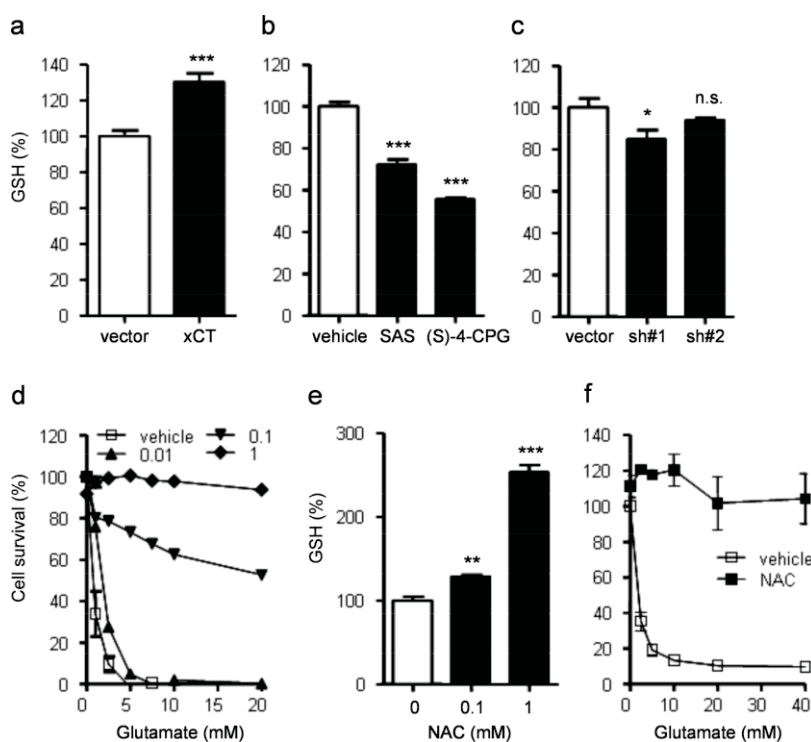
Figure 8 **xCT protects from oxidative glutamate toxicity by elevating glutathione levels.** Intracellular GSH levels and cell viability were determined 48 h after cell transfection or 24 h after treatment with xCT inhibitors or cysteine precursor NAC. (a) Increased GSH levels in xCT-overexpressing HT22 cells. Data from four independent experiments in triplicate are shown as means ± S.E.M. (*** $P<0.0001$, unpaired student's t-test). Both, (b) pharmacological inhibition of xCT with 50 μM SAS and 25 μM (S)-4-CPG and (c) xCT knockdown with vector-expressed shRNA, reduced GSH levels in glutamate-resistant HT22R cells. (d) Treatment with GSH-precursor NAC protects sensitive HT22 cells from glutamate-mediated cell death. HT22 cells were exposed to glutamate and 0.01 mM, 0.1 mM and 1 mM NAC for 24 h before cell viability was assayed by MTT assays in two independent experiments in quintuplicates. (e) NAC exposure significantly increased GSH levels in HT22 cells. HT22 cells were exposed to indicated concentrations of NAC, and intracellular GSH was measured enzymatically in four independent experiments in duplicate. (f) NAC-mediated increase in GSH levels is not detracted by induction of glutamate stress. HT22 cells were exposed to indicated glutamate concentrations and 1 mM NAC in three independent experiments in duplicate. (b, c, e) * $P<0.05$, ** $P<0.005$, *** $P<0.0001$ compared with vehicle-treated or empty vector-transfected cells by one-way ANOVA (Dunnett's).

N-acetyl-L-cysteine (NAC) is a synthetic precursor of cysteine and therefore used to maintain intracellular glutathione independently of cystine import and thus independently of the action of X_c^-. Treatment with 0.1 mM NAC partly and with 1 mM NAC completely protected HT22 cells against glutamate-induced cell death, even at 20 mM glutamate (Fig. 8 d). This protection could be traced back to increased GSH concentrations. HT22 cells incubated with 0.1 mM and 1 mM NAC contained 1.3-fold, respective 2.5-fold more GSH than control cells (Fig. 8 e). Moreover, elevated GSH levels were maintained by exposure to 1 mM NAC even at high glutamate concentrations (Fig. 8 f).

3.2.3   The role of xCT in neurite outgrowth

Increased activity of the antiporter system X_c^- leads to elevated concentrations of extracellular glutamate whose removal requires the action of glutamate transporters (Lewerenz et al., 2006). It has been shown that glutamate influences neurite outgrowth of neurons in culture (Berdan and Easaw, 1992). In addition, Pearce et al. have shown that neurite outgrowth is inhibited by enzymatic removal of glutamate and by NMDA class glutamate receptor inhibition indicating that glutamate stimulates neurite outgrowth through the activation of NMDA receptors (Pearce et al., 1987). Moreover, increased expression of EAAT transporters were reported during the differentiation of cultured astrocytes (Eng et al., 1997; Tawfik et al., 2006) and other cell types (Mordrelle et al., 2000; Pignataro et al., 2003). Given the cooperative action of X_c^- and glutamate transporters, it was of interest whether xCT plays a role in neurite outgrowth. To test this hypothesis, neuroblastoma N2a cells were transfected with either xCT or vectors encoding xCT-directed shRNAs, and cell differentiation was induced by exposure to 1 µM retinoic acid (RA) and withdrawal of FCS. After 7 days differentiation, neurite outgrowth was examined. Therefore, six cell categories were defined according to the dendrite length: cells without dendrites, cells with dendrites of the size of the cell body, and with dendrites of approximately 25 nm, 50 nm, 100 nm, and larger than 125 nm. Overexpression of xCT did not influence neurite outgrowth (Fig. 9). Also, the number of cells with dendrites was neither affected by xCT overexpression nor by xCT knockdown. However, an increased number of cells exhibited very small dendrites with lengths not exceeding the size of the cell body when xCT was knocked down with shRNAs, especially with sh#2 (Fig. 9 a), and fewer cells with larger dendrites were observed (Fig. 9 b). From these results it was concluded that inhibition of xCT activity impairs neurite outgrowth and that xCT may be involved in neuronal cell differentiation. xCT has been shown to play a role in differentiation of other cell types, and D'Angelo et al. recently reported xCT-mediated differentiation in dendritic cells (D'Angelo et al., 2010).
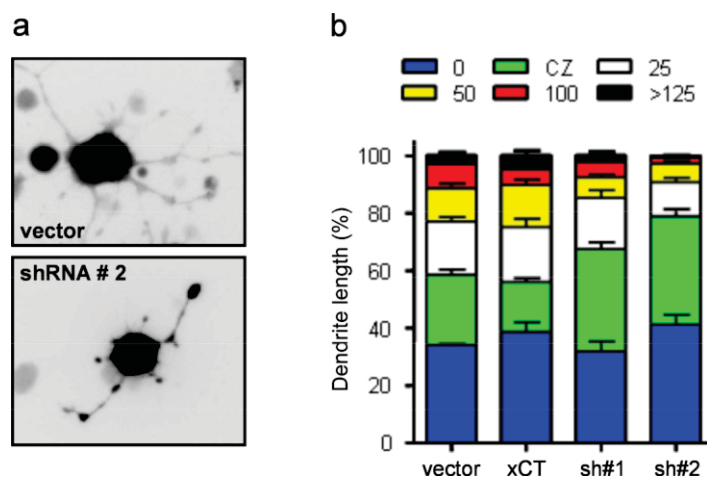
Figure 9 **Role of xCT in dendrite outgrowth.** xCT inhibition interferes with RA-induced dendritic growth. N2a cells were transfected with xCT or vectors encoding xCT-directed shRNAs before differentiation was induced by FCS privation and treatment with 1 µM RA. After 7 days differentiation, cells were categorized according to the length of their dendrites. (a) Light microscopy and (b) quantification show that xCT knockdown results in increased numbers of cells with short dendrites. Bars represent results from three independent experiments. At least 100 cells were counted per condition (CZ: dendrites with lengths not exceeding cell body size, numbers in nm).

3.2.4 The role of X_c^- in models of inflammation and ischemic stroke

Another set of preliminary experiments aimed at the analysis of the role of X_c^- during inflammation. Activated macrophages release large amounts of glutamate and thereby induce neuronal cell death by excitotoxicity. Moreover, it has been shown that this glutamate release is due to the action of X_c^- (Barger et al., 2007; Piani and Fontana, 1994; Sato et al., 2001; Watanabe and Bannai, 1987). In addition, it has been shown that X_c^- mediates microglial toxicity and thereby causes excitotoxic oligodendrocyte cell death, progressive oligodendrocyte loss, and demyelination in disorders like multiple sclerosis (Domercq et al., 2007). Therefore, xCT expression was analyzed in dependence of macrophage activation. To this end, BV2 microglia cells were stimulated with 10 ng/ml lipopoysaccharides (LPS), and xCT expression levels were analyzed in a 72 h time course (Fig. 10 a). 24 h after activation by LPS, BV2 microglia expressed 4.3 times more xCT than untreated cells, and 10.2 times more after 36 h. At 48 h, when xCT transcript levels decreased, medium was exchanged with fresh LPS-containing medium. Following this treatment, xCT expression in activated BV2 cells was found to be increased 12.8-fold after 60 h and 17.5-fold after 72 h but was not altered in nonactivated cells.

To examine the role of X_c^- during inflammatory processes *in vivo*, xCT expression was analyzed in peritoneal macrophages in C57BL/6 mice in that experimental autoimmune encephalomyelitis (EAE), a mouse model of multiple sclerosis, was induced. Peritoneal

macrophages were isolated at day 6 and day 15 of EAE, thus before and after onset of disease, which typically occurs at day 11 or 12 after EAE induction, and from control mice that were treated with CFA only. Peritoneal macrophage cDNAs were a kind gift of Patrick Vollmar. Quantitative RT-PCR revealed 2.8-fold and 3.4-fold increases of xCT expression at day 6 and day 15, respectively (Fig. 10 b). Thus, xCT expression is induced in peritoneal macrophages before the onset of disease and even increases at the first peak of EAE, when clinical symptoms are fully developed. In summary, upon activation, macrophages induce xCT expression both *in vitro* and *in vivo*.
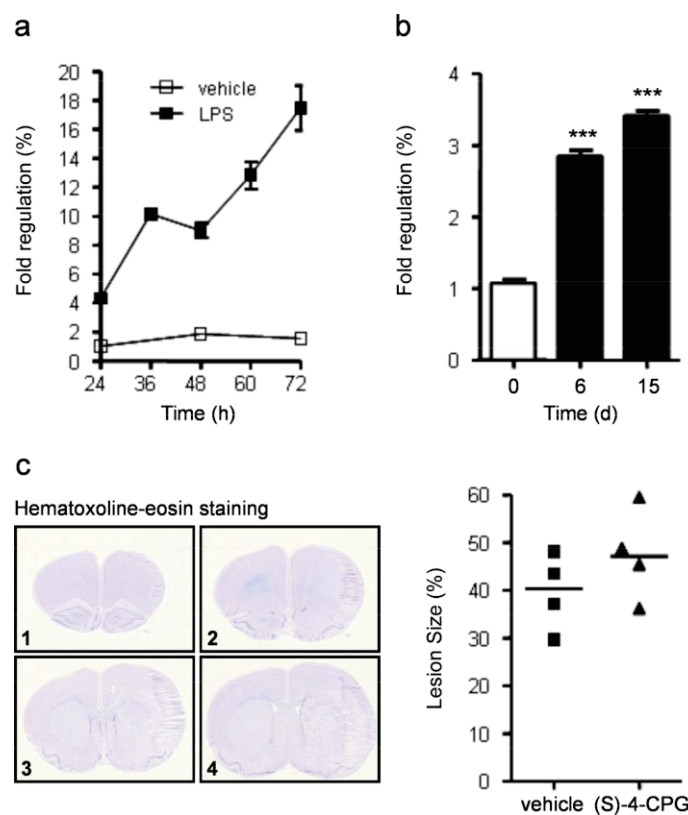
Figure 10 **Role of xCT in inflammation and ischemic stroke.** (a) Increased expression of xCT after LPS-induced activation of BV2 cells as quantified by real-time RT-PCR. BV2 cells were activated with 10 ng/ml LPS 24 h and 72 h after seeding, and RNA was isolated at indicated time points. Data represent means ± S.E.M. from two independent experiments in triplicates. (b) Upregulation of xCT in peritoneal macrophages after EAE induction. cDNAs from peritoneal macrophages were obtained from Patrick Vollmar. Mice were treated with CFA and MOG to induce EAE (black bars) or with CFA only (control, white bar), and peritoneal macrophages were isolated at indicated time points. Quantitative real-time RT-PCR was carried out once in triplicate with samples from one animal per treatment and time point. Data represent means ± S.E.M. *** $P<0.0001$ compared to CFA only control by one-way ANOVA (Dunnett's). (c) Stroke lesions in rat brains after induction of ischemic stroke by tMCAO and pharmacological inhibition of xCT by (S)-4-CPG. Typical coronal slices from anterior to posterior positions (1 - 4, left panel). Quantification of lesion sizes (right panel) reveals that rats treated with (S)-4-CPG developed enlarged stroke lesions. Dots indicate lesion sizes of single animals from two independent experiments with two animals per treatment used for quantification. Results are not significant.

Another neurological condition, in which high glutamate concentrations cause neurotoxicity, is ischemic stroke. To analyze the role of X_c^- in the glutamate release and neurotoxicity in conditions of ischemic stroke, transient middle cerebral artery occlusion was induced in Wistar rats followed by X_c^- inhibition with (S)-4-CPG. Two days after stroke induction, xCT was inhibited with (S)-4-CPG by continuous application to the brain with the help of osmotic pumps. 400 µM (S)-4-CPG were used, a concentration that has been shown to successfully inhibit xCT in rat brains (Savaskan et al., 2008). After four days, rats were sacrificed, and cryoslices of whole brains were prepared. Cryoslices were stained with cresyl violet, and lesion volumes were determined. In Figure 10 c (left panel), typical coronal slices from anterior (1) to posterior (4) positions are depicted.

It was assumed that, also in ischemic stroke, high extracellular glutamate concentrations are due to glutamate release by macrophages. Therefore, the hypothesis was that xCT inhibition protects against excitotoxicity and thus against ischemic lesions. However, mice treated with (S)-4-CPG developed lesions covering 47.5% of the ischemic hemisphere, whereas lesions in vehicle-treated animals affected 39.6% (Fig. 10 c, right panel). Only two independent experiments were performed, each with only two animals that could be used for analysis. Therefore, the result was not statistically significant. Nevertheless, xCT inhibition caused a 20% increase in volume of ischemic lesions. From these result it could be concluded that the high glutamate concentrations during stroke are not derived by the activation of macrophages, or that X_c^- is not the key player in the release of glutamate. On the other hand, X_c^- could play a dual role as neurons might require the activity of X_c^- for GSH synthesis in order to cope with the high concentration of glutamate and other inducers of oxidative stress.

3.3   P2X3

3.3.1   P2X3 is up-regulated in glutamate-resistant HT22R cells but does not protect from glutamate toxicity

The Affymetrix chip analysis has revealed a ~692-fold upregulation of P2X3 in HT22R cells. To confirm this result, P2X3 transcript levels were quantified by real-time RT-PCR, which showed that P2X3 expression in HT22R cells was 30-fold stronger than in sensitive HT22 cells (Fig. 11 a). The difference in the rate of upregulation may be due to the different methods. P2X3 expression was not altered when glutamate-sensitive HT22 cells were exposed to glutamate for 24 h (Fig. 11 b).

To determine whether P2X3 protects against oxidative glutamate toxicity, glutamate-sensitive HT22 cells were transfected with P2X3, exposed to glutamate, and cell viability was measured 24 h later. P2X3 overexpression did not protect glutamate-sensitive HT22 against glutamate-induced cell death (Fig. 11 c). To analyze its role in the resistance of HT22R cells, P2X3 was inhibited with A-317491, a non-nucleotide that has been described to be a selective antagonist of P2X3 and P2X2/3 receptors without effecting other neurotransmitter receptors, ion channels or enzymes (Jarvis et al., 2002). Therefore, HT22R cells were exposed to glutamate and 0.1 μM or 1 μM A-317491 for 24 h. Cell viability assays revealed that inhibition of P2X3 did not alter the protection of HT22R cells against glutamate toxicity (Fig. 11 d). It remained unclear, why P2X3, despite its enormous upregulation in HT22R cells, had no anti-oxidative function.

As ionotropic ATP channels often form heterooligomers, one hypothesis was that P2X3 needs to be co-expressed with a second P2X receptor. Torres et al. (1999) examined the interactions among P2X family members by co-immunoprecipitation and showed that P2X3 forms heterooligomers with P2X1, P2X2 and P2X5, but not with P2X4, P2X6 and P2X7. Therefore, the expression of the other P2X receptors was analyzed by quantitative RT-PCR. In addition to P2X3, the receptors P2X2 and P2X7 were found to be upregulated in HT22R cells. P2X4 expression was equal in HT22 and HT22R cells whereas expression of P2X5 was slightly lower in HT22R cells (Fig. 11 e). P2X1 and P2X6 expression could not be analyzed because quantitative PCR with three primer pairs for P2X1 and P2X6 could not amplify the respective cDNA indicating that P2X1 and P2X6 might be not expressed in HT22 cells.

If P2X3 was protective as a heterooligomer with P2X2, inhibition with A-317491 would have decreased the cell viability of HT22R cells, since A-317491 is also a specific inhibitor of P2X2/3 receptor activity. Thus, the upregulation of P2X3 might fulfill another purpose for glutamate-resistant cells.

3.3.2   P2X7 is up-regulated in HT22R cells and after glutamate treatment

P2X7 expression was ~43 times higher in HT22R cells than in HT22 cells as determined by RT-PCR (Fig. 11 e). Moreover, when HT22 cells were exposed to glutamate for 24 h, P2X7 but not P2X3 expression increased in a concentration-dependent manner (Fig. 11 b, f). P2X7 is not able to form hetero-oligomeric assemblies (Torres et al., 1999). Its putative role in the defense against oxidative glutamate toxicity could therefore be analyzed by specific inhibition. A-438079 is a competitive blocker of P2X7 with a higher selectivity than other P2X7 antagonists and little or no effect on other P2X receptors, other cell-surface receptors or ion channels (Donnelly-Roberts and Jarvis, 2007). However, inhibition with A-438079 did not alter the glutamate-resistant phenotype of HT22R cells (Fig. 11 g).

Although P2X3 and P2X7 were upregulated significantly in HT22R cells, there was no indication for their involvement in the defense against oxidative glutamate toxicity. Since our group is interested in protection against oxidative stress, the role of P2X receptors in HT22R cells was not further investigated.
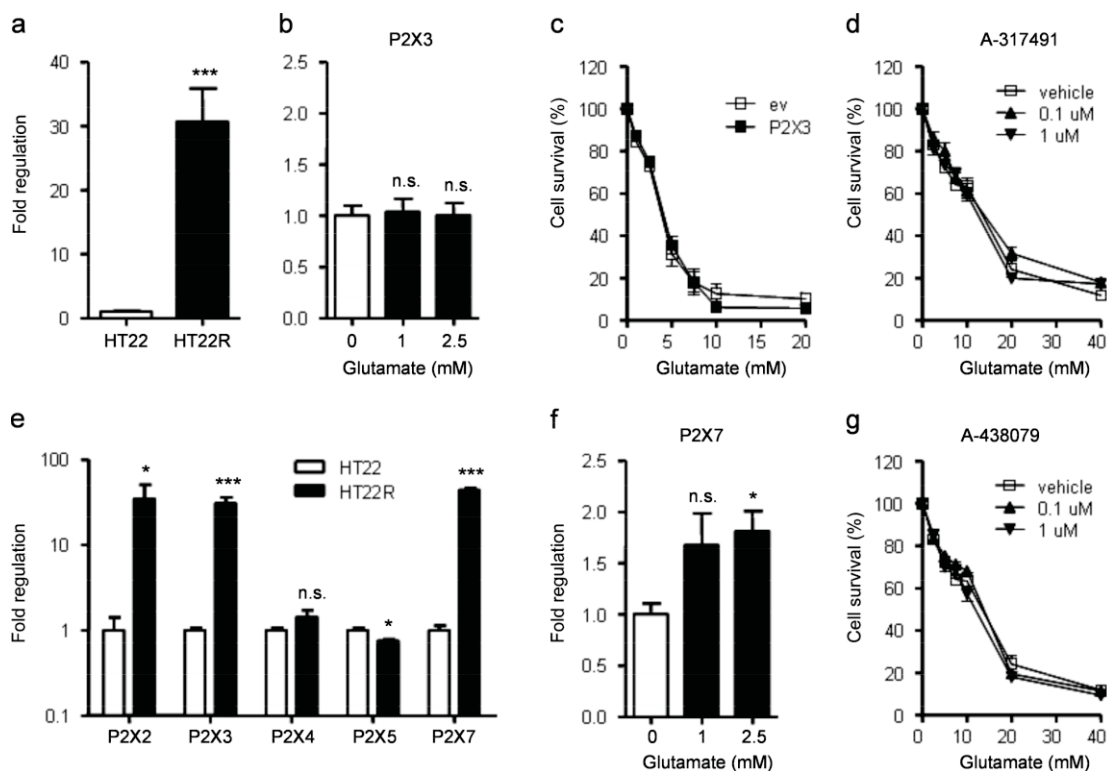
Figure 11 **P2X3 is up-regulated in HT22R cells but does not confer protection from glutamate toxicity.** (a) P2X3 mRNA is upregulated in HT22R cells, (b) but not in glutamate-exposed HT22 cells. Quantitative RT-PCR and normalization to housekeeping gene GAPDH. Data of three independent experiments in triplicate is shown as mean ± S.E.M. *** $P<0.0001$ ((a) unpaired student's t-test, (b) one-way ANOVA, Dunnett's). (c) Overexpression of P2X3 in HT22 cells or (d) P2X3 inhibition in HT22R cells do not alter susceptibility of cells to glutamate. Cell viability was measured with CTB 48 h after transfection or 24 h after exposure to 0.1 μM or 1 μM of the specific P2X3 inhibitor A-317491 in two independent experiments in quintuplicates. (e) The P2X receptor family members P2X2, P2X3 and P2X7 are significantly upregulated in glutamate-resistant HT22R cells as quantified by real-time RT-PCR. * $P<0.05$, *** $P<0.0001$ compared to glutamate sensitive cells by unpaired student's t-test (n = 2 except for P2X3, P2X7: n = 3). (b, f) P2X7 but not P2X3 is upregulated after glutamate exposure. HT22 cells were exposed to 1 mM or 2.5 mM glutamate for 24 h, and P2X3 and P2X7 mRNA was quantified by real-time RT-PCR in two independent experiments in triplicates. * $P<0.05$ (one-way ANOVA, Dunnett's). (g) Inhibition of P2X7 with 0.1 μM or 1 μM of the specific P2X7 inhibitor A-438079 does not reduce protection of HT22R cells against glutamate toxicity. Cell viability was measured in two independent experiments in quintuplicates.

3.4   GDAP1

3.4.1   GDAP1 is upregulated in HT22R cells and protects against oxidative glutamate toxicity

The upregulation of GDAP1 in HT22R cells shown by the Affymetrix array was reproduced both, on mRNA and protein level. On the transcript level, *Gdap1* was found to be upregulated ~15-fold as quantified by real-time RT-PCR (Fig. 12 a). Protein lysates from HT22 and HT22R cells were analyzed by Western blotting using an anti-GDAP1 antibody directed against amino acids 1 to 14 that was provided by Axel Niemann (ETH Zurich, Switzerland). Several bands were observed in lysates from HT22 and HT22R cells as well as in the mouse brain protein lysate that served as a control (Fig. 12 b). Two bands, one running above 60 kDa and one at ~40 kDa showed different patterns. The predicted molecular weight of GDAP1 is 41.5 kDa. The respective band at 40 kDa was quite faint, but stronger in HT22R cell lysates. Since the upper band was much more abundant in HT22R lysates it might be specific and correspond to a splice isoform of GDAP1. From these results it was concluded that GDAP1 is upregulated in HT22R cells on transcript and protein level.

The molecular function of GDAP1 is not yet known. Since it was upregulated in cells resistant to oxidative glutamate toxicity, it was interesting to know whether GDAP1 plays a role in the defense against oxidative stress. Therefore, HT22 cells were transiently transfected with *Gdap1* and exposed to glutamate for 24 h. Cell viability assays demonstrated that GDAP1 prominently protected HT22 cells against glutamate toxicity (Fig. 12 c). At 2.5 mM glutamate, cell viability of control cells was reduced to ~20% whereas ~80% of GDAP1-overexpressing cells survived. Control cells died at glutamate concentrations higher than 5 mM, a concentration, at which cell survival of GDAP1-overexpressing cells was only reduced to ~40%. Even at high glutamate concentration like 20 mM more than 30% of GDAP1-overexpressing cells were still alive. When sensitive HT22 cells were exposed to low concentrations of glutamate for 24 h, GDAP1 expression increased in surviving cells as quantified by real-time RT-PCR (Fig. 12 d). Supposedly, HT22 cells modulate their transcription levels towards factors that help tolerating glutamate toxicity and GDAP1 is one of these protecting factors.

A knockdown approach was applied to study the role of GDAP1 in the glutamate resistance of HT22R cells. To this end, vectors encoding three different *Gdap1*-directed shRNAs were generated and transfected into HT22R cells. The knockdown efficiency was analyzed by quantitative RT-PCR. shRNAs sh#1 and sh#2 reduced *Gdap1* expression to 39% and 28% of control levels, respectively, whereas sh#3 reduced transcript abundance by only 34% (Fig. 12 e). Due to the variability of *Gdap1* mRNA expression in control cells observed in different experiments, the results were not significant. Cell viability assays revealed that the two *Gdap1*-

directed shRNAs sh#1 and sh#3 significantly reduced cell survival of HT22R cells in the presence of 40 mM glutamate (Fig. 12 f). Despite its high knockdown efficiency, sh#2 could not reduce the resistance of HT22R cells against glutamate and was not used for further experiments. From these results it was concluded that GDAP1 protects against oxidative glutamate toxicity and partly accounts for the resistant phenotype of HT22R cells.
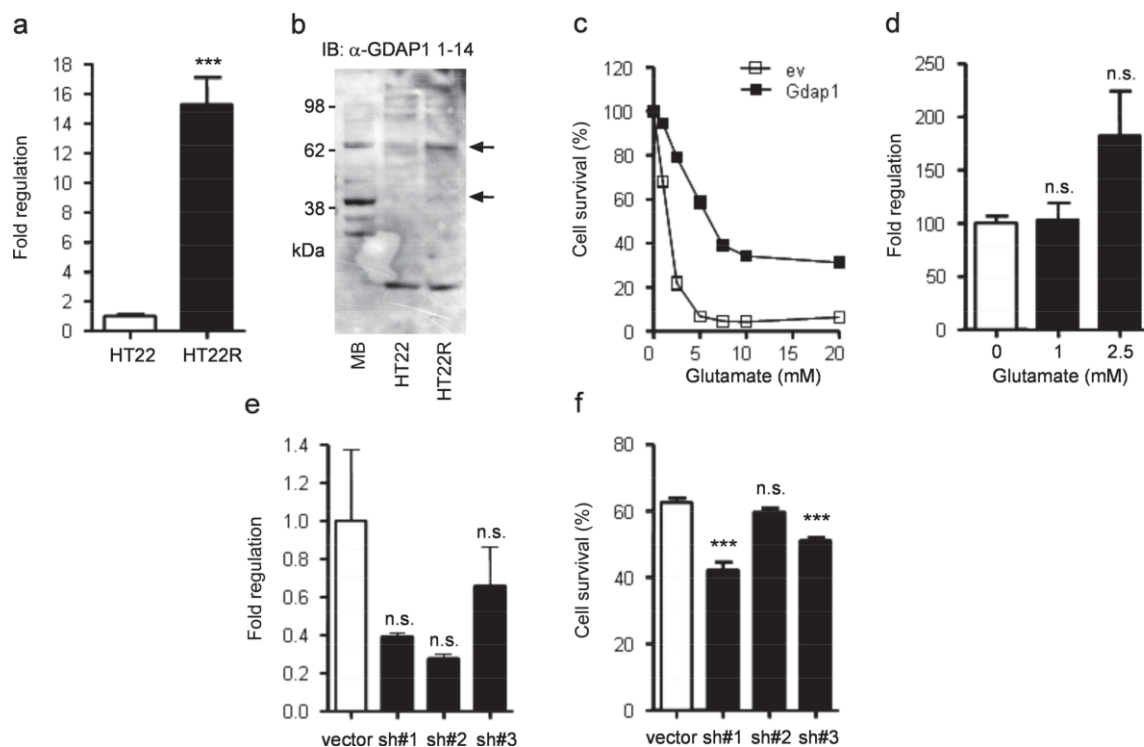
Figure 12 **GDAP1 is upregulated in glutamate-resistant HT22 cells and protects against glutamate toxicity.** (a) *Gdap1* mRNA is increased in HT22R cells as quantified by real-time RT-PCR and normalized to the expression of housekeeping gene *Gapdh*. Data is shown as mean ± S.E.M. Asterisks indicate *P*<0.005 as determined by unpaired student's t-test for two independent experiments in triplicates. (b) Immunoblot with protein lysates from HT22 and HT22R cells and mouse brain (MB) as positive control probed with antiserum against GDAP1 shows up-regulation of two distinct bands (arrows). Equal protein amounts were applied per lane. Molecular mass standards are indicated. (c) GDAP1 protects against oxidative glutamate toxicity. HT22 cells were transiently transfected with *Gdap1* and exposed to glutamate 48 h later. Cell viability was assayed by CTB assay. Data are presented as mean ± S.E.M. from ten independent experiments in quintuplicates. (d) *Gdap1* mRNA is upregulated in HT22 cells exposed to glutamate for 24 h as determined by real-time RT-PCR with *Gapdh* as endogenous control. Data are from three independent experiments done in triplicate. (e, f) HT22R cells were transiently transfected with shRNA constructs directed against *Gdap1* or control and (e) *Gdap1* mRNA abundance was quantified 48 h post-transfection by real-time RT-PCR in two independent experiments in triplicates. (f) Cell viability was quantified by CTB assay in two independent experiments in quintuplicates. (d – f) Data points correspond to means ± S.E.M. (*** *P*<0.0001, one-way ANOVA, Dunnett's).

3.4.2   GDAP1 induces mitochondrial fragmentation in HT22 cells

Overexpression of GDAP1 in COS-7 cells induces fragmentation of mitochondria (Niemann et al., 2005; Pedrola et al., 2008). Mitochondrial fragmentation is a key event in apoptosis (Lee et al., 2004). However, GDAP1 overexpression in COS-7 cells did not induce apoptosis and did not affect mitochondrial activity (Niemann et al., 2005). Since GDAP1-induced mitochondrial fragmentation has been shown only for COS-7 cells, the next set of experiments aimed at the analysis of mitochondrial morphology in HT22 cells transfected with *GDAP1*. To this means, HT22 cells were co-transfected with *GDAP1* and a mitochondria-targeted GFP (mitoGFP). Similar to the approach of Niemann et al., four mitochondrial morphologies were defined: tubular, vesicular, and fragmented mitochondria as well as mixed architectures comprising tubular and vesicular mitochondria (Fig. 13 a). Most control cells consisted of mixed mitochondrial architectures followed by cells with either tubular or vesicular mitochondria and only few cells with fragmented mitochondria. In contrast, GDAP1-overexpressing cells exhibited increased formations of vesicular and fragmented mitochondria at the expense of mixed and tubular forms (Fig. 13 b). Aggregated mitochondria, very dense accumulations of mitochondria at the nucleus, as described by Niemann et al. were not observed.
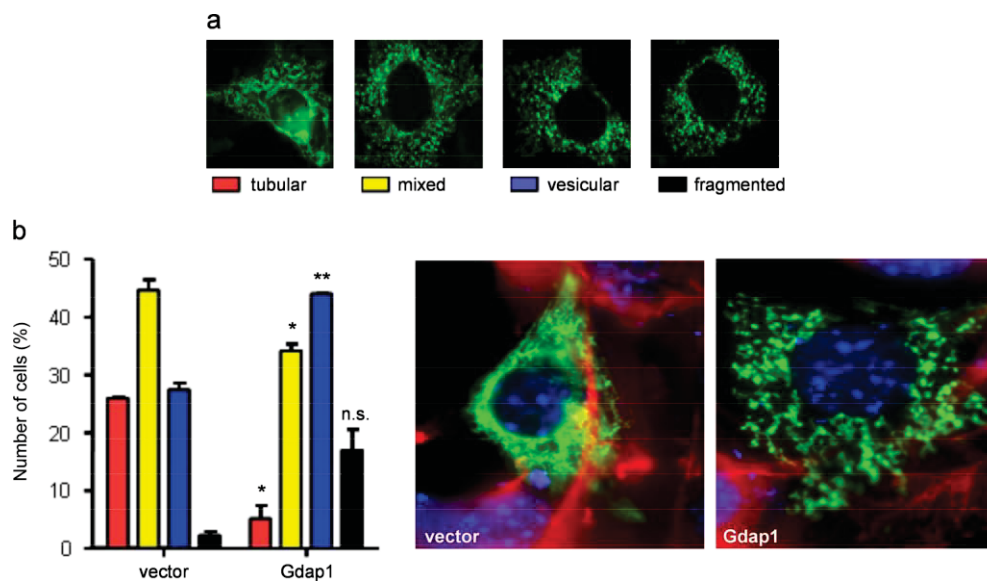
Figure 13 **GDAP1 induces mitochondrial fragmentation in HT22 cells.** (a) Mitochondrial morphology was quantified by classifying the appearance of mitochondria. Representative images of tubular, mixed, vesicular and fragmented mitochondria are shown. (b) Typical fluorescent images of control and GDAP1-overexpressing HT22 cells. HT22 cells were co-transfected with mitoGFP and empty vector or *Gdap1*, respectively. Nuclei were visualized with 0.5 µg/ml DAPI, and F-Actin was stained with 100 nM rhodamine phalloidin. Results were quantified to show percentages of cells with respective mitochondrial morphologies. At least 70 cells per condition were counted in three independent experiments. Date are represented as means ± S.E.M. * *P*<0.05, ** *P*<0.005 compared to control vector-transfected cells.

3.4.3   GDAP1 increases glutathione levels and protects from 12/15-LOX and tBid-induced cell death

Since GDAP1 was found to be protective against glutamate-induced cell death, its role in oxidative glutamate toxicity was studied more closely. The first step in the sequence of oxidative glutamate toxicity is the depletion of glutathione followed by an increase in levels of reactive oxygen species. In order to evaluate whether the protection of GDAP1 is mediated by glutathione, GSH levels were measured in GDAP1-overexpressing HT22 cells. Indeed, GDAP1 increased GSH levels of unchallenged cells to 109% (Fig. 14 a). Although the little increase in glutathione concentration does probably not account for the marked increase in survival of glutamate-treated cells, it is in line with the decreased levels of ROS in GDAP1-overexpressing cells measured by FACS analyses with H2DCFDA (Fig. 14 b).

Another hallmark of oxidative glutamate toxicity is the activation of 12/15-lipoxygenase. 12/15-LOX is activated by glutamate-induced GSH depletion and is required for oxidative glutamate toxicity, as it was shown that LOX inhibitors could prevent glutamate-mediated cell death (Li et al., 1997b). It directly attacks mitochondria leading to a breakdown of mitochondrial membrane potential, the release of pro-apoptotic factors like cytochrome *c* and the generation of ROS (Pallast et al., 2009). Therefore, it was examined whether GDAP1 could interfere with the action of 12/15-LOX. HT22 cells were transfected with 12/15-LOX, *Gdap1*, or both, and cell viability was measured. Viability of cells transfected with 12/15-LOX was reduced by 10% and could completely be restored by co-transfection with *Gdap1* (Fig. 14 c, upper left panel). In the presence of 10 mM glutamate, GDAP1 protected against cell death and again, restored cell viability of 12/15-LOX-transfected cells to levels of unchallenged cells (Fig. 14 c, lower left panel).

Upon induction of glutamate toxicity, pro-apoptotic Bcl-2 family member BID (BH3-interacting domain death agonist) translocates to mitochondria, which then accumulate at the nucleus. This event is followed by the translocation of AIF from mitochondria to the nucleus where it induces nuclear fragmentation (Landshamer et al., 2008). Caspase-3 activation is not required for BID-mediated glutamate neurotoxicity and AIF signaling. Moreover, upon glutamate treatment, BID has been shown to mediate mitochondrial fragmentation and the loss of mitochondrial membrane potential (Grohm et al., 2010). Cell viability assays revealed that overexpression of truncated and thus already activated BID (tBID) markedly induced cell death in HT22 cells (Fig. 14 c, upper right panel). Again, when cells were co-transfected with GDAP1, cell viability could be partly restored both, in the absence and presence of glutamate (Fig. 14 c, right panel).
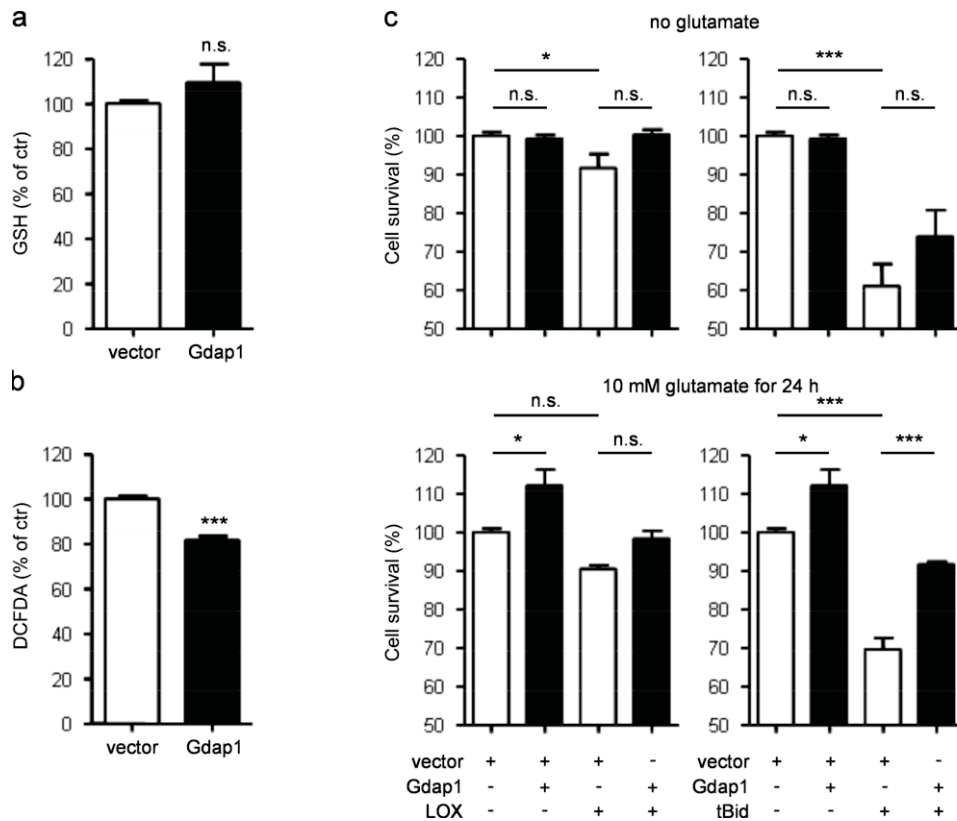
Figure 14 **GDAP1 increases glutathione levels and protects against 12/15-LOX and tBID-induced cell death.** Empty vector or *Gdap1* were transiently transfected into HT22 cells and (a) increased levels of glutathione were measured enzymatically in three independent experiments in triplicates. (b) Reduced levels of ROS in *Gdap1*-overexpressing cells were observed by FACS analysis with H2DCFDA in five independent experiments in duplicate. (a, b) Data correspond to means ± S.E.M. with *** $P<0.0001$ compared with vector-transfected cells (unpaired student's t-test). (c) GDAP1 protects against cell death induced by 12/15-LOX (left panel) and tBID (right panel) both in absence (upper panel) and presence (lower panel) of glutamate. HT22 cells were transiently transfected with empty vector, *Gdap1*, 12/15-LOX and *tBid* as well as co-transfected with *Gdap1* and 12/15-LOX or *tBid*, respectively. Cell viability was measured by CTB assay 24 h post transfection (c) or 24 h after 24 h exposure to 10 mM glutamate (d). Data are shown as mean ± S.E.M. of four independent experiments in triplicate. * $P<0.05$, *** $P<0.0001$ (one-way ANOVA, Bonferroni's).

3.4.4 GDAP1 causes a shift towards glycolysis despite increasing the mitochondrial membrane potential

Activation of 12/15-LOX and BID was shown to cause disruption of the mitochondrial membrane potential ($\Delta\Psi$m) (Grohm et al., 2010; Pallast et al., 2009). As GDAP1 protected against both, 12/15-LOX- and tBID-induced cell death, it was investigated whether GDAP1 could stabilize $\Delta\Psi$m. When $\Delta\Psi$m was studied by FACS analyses with the lipophilic, cationic dye JC-1 in GDAP1-overexpressing cells, a shift in JC-1 fluorescence from green to red was observed indicating an increase in $\Delta\Psi$m (Fig. 15 a, left panel). The ratio of geometric means of

red to green JC-1 fluorescence was used to quantify $\Delta\Psi m$. GDAP1 overexpression caused a 3.5-fold increased JC-1 ratio (Fig. 15 a, right panel). Experiments were reproduced with TMRE, another cell-permeant, cationic, fluorescent dye that accumulates in active mitochondria. TMRE fluorescence intensity was increased in GDAP1-overexpressing cells proving the increase in $\Delta\Psi m$ (Fig. 15 b). Moreover, the elevated mitochondrial membrane potential of HT22R cells could be reduced by GDAP1 knockdown with two shRNAs (Fig. 15 c).
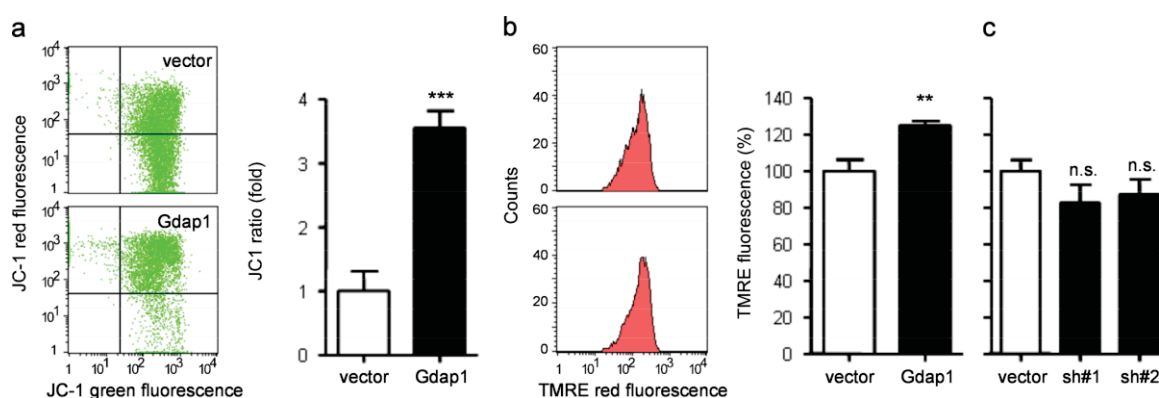

Figure 15 **GDAP1 overexpression stabilizes the mitochondrial membrane potential.** (a) FACS analyses revealed an increase in red to green JC-1 fluorescence ratio. Typical dot plots are shown (left panel). Quantification of JC-1 fluorescence ratio from four independent experiments in triplicates (right panel). Asterisks indicate $P<0.0001$ compared with control vector-transfected cells by unpaired student's t-test. (b) Increase in mitochondrial membrane potential $\Delta\Psi m$ of GDAP1-overexpressing cells confirmed by FACS analysis with TMRE. Increase in TMRE fluorescence is shown in typical histogram plots (left panel) and quantification from two independent experiments in triplicates (right panel). ** $P<0.005$ (unpaired student's t-test). (c) TMRE fluorescence is reduced after *Gdap1* knockdown in HT22R cells. HT22R cells were transfected with shRNA constructs 48 h prior to analysis (n = 6, one-way ANOVA, Dunnett's). Data points represent means ± S.E.M.

An increased mitochondrial membrane potential indicates a high capacity of oxidative phosphorylation. Therefore, it was supposed that GDAP1-overexpressing cells exhibit increased glucose consumption. Indeed, growth medium of GDAP1-transfected cells contained lower glucose concentrations compared to that of control cells indicating an increased metabolic rate (Fig. 16 b). However, the concentration of lactate was increased ~1.4 fold in medium of GDAP1-overexpressing cells (Fig. 16 a). Lactate is produced during glycolysis, which would lead to the assumption that cells overexpressing GDAP1 utilize the glycolytic pathway for energy production to a greater extent than control cells. At the same time, GDAP1-overexpressing cells had a growth advantage in glucose-containing medium, but did not grow faster in medium containing galactose, which poorly enters glycolysis (Fig. 16 c). Thus, the rate of glucose conversion is increased in GDAP1-overexpressing cells and glucose is increasingly converted to lactate. It was concluded that despite their elevated

mitochondrial membrane potential GDAP1-overexpressing cells shift their energy metabolism towards glycolysis.
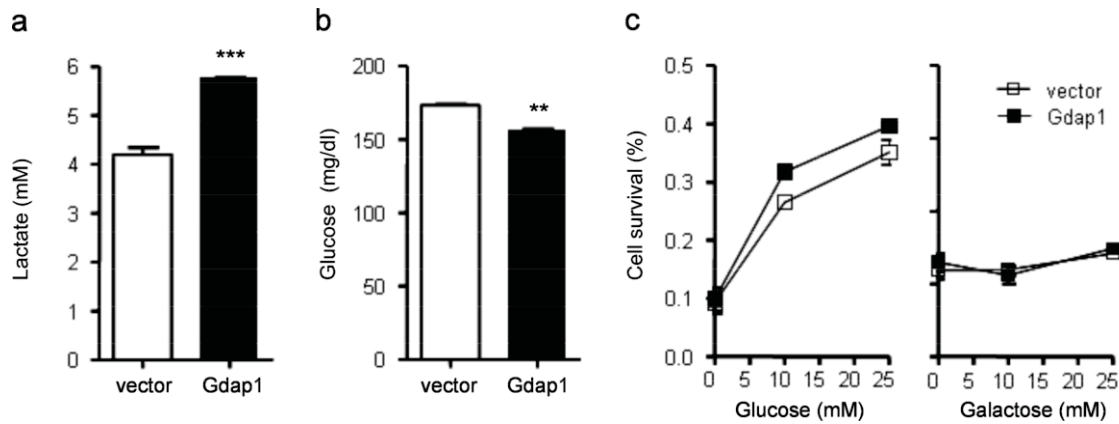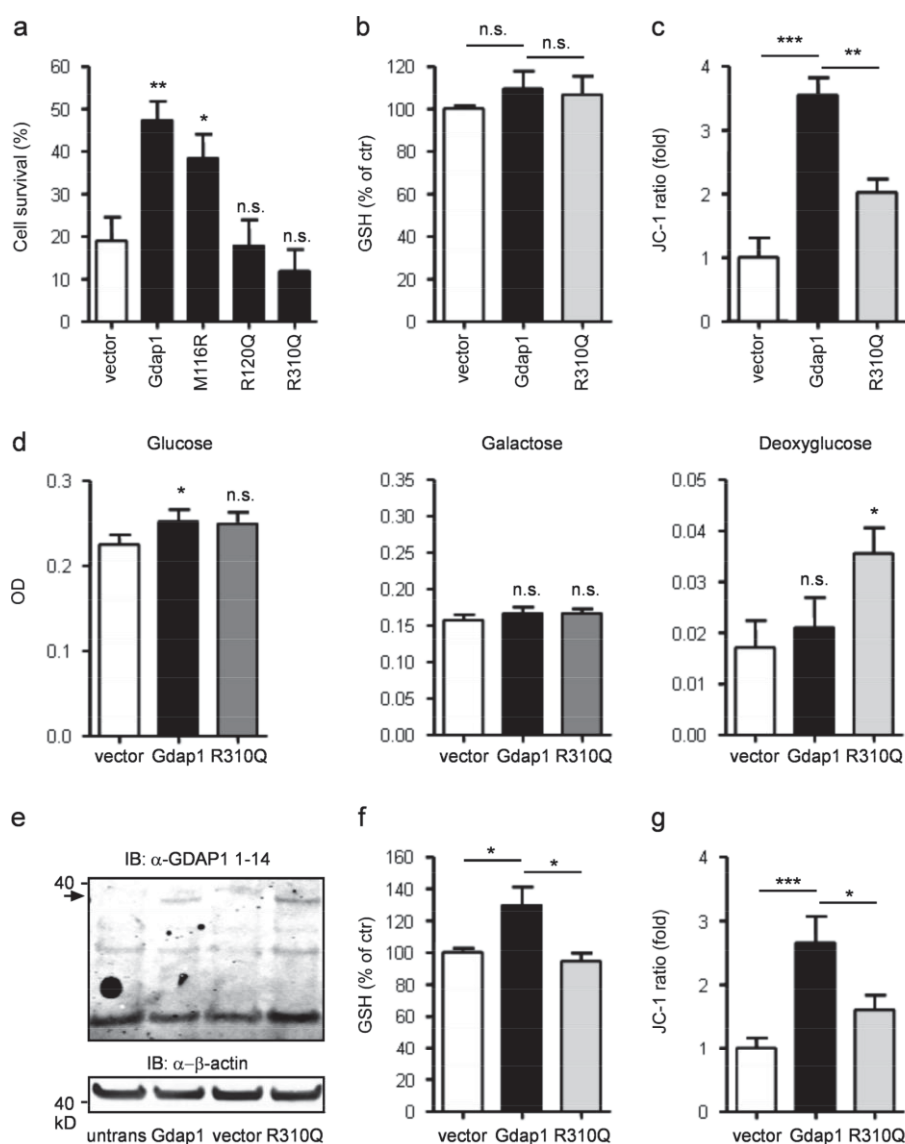

Figure 16 **GDAP1-overexpressing HT22 cells exhibit increased lactate production and a growth advantage in high glucose conditions.** (a, b) Medium from *Gdap1*-transfected cells contains (a) more lactate and (b) less glucose than medium from control cells. Transfection medium was changed after 24 h, the growth medium collected 24 h later and analyzed enzymatically. Data are represented as mean ± S.E.M. ** $P<0.005$, *** $P<0.0001$ (n = 2, one-way ANOVA, Dunnett's). (c) *Gdap1*-transfected cells have a concentration-dependent growth advantage when cultured in glucose but not in galactose. Cells were cultured in medium with indicated concentrations of glucose or galactose for 24 h and cell viability was measured by CTB assay in eight independent experiments in quintuplicates.

3.4.5   Autosomal-recessive mutations attenuate the function of GDAP1

In order to find out whether the presented observations were relevant for the pathology of CMT4A, different missense mutations of *Gdap1* were analyzed. Expression vectors encoding the recessive *Gdap1* point mutants M116R, R120Q and R310Q were obtained from Axel Niemann (ETH Zurich, Switzerland). The mutations M116R and R120Q lie within the GST-N domain and between the two GST domains of *Gdap1*, respectively. The mutation R310Q is located at the C-terminal end of the hydrophobic domain. R120Q causes a demyelinating CMT phenotype while the mutations M116R and R310Q are associated with intermediate forms (Azzedine et al., 2003; Boerkoel et al., 2003; Di Maria et al., 2004). Cell viability assays with transiently transfected HT22 cells revealed that the protection of GDAP1 against oxidative glutamate toxicity is reduced or abolished when *Gdap1* is mutated (Fig. 17 a). At 10 mM glutamate, only the mutant M116R increased cell survival, although to a lesser extent than wild-type GDAP1. Interestingly, the ability of the GDAP1 mutants to protect against glutamate toxicity correlated with their ability to induce mitochondrial fragmentation as shown by Niemann and colleagues (Niemann et al., 2005)). In the cell viability assay, the mutant R310Q caused a complete loss of the protective function of GDAP1 and was therefore selected for further experiments.

Figure 17 **Disease-causing mutations attenuate or even abolish GDAP1's effect on cell protection and mitochondrial membrane potential.** Upper and middle panel: transiently transfected HT22 cells, lower panel: stably overexpressing HT22 cells. (a) GDAP1 mutants diminish GDAP1's protection against oxidative glutamate toxicity. Cell viability assay of HT22 cells transiently transfected with WT or mutated *Gdap1* and exposed to 10 mM glutamate for 24 h. Data are from three independent experiments in quadruplicate. * $P<0.05$, ** $P<0.005$ compared to vector-transfected cells by one-way ANOVA (Dunnett's). (b) Both, transiently transfected WT and mutant *Gdap1*, increase intracellular glutathione levels. GSH was measured 48 h after transfection three times in triplicate. (c) HT22 cells expressing the point mutation R310Q increase mitochondrial membrane potential in a significantly lower rate than GDAP1-overexpressing cells. ΔΨm was determined by FACS analysis in four independent experiments in triplate. (b, c) Data points represent means ± S.E.M. ** $P<0.005$, *** $P<0.0001$ compared with vector-transfected cells by one-way ANOVA (Bonferroni's). (d) Growth rates of WT and mutant overexpressing cells were analyzed in ten independent cell viability assays. HT22 cells were transfected with *Gdap1*, the mutant R310Q or control vector. 24 h after transfection, medium was exchanged for medium containing glucose, galactose or deoxyglucose and cell viability was measured 48 h later by CTB assay. Cells expressing R310Q do not significantly increase growth rates in high glucose conditions. As GDAP1-overexpressing cells, they do not

alter growth rates in galactose medium, but exhibit an increased survival in medium containing deoxyglucose. * P<0.05 as determined by one-way ANOVA (Dunnett's). (e) Immunoblot of HT22 cells stably transfected with *Gdap1*, R310Q or control vector. The arrow indicates the band corresponding to GDAP1. Immunoblot against β-Actin is used as a control for equal protein amounts per lane. (f) Cells stably overexpressing R310Q do not increase intracellular GSH levels (three independent experiments in triplicates). (g) Lack of increase in ΔΨm in cells stably expressing R310Q was determined by FACS with JC-1 in four independent experiments in triplicates. (f, g) Data points represent means ± S.E.M. * P<0.05, *** P<0.0001 compared with vector-transfected cells by one-way ANOVA (Bonferroni's).

The elevated GSH level found in GDAP1-overexpressing cells was slightly reduced when cells were transfected with the mutant R310Q, but results were not significant (Fig. 17 b). ΔΨm was measured in R310Q-transfected cells with JC-1 and found to be higher than in control cells. However, mutated GDAP1 increased ΔΨm to a significantly reduced level than the wild-type protein (Fig. 17 c) indicating that the mutation affected the ability of GDAP1 to stabilize the mitochondrial membrane potential. Overexpressed R310Q mutant was also not capable to statistically increase the growth in glucose-containing medium (Fig. 17 d, left panel). Like the wild-type, R310Q overexpression did not alter the growth rate in galactose (Fig. 17 d, middle panel). However, in contrast to control or *Gdap1*-transfected cells, R310Q-overexpressing cells were able to proliferate on medium containing deoxyglucose, which cannot be converted by hexokinases (Fig. 17 d, right panel).

The features of GDAP1 presented so far, particularly its protection from oxidative stress and the stabilization of the mitochondrial membrane potential, have been obtained from transiently transfected cells. In order to have a more stable and more practical model at hand, HT22 cells were stably transfected with *Gdap1*, R310Q or the control vector by the medical student Svenja Frede. GDAP1 expression in these cells was analyzed by immunoblotting. The ~40 kDa band was evident in lysates from stably GDAP1- and R310Q overexpressing cells (Fig. 17 e). The stable cell lines were regularly checked for overexpression by quantitative RT-PCR (not shown). Stably GDAP1-overepressing cells exhibited the effects of GDAP1 on GSH content and mitochondrial membrane potential (Fig. 17 f and g). Moreover, the increase in GSH levels was more prominent compared to the transiently transfected cells. In cells stably overexpressing the mutant R310Q, the GSH concentration was at the level of control cells (Fig. 17 f). Similar to the situation in transiently transfected cells, stable overexpression of R310Q increased ΔΨm, but again to a much lower extent than the wild-type (Fig. 17 g).

In conclusion, the ability to protect against oxidative stress, to increase intracellular glutathione concentrations, and to stabilize the mitochondrial membrane potential is impaired when *Gdap1* is mutated. Moreover, these cellular changes were observed in transiently and stably overexpressing cells showing that they were not due to a short-term overexpression but rather to the protective function of GDAP1. Furthermore, the stable cell lines were easier to handle and allowed experiments at the level of cell compartments.

3.4.6   Wild-type and mutant GDAP1 stabilize mitochondrial hexokinase localization

The increased proliferation in glucose-containing medium and the increased production of lactate observed in GDAP1-overexpressing cells are typical features of cancerous tumors (Pedersen, 2007). Especially the shift from oxidative phosphorylation to glycolysis despite sufficient oxygen supply is one of the most common phenotypes of cancers and known as the Warburg effect, defined as elevated glycolysis in the presence of oxygen. Pedersen and colleagues have shown that in tumors exhibiting the Warburg effect, the hexokinase isoform hexokinase-2 (HK-2) is upregulated and binds to the voltage-dependent anion channel (VDAC) of the MOM. In contrast to cytosolic hexokinases, mitochondrial bound HK-2 is not inhibited by its product glucose-6-phosphate and gains preferred access to ATP synthesized by the ATP synthase located in the inner mitochondrial membrane, which results in an increased HK-2 activity (Pedersen, 2007). The importance of HK-2 and its mitochondrial receptor VDAC has been emphasized by studies in that glycolysis was markedly suppressed by removal of HK-2-loaded mitochondria from tumor cell lysates and completely restored by re-addition of the tumor mitochondria to the cytosolic fraction (Bustamante et al., 1981). During apoptosis, the pro-apoptotic factor BAX translocates to the mitochondria where it also binds to VDAC. Mitochondria-bound HK-2 suppresses the ability of BAX to bind to VDAC and induce cytochrome *c* release thus preventing apoptosis (Pastorino et al., 2002).

Since GDAP1 overexpression resembled tumor cells in their shift towards glycolysis and protected against cell death induced by the pro-apoptotic factor BID, one hypothesis was that GDAP1, which is also localized at the MOM, increases the binding of HK-2 to VDAC thereby causing a shift towards glycolysis. Western blot analyses with mitochondria-enriched and cytosolic cell fractions served to test this hypothesis. Mitochondria were isolated from stably overexpressing cells in order to obtain sufficient amounts for analysis. Since HK-2 is not very abundant, but HK-1 is more prominent in neurons, expression and localization of both, HK-1 and HK-2 were examined. Immunoblots were additionally probed with antibodies against β-Actin and the mitochondrial marker mitochondrial heat shock protein 70 (MHSP70) to allow for normalization and quantification of expression levels. A typical Western blot is shown in Figure 18 a (left panel). HK-1 was observed in cytosolic and mitochondrial fractions in all cell lines, whereas HK-2 was detected mainly in the mitochondrial fraction, especially of GDAP1 and R310Q overexpressing cells. Quantification of three blots revealed that both hexokinases HK-1 and HK-2 are increasingly bound to mitochondria in HT22 cells overexpressing GDAP1 or the mutant R310Q (Fig. 18 a, right panel), although results were not significant.

It has been shown that HK-2 mRNA is upregulated in cancers (Altenberg and Greulich, 2004). Quantitative real-time PCR served to analyze whether GDAP1-overexpressing HT22 cells also increase the expression of HK-2. Increased expression of HK-2 (Fig. 18 b) and downregulation

of HK-1 (Fig. 18 c) were observed in cells overexpressing GDAP1 or the mutant R310Q. However, only the HK-2 upregulation in R310Q-overexressing cells was found to be significant. In summary, HK-2 is upregulated and mitochondria-bound in WT and mutant GDAP1-overexpressing cells, which thus resemble the phenotype of cancer cells.

Another mechanism leading to the phenotype of hyperpolarized and fragmented mitochondria displaying a shift to glycolysis has been described in cancer cells (Bonnet et al., 2007) and in pulmonary artery smooth muscle cells from patients with pulmonary arterial hypertension (Archer et al., 2008). Here, the reduction in mitochondrial H_2O_2 production caused by the reduced oxidative phosphorylation suppresses plasma membrane voltage-gated K^+ (Kv) currents, leading to plasma membrane depolarization and an elevation of cytosolic K^+ and Ca^{2+}. This is mediated through a normoxic activation of hypoxia-inducible factor 1α (HIF-1α) and a decreased expression of the K^+ channel Kv1.5 (Archer et al., 2008). The reduced K^+ current leads to an accumulation of intracellular K^+, which inhibits caspases and impairs apoptosis. Therefore, another hypothesis was that GDAP1 induces HIF-1α and decreases plasma membrane Kv currents through a reduction in the amount of redox-sensing Kv channels. Expression of Kv1.5 was analyzed by RT-PCR. Indeed, decreased Kv1.5 mRNA expression was observed in cells overexpressing GDAP1. However, Kv1.5 expression was also, and even significantly, decreased in cells overexpressing the mutant R310Q (Fig. 18 d).

Further experiments addressed the role of HIF-1α. Under normal conditions, HIF-1α is permanently subject to degradation via the ubiquitin/proteasome pathway. Upon activation, HIF-1α is stabilized and translocates to the nucleus where it binds to hypoxia-responsive element (HRE) causing transcription activation. Therefore, two approaches were applied to examine HIF-1α activation: analysis of the cellular localization of HIF-1α and of HRE-dependent transcription activation. The localization of HIF-1α in GDAP1-overexpressing HT22 cells should be analyzed by Western blots with cytosolic and nuclear cell fractions. However, HIF-1α could not be detected due to either the insufficient quality of the cellular fragmentation, the HIF-1α antibody, or both (data not shown). The induction of HRE-dependent transcription was examined by co-transfection with a construct that expresses luciferase in dependency of the activation of the HRE. Luciferase assays revealed contradicting results. When the HRE response was normalized to protein concentrations, it was found to be decreased in GDAP1 WT and mutant overexpressing cells. In contrast, an increase in HRE response was observed when a control luciferase was applied (data not shown). Thus, although the Kv1.5 channel and HIF-1α activation might play a role in the GDAP1-mediated cell protection, due to experimental limitations this pathway could not be further examined.

Another mechanism that might explain the glycolytic phenotype induced by GDAP1 overexpression is the inhibition of pyruvate dehydrogenase (PDH) by PDH kinase 2 (PDK2). Altenberg and Greulich showed that enzymes of the glycolytic pathway, especially

glyceraldehyde-3-phosphate dehydrogenase, enolase 1, and pyruvate kinase, are upregulated in 24 examined cancer classes that represent more than 70% of all cancer cases worldwide (Altenberg and Greulich, 2004). Moreover, in cancer cells, PDH that converts pyruvate to acetyl-CoA, which in turn enters the Krebs cycle, is inhibited by phosphorylation (Bonnet et al., 2007). If the GDAP1-mediated shift towards glycolysis was caused by the inhibition of PDH by PDK2, increased PDK2 expression and activity would be expected. The expression of *Pdk2* mRNA, however, was decreased in both GDAP1 WT and mutant overexpressing cells (Fig. 18 e). Nevertheless, to further study the increased glycolytic rate in GDAP1-overexpressing cells, the activities of glycolysis enzymes like glyceraldehyde-3-phosphate dehydrogenase and pyruvate kinase could be analyzed.
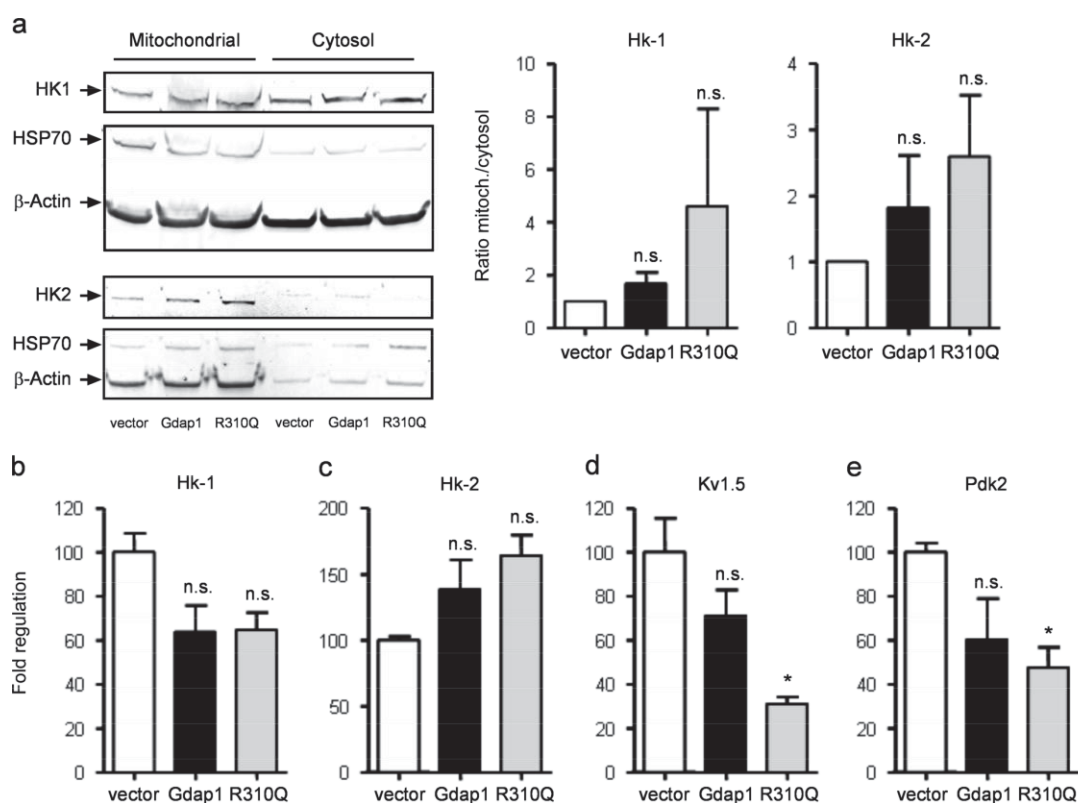
Figure 18 **Hexokinase 2 is upregulated and hexokinases 1 and 2 are bound to mitochondria in GDAP1- and R310Q-overexpressing HT22 cells.** (a) Immunoblot with mitochondrial and cytosolic fractions of HT22 cells stably transfected with *Gdap1* and the point mutant R310Q. The blot was probed with antibodies against hexokinases HK-1 and HK-2, β-Actin and the mitochondrial marker MHSP70. Quantification of three immunoblots. HK-1 and HK-2 expression were normalized to MHSP70 and β-Actin expression before the ratio between mitochondria-bound and cytosolic hexokinases was determined. (b) Decreased *Hk-1* and (c) increased *Hk-2* expression in cells stably expressing GDAP1 or R310Q was determined by quantitative RT-PCR in two independent experiments in triplicates. (d) Downregulation of potassium channel Kv1.5 (*Kcna5*) and (e) pyruvate dehydrogenase kinase 2 (*Pdk2*) in Gdap1- and R310Q-overexpressing cells was observed in two independent quantitative RT-PCR experiments. (a – e) Data are presented as mean ± S.E.M. * $P<0.05$ (one-way ANOVA, Dunnett's).

3.4.7   GDAP1 increases mitochondrial complex II abundance and function

The pathophysiology of Charcot-Marie-Tooth disease has been associated with mitochondrial defects (Cassereau et al., 2010; Loiseau et al., 2007). In fibroblasts from patients with an autosomal-dominant *GDAP1* mutation, impaired function of mitochondrial respiratory chain complex I has been observed (Cassereau et al., 2009). Therefore, the effect of GDAP1 on mitochondrial OXPHOS complexes was investigated. An antibody mixture containing antibodies against proteins of each of the five OXPHOS complexes was used to analyze their relative abundance. Western blot analysis showed that the 30 kDa subunit of complex II was upregulated in the stable GDAP1 and R310Q cell lines (Fig. 19 a, left panel). Three independent blots were quantified and the overall abundance of the complexes was set to 100% indicating an increase in complex II subunit abundance at the expense of the complex V subunit (Fig. 19 a, right panel). Complex II, succinate dehydrogenase or succinate-coenzyme Q reductase, contains four subunits in a fixed stocheometric composition. Thus, the increased abundance of the 30 kDa subunit might implicate the elevated abundance and activity of complex II. Moreover, the activity of complex V, or ATP synthase might be impaired.

Succinate dehydrogenase catalyzes the oxidation of succinate to fumarate and thereby passes electrons to the redox carrier ubiquinone. The activity of complex II was measured with a microplate assay, in which the enzyme was purified from the cell lysate, and the production of ubiquinol was quantified by the coupled reduction of the dye DCPIP and its change in absorption. In HT22 cells stably overexpressing GDAP1, complex II activity was increased 2.3-fold, and a 1.8-fold increase was observed in cells stably overexpressing the mutant R310Q (Fig. 19 b). However, the result was statistically significant only for WT Gdap1. The increased complex II function was also measured in transiently transfected cells. Here, GDAP1 and R310Q induced 1.3-fold and 1.1-fold activity increases, respectively, but results were not significant (Fig. 19 c).

Thus, GDAP1 overexpression induces the expression and function of mitochondrial complex II indicating a regulatory function of GDAP1 in oxidative phosphorylation. It remains unclear whether the effect of GDAP1 on complex II is affected in CMT4A.

Moreover, the effects of DRP1, another fission factor, and the fusion factor MFN1 on complex II activity were analyzed. Similar to GDAP1, DRP1 increased complex II activity (Fig. 19 d) indicating a connection between mitochondrial fission and oxidative phosphorylation at complex II. Complex II function was not altered by MFN1, but was elevated when co-transfected with *Gdap1*. Since GDAP1-induced mitochondrial fission has been shown to be counterbalanced by MFN1 (Niemann et al., 2005), function of GDAP1 on mitochondrial complex II might be independent of its fission activity.

The activity of complex V was not measured. However, ATP production was not impaired in WT GDAP1 and R310Q overexpressing cells (data not shown).
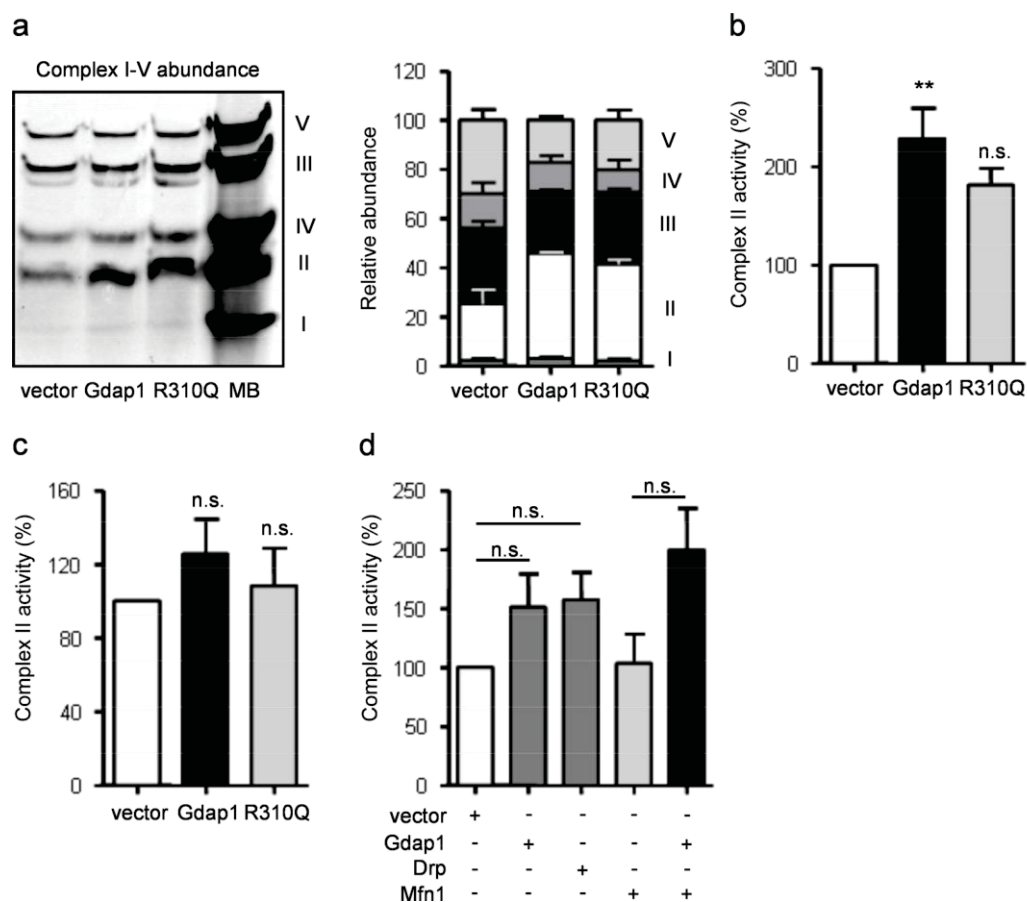
Figure 19 **GDAP1 increases mitochondrial complex II abundance and function.** (a) Immunoblot with mitochondrial fractions from stably GDAP1- and R310-overexpressing HT22 cells and mouse brain mitochondria (MB) probed with antibody mix against mitochondrial complex proteins. Quantification of three immunoblots. Data are shown as mean ± S.E.M. Both, (b) stably and (c) transiently GDAP1- and R310Q-overexpressing cells exhibit high mitochondrial complex II activities. Transiently transfected cells were analyzed two days after transfection. Using a commercial assay, mitochondrial complex II was purified from cell lysates and activity was measured as decrease in absorbance of DCPIP that is reduced by the complex II product ubiquinol. ** *P*<0.005 (n = 3, one-way ANOVA, Dunnett's). (d) Fission factors DRP1 and GDAP1 increase mitochondrial complex II activity and GDAP1 increases complex II activity in the presence of fusion factor MFN1. Complex II activity assay with HT22 cells transiently transfected with *Gdap1*, *Drp1*, *Mfn1*, and co-transfected with *Gdap1* and *Mfn1*. Experiments were carried out three times (one-way ANOVA, Bonferroni's).

3.4.8 GDAP1 is mainly expressed by neurons of the peripheral and central nervous system

GDAP1 expression has been shown in nerve cells (Niemann et al., 2005; Pedrola et al., 2008; Pedrola et al., 2005) but whereas Niemann and colleagues showed GDAP1 expression in Schwann cells by immunohistochemistry, Pedrola et al. could not detect GDAP1 in cultured rat Schwann cells. Thus, the question about GDAP1 being expressed in Schwann cells or not

remained open. To address this issue, *Gdap1* mRNA expression in rat extracts was analyzed by quantitative RT-PCR. cDNA of rat Schwann cells, dorsal root ganglia (DRG), astrocytes, and cortex neurons were a kind gift of Mark Stettner (Neurology, University Clinic, Düsseldorf). DRG cultures contain both neurons and Schwann cells. In comparison to DRG, *Gdap1* mRNA was much less abundant in pure Schwann cell cultures (Fig. 20 a). Also in cells of the CNS, *Gdap1* was much higher expressed in cortical neurons than in primary astrocytes (Fig. 20 b) confirming Pedrola's observation that in brain sections only the grey matter could be positively stained for GDAP1. In primary DRG cultures, the neuronal subpopulation is diminished over time, associated with decreased expression of the neuronal marker β-III-tubulin. The synchronous decrease in *Gdap1* mRNA expression (Fig. 20 c) supports the finding that GDAP1 is mainly expressed in neurons and is in line with the observations of Pedrola et al. (2008) who showed that in DRG cultures, all cells immunopositive for GDAP1 were also stained against β-III-tubulin. From these results it was concluded that GDAP1 is expressed both, in neurons and, although to a much lower extent, in Schwann cells.

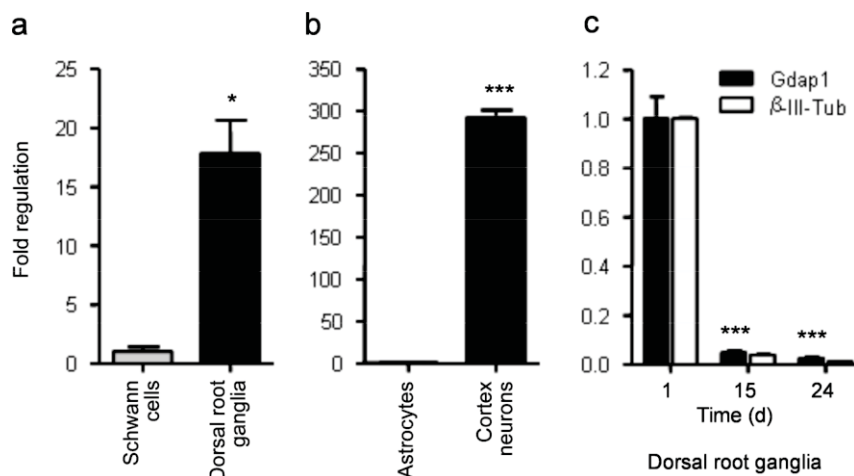

Figure 20 **Gdap1 is expressed in neurons of the central and peripheral nervous system.** Quantification of *Gdap1* mRNA by real-time RT-PCR. (a) In the PNS, a high *Gdap1* expression in DRG was observed. (b) In the CNS of rats, *Gdap1* is much more expressed in neurons than in astrocytes. (c) As neurons are diminished from DRG culture, *Gdap1* expression is decreased. (a - c) Bars represent means ± S.E.M. of two experiments in triplicates, respectively. *$P<0.05$, *** $P<0.0001$ as determined by unpaired student's t-test (except for (c) one-way ANOVA, Dunnett's).

3.4.9   GDAP1 mediates protection of NSC34 motor neurons against BSO-induced glutathione depletion

Since GDAP1 was found to be mainly expressed in neurons, and because CMT primarily affects motor neurons, experiments were reproduced with the motor neuron cell line NSC34 (Fig. 21 a). These cells were shown to exhibit properties of motor neurons including the

generation of action potentials (Cashman et al., 1992). Cell viability assays revealed that these cells can withstand glutamate concentrations of up to 100 mM (Fig. 21 b). In comparison, HT22 cells died after treatment with 7.5 mM to 10 mM glutamate, and even the cell survival of resistant HT22R cells was reduced by glutamate treatment. However, NSC-34 cells were susceptible to oxidative stress induced directly by treatment with H_2O_2 (Fig. 21 c) and GSH depletion by treatment with BSO (Fig. 21 d) as well as to tunicamycin that induces endoplasmatic reticulum stress (Fig. 21 e). Overexpression of GDAP1 but not the mutant form R310Q slightly increased the survival of NSC-34 cells treated with BSO, but did not affect cell death induced by H_2O_2 or tunicamycin (Fig. 21 c - e, upper panel). Similarly, *Gdap1* knockdown with two shRNAs increased the susceptibility of cells only to BSO (Fig. 21 c - e, lower panel). Thus, GDAP1 protects motor neurons against cell death induced by GSH depletion.
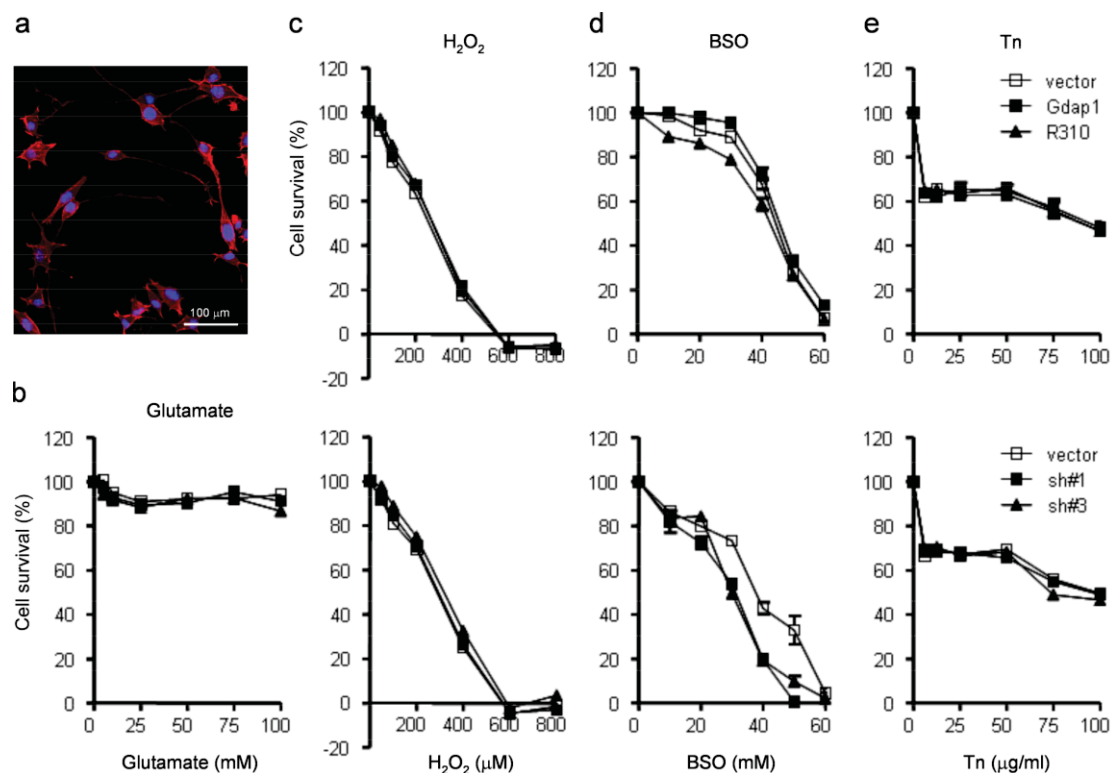

Figure 21 **GDAP1 confers resistance to BSO, but not to hydrogen peroxide or tunicamycin.** (a) Fluorescence microscopy image of NSC-34 motor neuronal cells stained with rhodamine phalloidin and DAPI. (b - e) Cell viability of NSC-34 cells transfected with *Gdap1* (upper panel) or *Gdap1*-directed shRNA constructs (lower panel) was assayed after treatment with (b) glutamate, (c) hydrogen peroxide, (d) BSO and (e) tunicamycin by CTB assay. NSC-34 cells are not susceptible to glutamate. Overexpression or knockdown of *Gdap1* did not affect cell death induced by hydrogen peroxide or tunicamyin. Overexpression of GDAP1 but not the mutant R310Q slightly protected NSC-34 cells from BSO toxicity, and *Gdap1* knockdown enhanced the susceptibility to BSO-induced cell death. Cell death experiments were carried out two or three times in quintuplicates. Data are shown as mean ± S.E.M.

3.4.10   Reduced GDAP1 expression, GSH levels and mitochondrial membrane potential in fibroblasts from CMT4A patients

In order to analyze the role of *GDAP1* mutations in CMT4A, experiments were reproduced in fibroblasts from two patients. Fibroblasts from eight healthy persons served as controls.

The fibroblast cell line CMT#1 originated from a skin biopsy of a 25-year-old male Polish patient harboring the heterozygous L239F/R273G mutation. He is the third child of healthy parents and no consanguinity is known in this family (Fig. 22 a). The clinical characteristics of the patient were described by Kabzinska and colleagues (Kabzinska et al., 2010). The patient showed first symptoms in the first decade, and sensory disturbances, hand tremor and hoarseness were observed.

The second fibroblast cell line CMT#2 was derived from a skin biopsy of a German patient carrying the homozygous mutation (c.579 + 1G>A), a mutation first detected by Senderek at al. (2003) in a 6-year-old female patient. The mutation lies within the intron 4 donor splice site and will probably result in skipping of exon 4. The patient described by Senderek et al. presented with foot deformities, wasting of foot and hand muscles, and disturbed walking and fine motor activities. Both, motor conduction velocities and action potentials were found to be reduced. Moreover, degenerating neurons, demyelination and onion bulb formations have been observed (Senderek et al., 2003). These findings suggest that the (c.579 + 1G>A) mutation causes an intermediate form of CMT. The donor of the CMT#2 cell line, a 40-year-old male, revealed first symptoms in early childhood. He had difficulties to walk and became wheelchair-bound at the age of ten years. He presented with paralyses of hands, arms and vocal cord. He is a descendant of an inbred family; his parents were cousins both, from the maternal and paternal side, as the grandparents were siblings (Fig. 22 b).

To analyze the *GDAP1* transcript in the CMT fibroblasts, PCR was performed with primers amplifying *GDAP1* cDNA from exon 2 to the end of the transcript. As predicted by Senderek and colleagues (Senderek et al., 2003), the amplification of *GDAP1* cDNA of CMT#2 fibroblasts resulted in a shortened transcript indicating the lack of exon 4 (Fig. 22 c). The PCR products from patient and control fibroblasts were cloned into the pGEM-T Easy vector and sequenced. In the CMT#1 sequence, the C>T point mutation causes the change in the amino acid sequence from leucine to phenylalanine (Fig. 22 d). The sequence alignment of the CMT#2 and the control sequence revealed matches excluding exon 4 (Fig. 22 c, e). On the RNA level, the skipping of exon 4 leads to a frameshift and the occurrence of a stop codon resulting in a truncated protein (Fig. 22 e).

Fibroblasts derived from the two CMT patients exhibited similar cell morphologies as control fibroblasts from healthy donors (Fig. 23 a). Quantitative RT-PCR revealed a very low *GDAP1* mRNA expression in all fibroblast cell lines examined. Fibroblasts expressed 27 times less *GDAP1* than motor neurons (Fig. 23 b), and *GDAP1* expression in CMT-derived fibroblasts was even lower. As quantified by real-time RT-PCR, *GDAP1* expression in the CMT#1 and CMT#2 cell lines was reduced to 6% and 10% of control levels, respectively (Fig. 23 c). Apparently cells downregulate mutated *GDAP1*. Moreover, as CMT4A-associating *GDAP1*

mutations are inherited recessively, they probably cause a loss of function of the GDAP1 protein. It was therefore assumed that the protective features, like protection from glutamate-induced cell death and elevated GSH levels, are reduced in patient-derived fibroblasts.
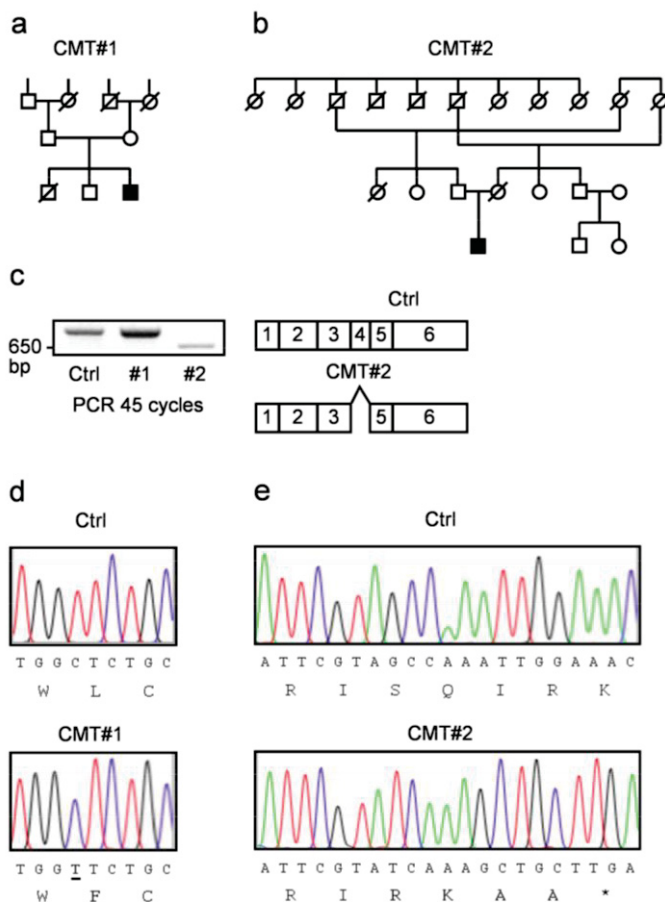

Figure 22 **Pedigrees and *GDAP1* mutations of CMT4A patients that donated the skin biopsies used in this work.** (a) Pedigree of a 25-year-old Polish patient harbouring the heterozygous L239F mutation (pedigree was adopted from (Kabzinska et al., 2010)). (b) Pedigree of 40-year-old German patient with the homozygous mutation (c.579 + 1G>A). Females are denoted by circles, males by squares. Filled symbols indicate CMT-affected patients. (c) Agarose gel of PCR products with PCR primers amplifying *GDAP1* cDNA from exon 2 to the end of the transcript reveals a shortened *GDAP1* transcript in CMT2 fibroblasts (left panel) confirming the skipping of exon 4 (right panel). (d, e) Sequence alignments of *GDAP1* cDNA from (d) CMT#1 and (e) CMT#2 fibroblasts (lower sequences) and cDNA from control fibroblasts (upper sequences) at mutation sites. (d) The C<T basepair exchange in CMT#1 leads to the L239F protein. (e) Skipping of exon 4 in CMT#2 leads to a frameshift and a truncated GDAP1 protein.

Due to the differences in growth rates, cell viability assays could not be used to study glutamate toxicity in fibroblasts. GSH levels were measured enzymatically and were found to be reduced in both patient cell lines compared to control fibroblasts (Fig. 23 d). CMT#1 contained 42.9% less GSH than control cells, and in CMT#2 cells, the GSH concentration was

reduced by 18.6%. FACS analysis with TMRE revealed decreased mitochondrial membrane potentials in the two patient cell lines with a statistically significant reduction only for CMT#1 (Fig. 23 e). The activity of complex II in patient fibroblast cell lines showed a similar pattern as the GSH levels and $\Delta\Psi m$ although results were not significant (Fig. 23 f). In summary, GSH concentration, $\Delta\Psi m$, and complex II activity that are elevated after GDAP1 overexpression, were impaired in fibroblasts of two CMT4A patients with different *GDAP1* mutations.

However, the low GDAP1 expression is a limitation of the fibroblast cell model. In order to have a better model at hands, motor neurons will be generated from induced pluripotent stem cells (iPCS) derived from patient fibroblasts as described by Karumbayaram et al. (Karumbayaram et al., 2009).
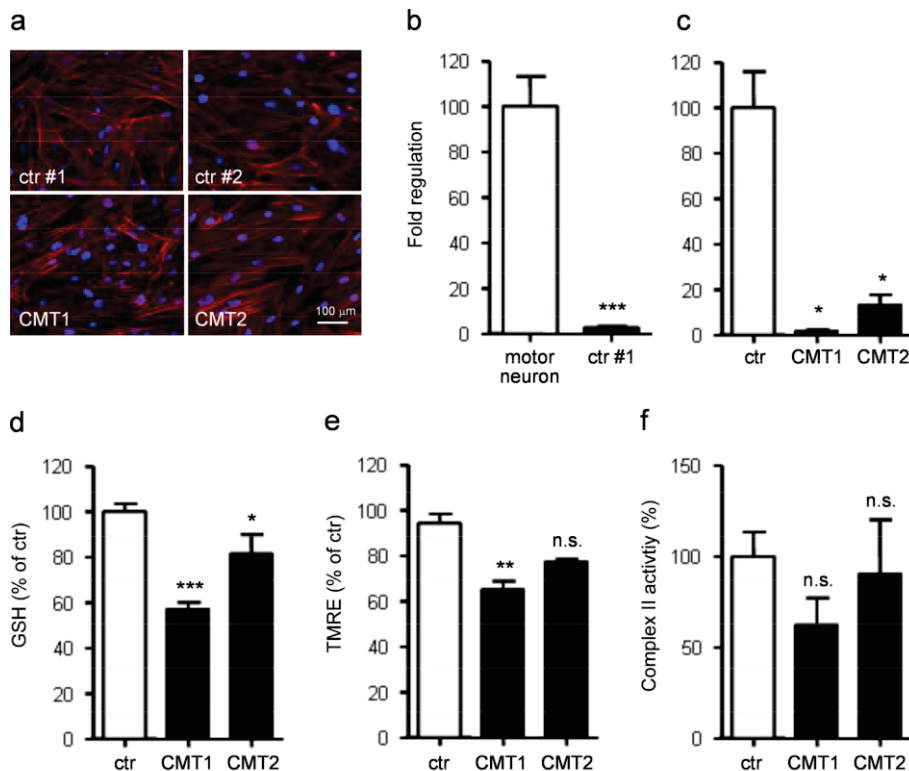
Figure 23 **CMT4A-derived fibroblasts express less Gdap1 and exhibit reduced GSH levels, mitochondrial membrane potentials and mitochondrial complex II activities.** (a) Morphology of control and CMT4A patient fibroblasts. F-Actin was stained with rhodamine phalloidin, nuclei with DAPI. (b, c) Quantification of Gdap1 mRNA by real-time RT-PCR in (b) motor neurons and fibroblasts and (c) in patient and control fibroblasts. Bars represent mean ± S.E.M. of three independent experiments, respectively. (d) Decreased GSH levels in patient fibroblast cell lines CMT#1 and CMT#2 as measured enzymatically in three independent experiments in duplicate. (e) Patient fibroblasts exhibit decreased $\Delta\Psi m$ as determined by FACS analysis with TMRE in two independent experiments in duplicate. (f) Complex II activity in patient fibroblast cell lines from three independent experiments. (b - f) Bars represent mean ± S.E.M., respectively. * $P<0.05$, ** $P<0.005$, *** $P<0.0001$ compared to control fibroblasts by (b) student's *t*-test or (c-f) one-way ANOVA (Dunnett's).

4.   Discussion

4.1   xCT and GDAP1 protect against oxidative glutamate toxicity

HT22 cells are an excellent model to study oxidative glutamate toxicity, and the glutamate-resistant cell line HT22R is used to identify protective factors. The transcript levels of HT22 and HT22R cells have been compared previously by subtractive suppression hybridization, and several proteins have been identified to protect against oxidative stress, including xCT (Lewerenz et al., 2006), BCL-2 (Sahin et al., 2006), the orphan G-protein-coupled receptor GPR39 (Dittmer et al., 2008), and the newly identified superoxide dismutase TIGR (transcript increased in glutamate resistance) (Toutzaris et al., 2010). The Affymetrix array analysis aimed at the identification of further players involved in cell protection. The highest increases in transcription levels were found for the P2X receptor P2X3, the transcription factor DACHSHUND2, GDAP1, VLDLR (Very low density lipoprotein receptor), and a serine dehydrogenase. Moreover, the up-regulation of xCT was reproduced.

Three of the differentially expressed transcripts, namely xCT, P2X3, and GDAP1 were analyzed in this study. Their increased expression was confirmed by quantitative RT-PCR. In this way, another P2X receptor, P2X7, was found to be upregulated in HT22R cells. The protective function of the candidate transcripts was analyzed by overexpression in glutamate-sensitive HT22 cells. Only xCT and GDAP1 were able to remarkably protect against glutamate toxicity, and it remains elusive why the P2X receptors P2X3 and P2X7, despite their huge upregulation in HT22R cells, could not protect against glutamate-induced cell death. The protection of xCT against glutamate toxicity has been described before (Lewerenz et al., 2006). The increase in the expression and activity of xCT results in increased cystine uptake and thus in elevated levels of the antioxidant GSH. That the protection of xCT is mediated by GSH was proven by the finding that N-acetyl-L-cysteine, a precursor of GSH, completely protected HT22 cells against glutamate-induced cell death.

However, protection of cells against oxidative stress and increased survival in cancer are two sides to a coin. It is therefore not astonishing that xCT has been shown to play a crucial role in the growth of different cancers including brain and pancreatic cancer (Chung et al., 2005; Lo et al., 2008a; Savaskan et al., 2008; Ye et al., 1999). Moreover, other proteins that were identified in HT22R cells have been associated with cancer. GPR39 has been suggested as a therapeutical target in cancer (Dittmer et al., 2008) and recently shown to contribute to tumor progression in human esophageal cell carcinoma (Xie et al., 2011), and BCL-2 is implicated in various cancers, including breast, lung, and prostate carcinoma (Alsabeh et al., 1996; Catz and Johnson, 2003; Martin et al., 2003). A role for GDAP1 in cancer is not known. However, Ratajewski and Pulaski showed GDAP1 expression in various cancer cell lines (Ratajewski and Pulaski, 2009).

4.2   The dual role of xCT in neuroprotection and neurotoxicity

Oxidative stress and xCT have been associated with various diseases including neurological disorders. Preliminary experiments addressed the role of xCT during inflammation and neurodegeneration in cell and animal models.

When microglial cells are activated by proinflammatory stimuli, they release substantial levels of glutamate. Several studies suggest that, next to the release of other compounds such as cytokines and nitric oxide, the release of glutamate is the key determinant of microglial neurotoxicity (Barger et al., 2007). Glutamate release of microglia activated with LPS or the β-amyloid precursor protein could be blocked by inhibition of X_c^- with α-aminoadipate or use of cystine-free medium (Barger and Basile, 2001; Piani and Fontana, 1994) suggesting that glutamate release from activated microglia is mainly mediated by the antiporter system X_c^-. Accordingly, increase in xCT expression was shown in LPS-induced BV2 microglial cells. To evaluate the role of xCT during inflammatory processes *in vivo*, its expression in the multiple sclerosis mouse model EAE was examined. Changes in the expression of the glutamate transporters GLT-1, GLAST and EAAC1 have been reported previously in this model (Ohgoh et al., 2002). Here, the expression of xCT was shown to be induced in peritoneal macrophages of EAE mice. xCT is therefore suggested to be a therapeutic target. However, pharmacological inhibition with sulfasalazine led to a more severe clinical course in EAE-induced rats (Correale et al., 1991). Knockdown experiments in EAE mice are going to be conducted in order to analyze the role of xCT for disease progression.

High glutamate concentrations are also responsible for neuronal cell death during stroke. It was assumed that, like during inflammation, macrophages were responsible for the glutamate release, and that xCT inhibition would therefore decrease neurotoxicity. This hypothesis was tested by inducing focal ischemia using tMCAO in Wistar rats. However, pharmacological inhibition of xCT with (S)-4-CPG did not protect against neuronal cell death; on the contrary, xCT inhibition caused increased ischemic lesions. The inhibition of xCT activity might render

neurons even more susceptible to glutamate toxicity rather than to protect them by decreasing the glutamate release from migrating macrophages. These results reveal a dual role of xCT in neurological disorders.

4.3 GDAP1 protects against cell death implying GSH and elevates cellular GSH levels

GDAP1 protected against oxidative stress induced by glutamate or BSO, both reducing intracellular GSH levels. Similarly, GDAP1 silencing increased the susceptibility of NSC-34 cells to BSO. GDAP1 did not protect cells against direct oxidative stress induced by H_2O_2 nor against endoplasmic reticulum stress induced by tunicamycin. These results indicate that GDAP1-mediated protection is specific for cell death implying changes in glutathione metabolism. Glutathione depletion is an early step in oxidative glutamate toxicity and apoptotic cell death. It has been shown that GSH depletion and inhibition of γ-glutamylcysteine synthase (γ-GCS) that catalyzes the first step in GSH synthesis induce apoptosis, while overexpression of γ-GCS and high intracellular GSH levels conveyed resistance against apoptosis induced by various stimuli. Moreover, GSH depletion leads to post-translational modifications of proteins by glutathionylation, which has been shown to be involved in the regulation of apoptosis (Franco and Cidlowski, 2009). GDAP1 overexpression slightly elevated GSH levels in HT22 cells even in the presence of low concentrations of glutamate, maybe by increasing GSH synthesis. However, it is not probable that the small increase in GSH concentration is sufficient to account for the protection of GDAP1 against glutamate toxicity.

GDAP1 exhibits structural similarities to glutathione *S*-transferases (Marco et al., 2004; Pedrola et al., 2005; Shield et al., 2006). The catalytic activity of GSTs depends on their dimerization and their ability to bind GSH. GDAP1 has been shown to form homodimers (Shield et al., 2006), but until recently no GST activity was detected (Pedrola et al., 2005; Shield et al., 2006). A truncated, eukaryotically expressed GDAP1 X288 protein lacking the transmembrane domain, however, binds GSH and exhibits GST function, although only for some of the tested substrates and with relatively low activities (Wagner, 2009). It is not known whether full-length and membrane-anchored GDAP1 can act as a GST. But given its ability to bind GSH, to protect against cell death by glutathione depletion, and to trigger GSH production led to the assumption that GDAP1 might act as a GSH sensor. It is not known, whether any of the described effects of GDAP1 depends on GSH nor how GDAP1 might be involved in such a signaling cascade. However, a further set of experiments will address this issue by analyzing the most prominent effect of GDAP1 overexpression, namely the mitochondrial fragmentation under conditions of low and high GSH concentrations.

4.4   GDAP1 protects against glutamate toxicity by stabilizing ΔΨm, AIF, and the binding of HK-2 to VDAC

A key factor implicated in neuronal cell death is AIF, a flavoprotein with NADH oxidase activity (Vahsen et al., 2004). Under normal conditions, AIF is located in the mitochondrial intermembrane space or loosely associated with the inner mitochondrial membrane. Upon apoptosis induction or in response to glutamate toxicity, AIF translocates to the nucleus, where it causes nuclear fragmentation and caspase-independent cell death within minutes (Landshamer et al., 2008). The translocation of AIF is mediated by the activation of BH3-interacting domain death agonist (BID). BID is a member of the proapoptotic BCL-2 family. Activation of BID results in its truncated form, tBID that interacts with another BCL-2 family member, BAX, leading to the insertion of BAX into the outer mitochondrial membrane. BAX binds to and opens the voltage-dependent anion channel (VDAC) causing the release of cytochrome *c* and other proapoptotic factors like AIF (Tsujimoto and Shimizu, 2000). Other studies suggest that BCL-2 antagonist/killer (BAK) and BAX, activated by BID, oligomerize and form a pore, through which cytochrome *c* is released (Korsmeyer et al., 2000). The activation of BID has been shown to cause mitochondrial membrane permeabilization (Grohm et al., 2010; Landshamer et al., 2008), and overexpression of tBID leads to cell death. GDAP1, on the other hand, stabilized the mitochondrial membrane potential (ΔΨ,) and protected against tBID-induced cell death. This and the localization of GDAP1 at the MOM suggests that it inhibits the action of BID and thus prevents cell death by either inhibiting the interaction of BAX and VDAC or by stabilizing AIF at the mitochondria and thereby preventing AIF translocation to the nucleus. To prove these assumptions, the localization of AIF in dependency of tBID and GDAP1 overexpression could be analyzed.

It has been shown in this study that GDAP1 increases the binding of hexokinases HK-1 and HK-2 to the mitochondrial outer membrane. HK-2 bound to VDAC suppresses BAX-induced cytochrome *c* release and apoptosis (Pastorino et al., 2002), and tBID partly acts by eliciting the dissociation of HK-2 from mitochondria (Majewski et al., 2004a; Majewski et al., 2004b). Therefore, another hypothesis is that GDAP1 protects against cell death by increasing the binding of HK-2 to VDAC and thereby blocking the interaction of VDAC with BAX.

4.5   Cell protection and mitochondrial fission

GDAP1 has been shown to induce fragmentation of mitochondria in COS-7 cells (Niemann et al., 2005; Pedrola et al., 2008). Also in HT22 cells, GDAP1 overexpression led to mitochondrial fission. In this study, GDAP1 powerfully protected against cell death induced by glutamate. However, mitochondrial fragmentation is commonly associated with apoptosis and oxidative stress (Grohm et al., 2010; Jahani-Asl et al., 2007). Mitochondrial fragmentation and MOM

permeabilization are followed by the release of factors like cytochrome *c* and SMAC/DIABLO into the cytosol (Cereghetti and Scorrano, 2006). Moreover, fusion and fission factors were shown to be involved in apoptosis regulation. Frank et al. showed that DRP1 is recruited to the mitochondria upon apoptosis and that its inhibition prevented breakdown of the mitochondrial membrane potential and release of cytochrome *c* (Frank et al., 2001). Cytochrome *c* release, in turn, involves the destabilization of the fusion factor OPA1 (Delivani and Martin, 2006). Furthermore, overexpression of mitofusins was shown to interfere with the activation of BAX and BAK (Neuspiel et al., 2005), to block mitochondrial fusion and to protect neurons against acute injury (Jahani-Asl et al., 2007). Downregulation of the fission factors DRP1 and FIS1 induced resistance to apoptosis, whereas cells depleted of the fusion factor OPA1 were extremely sensitive to apoptosis induction (Lee et al., 2004). Similarly, pro- and antiapoptotic factors were found to act on mitochondrial network mediators. BAX and BAK were found to interact with MFN1 and MFN2 and thereby regulate mitochondrial fusion (Karbowski et al., 2006). Moreover, the proapoptotic factors BAX and BAK mediate sumoylation and accompany stable association of DRP1 with the mitochondrial membrane (Santel and Frank, 2008; Wasiak et al., 2007). On the other hand, the antiapoptotic BCL-XL stimulated DRP1 GTPase activity and promoted mitochondrial fission (Li et al., 2008). Thus, mitochondrial fragmentation does not necessarily indicate apoptosis. Instead, the mitochondrial network regulation is much more complex. However, it is not clear whether GDAP1-induced fragmentation and its protection against oxidative glutamate toxicity are connected. It has been proposed before that HK-2 binding to VDAC blocks the binding of BAX (Fulda et al., 2010; Pastorino et al., 2002), which might in this way account for the GDAP1-mediated cell protection. Moreover, the ability of GDAP1 mutants to cause mitochondrial fission directly correlated with their ability to protect against glutamate toxicity. On the other hand, oxidative glutamate toxicity comprises mechanisms distinct of that of apoptosis. A connection between mitochondrial fission and protection against oxidative stress is therefore highly speculative.

4.6   GDAP1 overexpression increases glycolysis rates although elevating the mitochondrial membrane potential

GDAP1 overexpression caused an increased mitochondrial membrane potential, a growth advantage in glucose-containing medium and increased uptake of glucose, findings that at first indicated elevated oxidative phosphorylation. However, lactate production was increased in GDAP1-overexpressing cells. This phenotype, increased glycolysis in the presence of oxygen and despite the stable membrane potential, resembled the Warburg effect, which is frequently observed in cancer cells (Altenberg and Greulich, 2004). Here, the binding of HK-2

to the VDAC enhances the hexokinase reaction by abrogating product inhibition and facilitating the access to ATP synthesized in the inner mitochondrial membrane (Pedersen, 2007). Thus, in addition to its role in protection against cell death, the increased binding of HK-2 to VDAC at the MOM could also account for the observed increase in glycolysis due to GDAP1 overexpression.

Moreover, elevated lactate production has been observed in AIF-deficient mice (Vahsen et al., 2004) suggesting that, next to inhibiting its translocation to the nucleus, GDAP1 might suppress AIF's function as a NADH oxidase. Interestingly, a physical interaction between AIF and HK-2 has been shown by co-immunoprecipitation (Chen et al., 2009). However, because AIF is located in the intermembrane space, while HK-2 is bound to the mitochondrial outer membrane at the cytosolic side, another protein crossing the outer membrane is required for this interaction. Since GDAP1 spans the MOM with its C-terminus located in the intermembrane space (Wagner et al., 2009) it could be a putative interaction partner. Immunoprecipitation assays have to be conducted to test this hypothesis.

Another mechanism that might explain the glycolytic phenotype of GDAP1-overexpressing cells is the HIF-1α-Kv1.5 pathway. Here, the low expression of the K^+ channel Kv1.5 and the inhibition of PDH by PDK2 contributed to apoptosis resistance and the shift to glycolysis in cancer cells (Archer et al., 2008; Bonnet et al., 2007). The reduced efflux of K^+ from the cell leads to an increased K^+ concentration that inhibits caspases and thus apoptosis. The decreased Kv1.5 expression is mediated by the hypoxia-inducible factor 1α and an inhibition loop in that the low Kv currents lead to plasma membrane depolarization and elevated entry of Ca^{2+} activating the transcription factor NFAT that in turn suppresses expression of Kv1.5. Moreover, PDK2 phosphorylates and thus inhibits PDH thereby preventing pyruvate to enter the Krebs cycle. To test the role of the HIF-1α-Kv1.5 pathway for the glycolytic phenotype of GDAP1, Kv1.5 and PDK2 expression levels were analyzed. PDK expression was decreased in GDAP1-overexpressing cells disproving the assumption that the increased glycolytic rate is caused by inhibition of PDH. Nevertheless, Kv1.5 expression was reduced indicating the involvement of the HIF-1α-Kv1.5 pathway. Therefore, further experiments were conducted to examine the role of HIF-1α. The hypothesis that HIF-1α contributes to the shift to glycolysis has been strengthened by another study showing that during inflammation, HIF-1α was stabilized by impaired oxidative phosphorylation, and that the mitochondrial defect and HIF-1α stabilization synergized to activate glycolysis as measured by lactate release (Garedew and Moncada, 2008). However, due to experimental limitations, further evidence on the implication of HIF-1α could not be obtained. Western blots with cytosolic and nuclear cell fractions aimed to examine the cellular localization of HIF-1α but failed because of the poor quality of the HIF-1α antibody. Moreover, the investigation of HRE-dependent transcription by luciferase assays resulted in contradictory results depending on the use of different control luciferases. The same was true for the analysis of the role of the transcription factor NFAT.

Although the implication of HIF-1α remains elusive, several mechanisms have been identified that might account for GDAP1's shift in energy metabolism towards glycolysis, namely the increased binding of HK-2 to VDAC, the inhibition of nuclear translocation of AIF, and the low expression of Kv1.5.

4.7 *GDAP1* mutations impair oxidative phosphorylation

In this study, GDAP1 overexpression was shown to increase the mitochondrial membrane potential that is required for oxidative phosphorylation. But at the same time it enhanced the rate of glycolysis. Like true for cancer cells, increased glycolysis does not necessarily imply impaired oxidative phosphorylation. On the contrary, mitochondrial energy production is normally not impaired in tumors, and even in rapidly growing tumor cells the contribution of glycolysis to total energy production does not exceed 50% (Pedersen, 2007). The complex II 30 kDa protein is part of the soluble succinate dehydrogenase and was found to be upregulated in GDAP1-overexpressing cells. In addition, complex II activity was increased by GDAP1. Succinate dehydrogenase is *S*-glutathionylated depending on the redox state of the cell, and *S*-glutathionylation of purified enzyme results in increased electron transfer efficiency (Chen et al., 2007). Given GDAP1's effect on GSH metabolism and its putative function as GST, GDAP1 might enhance complex II activity and *S*-glutathionylation of succinate dehydrogenase. The activity of the other subunits was not investigated nor the overall oxidative phosphorylation capacity. Thus it is not clear whether the GDAP1-induced increase in glycolysis is the consequence of compromised respiration. However, oxidative phosphorylation might be impaired in CMT4A since patient fibroblasts exhibited decreased ΔΨm and decreased CII activity. Moreover, defects in complex II have been linked to the pathogenesis of certain diseases (Chen et al., 2007), and OXPHOS dysfunction has been associated with other CMT forms (Cassereau et al., 2010). In fibroblasts from three patients of a CMT2K family with the dominant *GDAP1* mutation C240Y, the activity of mitochondrial NADH ubiquinone oxidoreductase (complex I) was reduced accompanied by reduced oxygen consumption rate and decreased ATP production while no other OXPHOS complex was impaired. In these cells, increased mitochondrial mass, more fragmented mitochondria and tubular mitochondria with increased diameters were observed (Cassereau et al., 2009). Furthermore, reduced ΔΨm, impaired energetic coupling, and decreased glucose oxidation were observed in fibroblasts or muscle cells from CMT2A patients with *MFN2* mutations (Loiseau et al., 2007; Pich et al., 2005). Therefore, impaired oxidative phosphorylation is supposedly implied in the pathogenesis of CMT4A, and might be due to a defect in complex II.

4.8   Impaired mitochondrial network organization cause OXPHOS defects

Increasing evidence suggest that imbalanced fusion and fission lead to deficiencies in mitochondrial energy production. Both fusion and fission defects have been associated with bioenergetic defects (Grandemange et al., 2009). Increased oxidative phosphorylation has been found to be accompanied by mitochondrial fusion (Rossignol et al., 2004), and cells lacking OPA1 or both MFN1 and MFN2 showed decreased cellular respiration as measured by oxygen consumption studies (Chen et al., 2005). It has been suggested that impaired mitochondrial fusion leads to a loss in total mitochondrial DNA that in turn causes respiration defects (Grandemange et al., 2009). In Parkinson's disease, a defect in DJ-1 leads to mitochondrial fragmentation and decreased respiratory rates (Krebiehl et al., 2010). Moreover, mitochondrial fusion depends on the mitochondrial membrane potential and OXPHOS activity. Legros and colleagues have shown that mitochondrial fusion is completely inhibited by protonophores that dissipate ΔΨm (Legros et al., 2002). How ΔΨm influences mitochondrial network regulation is not yet known, but the proteolytic cleavage of fusion factor OPA1 was found to be affected by ΔΨm (Ishihara et al., 2006). Similarly, several studies have proven a relationship between mitochondrial fission and energy production. Benard et al. examined the connection between mitochondrial fission and function and found that the inhibition of mitochondrial fragmentation by *Drp1* knockdown resulted in insufficient OXPHOS and that the inhibition of mitochondrial complex I by rotenone or uncoupling OXPHOS with CCCP reduced ΔΨm and induced mitochondrial fragmentation suggesting a bidirectional relationship (Benard et al., 2007). In addition to balanced mitochondrial fusion and fission, mitochondrial transport is crucial for OXPHOS activity. In yeast the disruption of a protein involved in mitochondrial transport resulted in abnormalities in mitochondrial morphology and poor respiratory activity (Detmer and Chan, 2007). Therefore, the observed OXPHOS defects in GDAP1 mutants might be due to a loss of its mitochondrial fission activity.

4.9   CMT4A causes mainly axonal defects

Neuropathies provoked by mutations in *GDAP1* lead to axonal and demyelinating phenotypes. In order to examine how *GDAP1* mutations contributed to the disease mechanism, Niemann et al. (2005) analyzed GDAP1 expression in neurons and Schwann cells. By immunohistochemistry, they showed that GDAP1 colocalized with both neuronal and Schwann cell markers in cross sections of rat sciatic nerves. From these results they concluded that *GDAP1* mutations in both PNS neurons and Schwann cells affect cellular functions and lead to the complex phenotypes in CMT4A. In comparison, Pedrola et al. could not detect

GDAP1 expression in RT-PCR analyses with mRNA from cultured rat Schwann cells (Pedrola et al., 2005). Moreover, immonohistochemical staining of different mouse brain regions (Pedrola et al., 2008) revealed ubiquitous GDAP1 expression in the grey matter of brain and spinal cord, but no expression in the white matter, from which they concluded that glial cells do not express GDAP1.

In this study, quantitative RT-PCR with rat cortex neurons, astrocytes, DRG, and Schwann cells served to find out, whether *GDAP1* mRNA is only expressed in neurons or in both, neurons and glia cells. *GDAP1* expression was detected in all cell types. However, expression levels were remarkably higher in cortical neurons than in primary astrocytes. Furthermore, *GDAP1* was found to be higher expressed in dorsal root ganglia cultures than in purified Schwann cells. Moreover, DRG cultures contain both neurons and Schwann cells, and the number of neuronal cells declines over time. Accordingly, a time course experiment showed decreasing *GDAP1* expression, which perfectly matched the expression of the neuronal marker β-III-tubulin. These results prove that GDAP1 is mainly expressed in neurons, both of the central and peripheral nervous system indicating that neuronal defects are the major cause of CMT4A disease. Given the marginal expression of GDAP1 in Schwann cells, it remains elusive how *GDAP1* mutations can cause demyelination. And although *GDAP1* mutations have been reported to cause both axonal and demyelinating types of CMT, the number of mutations causing axonal forms outweighs that of mutations with demyelinating phenotypes (Fig. 4).

Moreover, point mutations were shown to impair the fission ability of GDAP1 (Niemann et al., 2005). Balanced mitochondrial network regulation has been associated with the bioenergetic function of mitochondria. Due to their increased energy demand and the fact that mitochondria need to be transported over large distances to dendritic and axonal terminals, neurons are especially dependent on functional mitochondrial dynamics (Chen and Chan, 2006). Although GDAP1 is highly expressed in neurons of the CNS, *GDAP1* mutations lead only to peripheral disorders. This can be explained either by the assumption that GDAP1 function is compensated by another protein in the CNS (Wagner, 2009) or by the elevated susceptibility of peripheral neurons due to their increased axonal lengths again indicating the involvement of fusion/fission or transport defects in CMT disease. The findings that CMT2-associated *MFN2* mutations impair axonal transport along axons (Baloh et al., 2007) confirms the thesis that impaired fission at least partly accounts for the pathology of CMT and indicated that CMT is primarily caused by neuronal defects.

4.10 The point mutation R310Q attenuates the function of GDAP1

Niemann et al. reported that disease-causing mutations reduced the fission activity of GDAP1 (Niemann et al., 2005). Moreover, the facts that no *GDAP1* mutations in the TMD domain were

reported and that truncated proteins cause more severe CMT than point mutations suggest that CMT is caused by the loss of membrane anchoring and/or loss of fission activity. However, in addition to the MOM integration of GDAP1, only the TMD-bordering part and the cytosolic hydrophobic domain of GDAP1 are required for GDAP1-induced fission; and only a few disease-associated mutations cover the hydrophobic domain or the more C-terminal part while the majority of mutations lie within the cytosolic domains that do not interfere with mitochondrial fission. Thus, impaired fission can not alone account for the pathology of CMT.

In this study, further cellular functions of GDAP1 have been described, and several of them were attenuated by the mutation R310Q. GDAP1 prominently protected HT22 cells against glutamate-induced oxidative stress whereas the efficiency of several point mutants to protect against glutamate was reduced and correlated with their effect on mitochondrial fission. Moreover, WT but not mutant GDAP1 increased survival of NSC-34 motor neurons in that GSH synthesis was inhibited by BSO. These results indicate that the loss of neuroprotection may be involved in CMT4A. In addition, overexpression of R310Q did not increase GSH levels supporting the loss of neuroprotective function by mutations in *GDAP1*.

GDAP1 overexpression caused an increased mitochondrial membrane potential suggesting a high OXPHOS capacity, and increased expression and activity of mitochondrial complex II. While the expression of complex II was also elevated by overexpression of the mutant, increases in $\Delta\Psi m$ and complex II activity were not detected. Moreover, in fibroblasts from two CMT4A patients, the GSH concentration, $\Delta\Psi m$ and complex II activity were reduced. These results might imply a respiratory defect in CMT4A. However, since GDAP1 was also found to cause a shift towards glycolysis, this is highly speculative, and respiratory measurements are required to address the role of GDAP1 in oxidative phosphorylation and possible effects of *GDAP1* mutations. Other putative functions of GDAP1, including the increase of HK-2 expression and its increased binding to mitochondria, were not affected by the R310Q mutation. Although several suggestions have been made here and elsewhere, the cellular mechanisms that lead to the pathology of CMT4A are not yet elucidated. Impaired mitochondrial network organization and defective respiration have been shown to be associated with neurodegenerative diseases as discussed above. Similar to CMT2 where most of the *MFN2* mutations cluster in or near the GTPase domain, the GST domains of GDAP1 are frequent targets of mutations (Crimella et al., 2010) indicating that the putative GST function of GDAP1 is impaired in CMT4A. Nevertheless, mutations were found in all cytosolic domains, including the α4-α5 region between the two GST domains whose function has so far not been analyzed. Therefore, the cellular function of GDAP1, maybe as a GST, has to be elucidated in order to understand the molecular mechanisms that lead to CMT4A.

Bibliography

Albrecht, P., J. Lewerenz, S. Dittmer, R. Noack, P. Maher, and A. Methner. 2010. Mechanisms of oxidative glutamate toxicity: the glutamate/cystine antiporter system xc- as a neuroprotective drug target. *CNS Neurol Disord Drug Targets*. 9:373-382.

Alsabeh, R., C.S. Wilson, C.W. Ahn, M.A. Vasef, and H. Battifora. 1996. Expression of bcl-2 by breast cancer: a possible diagnostic application. *Mod Pathol*. 9:439-444.

Altenberg, B., and K.O. Greulich. 2004. Genes of glycolysis are ubiquitously overexpressed in 24 cancer classes. *Genomics*. 84:1014-1020.

Ammar, N., E. Nelis, L. Merlini, N. Barisic, R. Amouri, C. Ceuterick, J.J. Martin, V. Timmerman, F. Hentati, and P. De Jonghe. 2003. Identification of novel GDAP1 mutations causing autosomal recessive Charcot-Marie-Tooth disease. *Neuromuscul Disord*. 13:720-728.

Archer, S.L., M. Gomberg-Maitland, M.L. Maitland, S. Rich, J.G. Garcia, and E.K. Weir. 2008. Mitochondrial metabolism, redox signaling, and fusion: a mitochondria-ROS-HIF-1alpha-Kv1.5 O2-sensing pathway at the intersection of pulmonary hypertension and cancer. *Am J Physiol Heart Circ Physiol*. 294:H570-578.

Azzedine, H., M. Ruberg, D. Ente, C. Gilardeau, S. Perie, B. Wechsler, A. Brice, E. LeGuern, and O. Dubourg. 2003. Variability of disease progression in a family with autosomal recessive CMT associated with a S194X and new R310Q mutation in the GDAP1 gene. *Neuromuscul Disord*. 13:341-346.

Baker, D.A., K. McFarland, R.W. Lake, H. Shen, X.C. Tang, S. Toda, and P.W. Kalivas. 2003. Neuroadaptations in cystine-glutamate exchange underlie cocaine relapse. *Nat Neurosci*. 6:743-749.

Baloh, R.H., R.E. Schmidt, A. Pestronk, and J. Milbrandt. 2007. Altered axonal mitochondrial transport in the pathogenesis of Charcot-Marie-Tooth disease from mitofusin 2 mutations. *J Neurosci*. 27:422-430.

Banjac, A., T. Perisic, H. Sato, A. Seiler, S. Bannai, N. Weiss, P. Kolle, K. Tschoep, R.D. Issels, P.T. Daniel, M. Conrad, and G.W. Bornkamm. 2008. The cystine/cysteine cycle: a redox cycle regulating susceptibility versus resistance to cell death. *Oncogene*. 27:1618-1628.

Bannai, S. 1986. Exchange of cystine and glutamate across plasma membrane of human fibroblasts. *J Biol Chem*. 261:2256-2263.

Bannai, S., and T. Ishii. 1988. A novel function of glutamine in cell culture: utilization of glutamine for the uptake of cystine in human fibroblasts. *J Cell Physiol*. 137:360-366.

Bannai, S., and E. Kitamura. 1980. Transport interaction of L-cystine and L-glutamate in human diploid fibroblasts in culture. *J Biol Chem*. 255:2372-2376.

Barber, S.C., and P.J. Shaw. 2010. Oxidative stress in ALS: key role in motor neuron injury and therapeutic target. *Free Radic Biol Med*. 48:629-641.

Barger, S.W., and A.S. Basile. 2001. Activation of microglia by secreted amyloid precursor protein evokes release of glutamate by cystine exchange and attenuates synaptic function. *J Neurochem*. 76:846-854.

Barger, S.W., M.E. Goodwin, M.M. Porter, and M.L. Beggs. 2007. Glutamate release from activated microglia requires the oxidative burst and lipid peroxidation. *J Neurochem*. 101:1205-1213.

Barnham, K.J., C.L. Masters, and A.I. Bush. 2004. Neurodegenerative diseases and oxidative stress. *Nat Rev Drug Discov*. 3:205-214.

Bassi, M.T., E. Gasol, M. Manzoni, M. Pineda, M. Riboni, R. Martin, A. Zorzano, G. Borsani, and M. Palacin. 2001. Identification and characterisation of human xCT that co-expresses, with 4F2 heavy chain, the amino acid transport activity system xc. *Pflugers Arch*. 442:286-296.

Baxter, R.V., K. Ben Othmane, J.M. Rochelle, J.E. Stajich, C. Hulette, S. Dew-Knight, F. Hentati, M. Ben Hamida, S. Bel, J.E. Stenger, J.R. Gilbert, M.A. Pericak-Vance, and J.M. Vance. 2002. Ganglioside-induced differentiation-associated protein-1 is mutant in Charcot-Marie-Tooth disease type 4A/8q21. *Nat Genet*. 30:21-22.

Benard, G., N. Bellance, D. James, P. Parrone, H. Fernandez, T. Letellier, and R. Rossignol. 2007. Mitochondrial bioenergetics and structural network organization. *J Cell Sci*. 120:838-848.

Berdan, R.C., and J.C. Easaw. 1992. Modulation of sprouting in organ culture after axotomy of an identified molluscan neuron. *J Neurobiol*. 23:433-450.

Berger, P., P. Young, and U. Suter. 2002. Molecular cell biology of Charcot-Marie-Tooth disease. *Neurogenetics*. 4:1-15.

Boerkoel, C.F., H. Takashima, M. Nakagawa, S. Izumo, D. Armstrong, I. Butler, P. Mancias, S.C. Papasozomenos, L.Z. Stern, and J.R. Lupski. 2003. CMT4A: identification of a Hispanic GDAP1 founder mutation. *Ann Neurol*. 53:400-405.

Bonnet, S., S.L. Archer, J. Allalunis-Turner, A. Haromy, C. Beaulieu, R. Thompson, C.T. Lee, G.D. Lopaschuk, L. Puttagunta, G. Harry, K. Hashimoto, C.J. Porter, M.A. Andrade, B. Thebaud, and E.D. Michelakis. 2007. A mitochondria-K+ channel axis is suppressed in cancer and its normalization promotes apoptosis and inhibits cancer growth. *Cancer Cell*. 11:37-51.

Bouhouche, A., N. Birouk, A. Benomar, R. Ouazzani, T. Chkili, and M. Yahyaoui. 2007. A novel GDAP1 mutation P78L responsible for CMT4A disease in three Moroccan families. *Can J Neurol Sci*. 34:421-426.

Burdo, J., R. Dargusch, and D. Schubert. 2006. Distribution of the cystine/glutamate antiporter system xc- in the brain, kidney, and duodenum. *J Histochem Cytochem*. 54:549-557.

Burnstock, G. 2006. Purinergic signalling--an overview. *Novartis Found Symp*. 276:26-48; discussion 48-57, 275-281.

Burnstock, G. 2009. Purinergic mechanosensory transduction and visceral pain. *Mol Pain*. 5:69.

Bustamante, E., H.P. Morris, and P.L. Pedersen. 1981. Energy metabolism of tumor cells. Requirement for a form of hexokinase with a propensity for mitochondrial binding. *J Biol Chem*. 256:8699-8704.

Cashman, N.R., H.D. Durham, J.K. Blusztajn, K. Oda, T. Tabira, I.T. Shaw, S. Dahrouge, and J.P. Antel. 1992. Neuroblastoma x spinal cord (NSC) hybrid cell lines resemble developing motor neurons. *Dev Dyn*. 194:209-221.

Cassereau, J., A. Chevrollier, N. Gueguen, V. Desquiret, C. Verny, G. Nicolas, F. Dubas, P. Amati-Bonneau, P. Reynier, D. Bonneau, and V. Procaccio. 2010. Mitochondrial dysfunction and pathophysiology of Charcot-Marie-Tooth disease involving GDAP1 mutations. *Exp Neurol*.

Cassereau, J., A. Chevrollier, N. Gueguen, M.C. Malinge, F. Letournel, G. Nicolas, L. Richard, M. Ferre, C. Verny, F. Dubas, V. Procaccio, P. Amati-Bonneau, D. Bonneau, and P. Reynier. 2009. Mitochondrial complex I deficiency in GDAP1-related autosomal dominant Charcot-Marie-Tooth disease (CMT2K). *Neurogenetics*. 10:145-150.

Catz, S.D., and J.L. Johnson. 2003. BCL-2 in prostate cancer: a minireview. *Apoptosis*. 8:29-37.

Cereghetti, G.M., and L. Scorrano. 2006. The many shapes of mitochondrial death. *Oncogene*. 25:4717-4724.

Chan, D.C. 2006a. Mitochondria: dynamic organelles in disease, aging, and development. *Cell*. 125:1241-1252.

Chan, D.C. 2006b. Mitochondrial fusion and fission in mammals. *Annu Rev Cell Dev Biol*. 22:79-99.

Chan, D.C. 2007. Mitochondrial dynamics in disease. *N Engl J Med*. 356:1707-1709.

Chen, H., and D.C. Chan. 2006. Critical dependence of neurons on mitochondrial dynamics. *Curr Opin Cell Biol*. 18:453-459.

Chen, H., A. Chomyn, and D.C. Chan. 2005. Disruption of fusion results in mitochondrial heterogeneity and dysfunction. *J Biol Chem*. 280:26185-26192.

Chen, H., S.A. Detmer, A.J. Ewald, E.E. Griffin, S.E. Fraser, and D.C. Chan. 2003. Mitofusins Mfn1 and Mfn2 coordinately regulate mitochondrial fusion and are essential for embryonic development. *J Cell Biol*. 160:189-200.

Chen, Y.R., C.L. Chen, D.R. Pfeiffer, and J.L. Zweier. 2007. Mitochondrial complex II in the post-ischemic heart: oxidative injury and the role of protein S-glutathionylation. *J Biol Chem*. 282:32640-32654.

Chen, Z., H. Zhang, W. Lu, and P. Huang. 2009. Role of mitochondria-associated hexokinase II in cancer cell death induced by 3-bromopyruvate. *Biochim Biophys Acta*. 1787:553-560.

Choi, D.W. 1988. Glutamate neurotoxicity and diseases of the nervous system. *Neuron*. 1:623-634.

Christensen, H.N. 1990. Role of amino acid transport and countertransport in nutrition and metabolism. *Physiol Rev*. 70:43-77.

Chung, K.W., S.M. Kim, I.N. Sunwoo, S.Y. Cho, S.J. Hwang, J. Kim, S.H. Kang, K.D. Park, K.G. Choi, I.S. Choi, and B.O. Choi. 2008. A novel GDAP1 Q218E mutation in autosomal dominant Charcot-Marie-Tooth disease. *J Hum Genet*. 53:360-364.

Chung, W.J., S.A. Lyons, G.M. Nelson, H. Hamza, C.L. Gladson, G.Y. Gillespie, and H. Sontheimer. 2005. Inhibition of cystine uptake disrupts the growth of primary brain tumors. *J Neurosci*. 25:7101-7110.

Claramunt, R., L. Pedrola, T. Sevilla, A. Lopez de Munain, J. Berciano, A. Cuesta, B. Sanchez-Navarro, J.M. Millan, G.M. Saifi, J.R. Lupski, J.J. Vilchez, C. Espinos, and F. Palau. 2005. Genetics of Charcot-Marie-Tooth disease type 4A: mutations, inheritance, phenotypic variability, and founder effect. *J Med Genet*. 42:358-365.

Correale, J., T. Olsson, J. Bjork, G. Smedegard, B. Hojeberg, and H. Link. 1991. Sulfasalazine aggravates experimental autoimmune encephalomyelitis and causes an increase in the number of autoreactive T cells. *J Neuroimmunol*. 34:109-120.

Crimella, C., A. Tonelli, G. Airoldi, C. Baschirotto, M.G. D'Angelo, S. Bonato, L. Losito, A. Trabacca, N. Bresolin, and M.T. Bassi. 2010. The GST domain of GDAP1 is a frequent target of mutations in the dominant form of axonal Charcot Marie Tooth type 2K. *J Med Genet*. 47:712-716.

Cuesta, A., L. Pedrola, T. Sevilla, J. Garcia-Planells, M.J. Chumillas, F. Mayordomo, E. LeGuern, I. Marin, J.J. Vilchez, and F. Palau. 2002. The gene encoding ganglioside-induced differentiation-associated protein 1 is mutated in axonal Charcot-Marie-Tooth type 4A disease. *Nat Genet*. 30:22-25.

D'Angelo, J.A., E. Dehlink, B. Platzer, P. Dwyer, M.L. Circu, J. Garay, T.Y. Aw, E. Fiebiger, and B.L. Dickinson. 2010. The cystine/glutamate antiporter regulates dendritic cell differentiation and antigen presentation. *J Immunol*. 185:3217-3226.

Delivani, P., and S.J. Martin. 2006. Mitochondrial membrane remodeling in apoptosis: an inside story. *Cell Death Differ*. 13:2007-2010.

Detmer, S.A., and D.C. Chan. 2007. Functions and dysfunctions of mitochondrial dynamics. *Nat Rev Mol Cell Biol*. 8:870-879.

Di Maria, E., R. Gulli, P. Balestra, D. Cassandrini, S. Pigullo, L. Doria-Lamba, M. Bado, A. Schenone, F. Ajmar, P. Mandich, and E. Bellone. 2004. A novel mutation of GDAP1 associated with Charcot-Marie-Tooth disease in three Italian families: evidence for a founder effect. *J Neurol Neurosurg Psychiatry*. 75:1495-1498.

Dittmer, S., M. Sahin, A. Pantlen, A. Saxena, D. Toutzaris, A.L. Pina, A. Geerts, S. Golz, and A. Methner. 2008. The constitutively active orphan G-protein-coupled receptor GPR39 protects from cell death by increasing secretion of pigment epithelium-derived growth factor. *J Biol Chem*. 283:7074-7081.

Domercq, M., M.V. Sanchez-Gomez, C. Sherwin, E. Etxebarria, R. Fern, and C. Matute. 2007. System xc- and glutamate transporter inhibition mediates microglial toxicity to oligodendrocytes. *J Immunol*. 178:6549-6556.

Donnelly-Roberts, D.L., and M.F. Jarvis. 2007. Discovery of P2X7 receptor-selective antagonists offers new insights into P2X7 receptor function and indicates a role in chronic pain states. *Br J Pharmacol*. 151:571-579.

Eng, D.L., Y.L. Lee, and P.G. Lal. 1997. Expression of glutamate uptake transporters after dibutyryl cyclic AMP differentiation and traumatic injury in cultured astrocytes. *Brain Res*. 778:215-221.

Ennion, S., S. Hagan, and R.J. Evans. 2000. The role of positively charged amino acids in ATP recognition by human P2X1 receptors. *J Biol Chem*. 275:35656.

Finkel, T., and N.J. Holbrook. 2000. Oxidants, oxidative stress and the biology of ageing. *Nature*. 408:239-247.

Franco, R., and J.A. Cidlowski. 2009. Apoptosis and glutathione: beyond an antioxidant. *Cell Death Differ*. 16:1303-1314.

Frank, S., B. Gaume, E.S. Bergmann-Leitner, W.W. Leitner, E.G. Robert, F. Catez, C.L. Smith, and R.J. Youle. 2001. The role of dynamin-related protein 1, a mediator of mitochondrial fission, in apoptosis. *Dev Cell*. 1:515-525.

Frazier, A.E., C. Kiu, D. Stojanovski, N.J. Hoogenraad, and M.T. Ryan. 2006. Mitochondrial morphology and distribution in mammalian cells. *Biol Chem*. 387:1551-1558.

Fridovich, I. 1998. Oxygen toxicity: a radical explanation. *J Exp Biol*. 201:1203-1209.

Fulda, S., L. Galluzzi, and G. Kroemer. 2010. Targeting mitochondria for cancer therapy. *Nat Rev Drug Discov*. 9:447-464.

Garedew, A., and S. Moncada. 2008. Mitochondrial dysfunction and HIF1alpha stabilization in inflammation. *J Cell Sci*. 121:3468-3475.

Gasol, E., M. Jimenez-Vidal, J. Chillaron, A. Zorzano, and M. Palacin. 2004. Membrane topology of system xc- light subunit reveals a re-entrant loop with substrate-restricted accessibility. *J Biol Chem*. 279:31228-31236.

Gout, P.W., A.R. Buckley, C.R. Simms, and N. Bruchovsky. 2001. Sulfasalazine, a potent suppressor of lymphoma growth by inhibition of the x(c)- cystine transporter: a new action for an old drug. *Leukemia*. 15:1633-1640.

Grandemange, S., S. Herzig, and J.C. Martinou. 2009. Mitochondrial dynamics and cancer. *Semin Cancer Biol*. 19:50-56.

Griffith, O.W. 1999. Biologic and pharmacologic regulation of mammalian glutathione synthesis. *Free Radic Biol Med*. 27:922-935.

Grohm, J., N. Plesnila, and C. Culmsee. 2010. Bid mediates fission, membrane permeabilization and peri-nuclear accumulation of mitochondria as a prerequisite for oxidative neuronal cell death. *Brain Behav Immun*. 24:831-838.

Guan, J., M. Lo, P. Dockery, S. Mahon, C.M. Karp, A.R. Buckley, S. Lam, P.W. Gout, and Y.Z. Wang. 2009. The xc- cystine/glutamate antiporter as a potential therapeutic target for small-cell lung cancer: use of sulfasalazine. *Cancer Chemother Pharmacol*. 64:463-472.

Hales, K.G., and M.T. Fuller. 1997. Developmentally regulated mitochondrial fusion mediated by a conserved, novel, predicted GTPase. *Cell*. 90:121-129.

Halliwell, B. 2001. Role of free radicals in the neurodegenerative diseases: therapeutic implications for antioxidant treatment. *Drugs Aging*. 18:685-716.

Huang, X., C.S. Atwood, M.A. Hartshorn, G. Multhaup, L.E. Goldstein, R.C. Scarpa, M.P. Cuajungco, D.N. Gray, J. Lim, R.D. Moir, R.E. Tanzi, and A.I. Bush. 1999. The A beta peptide of Alzheimer's disease directly produces hydrogen peroxide through metal ion reduction. *Biochemistry*. 38:7609-7616.

Ishihara, N., Y. Fujita, T. Oka, and K. Mihara. 2006. Regulation of mitochondrial morphology through proteolytic cleavage of OPA1. *EMBO J*. 25:2966-2977.

Jahani-Asl, A., E.C. Cheung, M. Neuspiel, J.G. MacLaurin, A. Fortin, D.S. Park, H.M. McBride, and R.S. Slack. 2007. Mitofusin 2 protects cerebellar granule neurons against injury-induced cell death. *J Biol Chem*. 282:23788-23798.

Jarvis, M.F., and B.S. Khakh. 2009. ATP-gated P2X cation-channels. *Neuropharmacology*. 56:208-215.

Kabzinska, D., H. Drac, K. Rowinska-Marcinska, A. Fidzianska, A. Kochanski, and I. Hausmanowa-Petrusewicz. 2006a. Early onset Charcot-Marie-Tooth disease caused by a homozygous Leu239Phe mutation in the GDAP1 gene. *Acta Myol*. 25:34-37.

Kabzinska, D., A. Kochanski, H. Drac, K. Rowinska-Marcinska, B. Ryniewicz, L. Pedrola, F. Palau, and I. Hausmanowa-Petrusewicz. 2006b. A novel Met116Thr mutation in the GDAP1 gene in a Polish family with the axonal recessive Charcot-Marie-Tooth type 4 disease. *J Neurol Sci*. 241:7-11.

Kabzinska, D., A. Kochanski, H. Drac, B. Ryniewicz, K. Rowinska-Marcinska, and I. Hausmanowa-Petrusewicz. 2005. Autosomal recessive axonal form of Charcot-Marie-Tooth

Disease caused by compound heterozygous 3'-splice site and Ser130Cys mutation in the GDAP1 gene. *Neuropediatrics*. 36:206-209.

Kabzinska, D., G.M. Saifi, H. Drac, K. Rowinska-Marcinska, I. Hausmanowa-Petrusewicz, A. Kochanski, and J.R. Lupski. 2007. Charcot-Marie-Tooth disease type 4C4 caused by a novel Pro153Leu substitution in the GDAP1 gene. *Acta Myol*. 26:108-111.

Kabzinska, D., H. Strugalska-Cynowska, A. Kostera-Pruszczyk, B. Ryniewicz, R. Posmyk, A. Midro, P. Seeman, L. Barankova, M. Zimon, J. Baets, V. Timmerman, V. Guergueltcheva, I. Tournev, S. Sarafov, P. De Jonghe, A. Jordanova, I. Hausmanowa-Petrusewicz, and A. Kochanski. 2010. L239F founder mutation in GDAP1 is associated with a mild Charcot-Marie-Tooth type 4C4 (CMT4C4) phenotype. *Neurogenetics*. 11:357-366.

Karbowski, M., K.L. Norris, M.M. Cleland, S.Y. Jeong, and R.J. Youle. 2006. Role of Bax and Bak in mitochondrial morphogenesis. *Nature*. 443:658-662.

Karumbayaram, S., B.G. Novitch, M. Patterson, J.A. Umbach, L. Richter, A. Lindgren, A.E. Conway, A.T. Clark, S.A. Goldman, K. Plath, M. Wiedau-Pazos, H.I. Kornblum, and W.E. Lowry. 2009. Directed differentiation of human-induced pluripotent stem cells generates active motor neurons. *Stem Cells*. 27:806-811.

Korsmeyer, S.J., M.C. Wei, M. Saito, S. Weiler, K.J. Oh, and P.H. Schlesinger. 2000. Pro-apoptotic cascade activates BID, which oligomerizes BAK or BAX into pores that result in the release of cytochrome c. *Cell Death Differ*. 7:1166-1173.

Krebiehl, G., S. Ruckerbauer, L.F. Burbulla, N. Kieper, B. Maurer, J. Waak, H. Wolburg, Z. Gizatullina, F.N. Gellerich, D. Woitalla, O. Riess, P.J. Kahle, T. Proikas-Cezanne, and R. Kruger. 2010. Reduced basal autophagy and impaired mitochondrial dynamics due to loss of Parkinson's disease-associated protein DJ-1. *PLoS One*. 5:e9367.

La Bella, V., F. Valentino, T. Piccoli, and F. Piccoli. 2007. Expression and developmental regulation of the cystine/glutamate exchanger (xc-) in the rat. *Neurochem Res*. 32:1081-1090.

Landshamer, S., M. Hoehn, N. Barth, S. Duvezin-Caubet, G. Schwake, S. Tobaben, I. Kazhdan, B. Becattini, S. Zahler, A. Vollmar, M. Pellecchia, A. Reichert, N. Plesnila, E. Wagner, and C. Culmsee. 2008. Bid-induced release of AIF from mitochondria causes immediate neuronal cell death. *Cell Death Differ*. 15:1553-1563.

Lee, Y.J., S.Y. Jeong, M. Karbowski, C.L. Smith, and R.J. Youle. 2004. Roles of the mammalian mitochondrial fission and fusion mediators Fis1, Drp1, and Opa1 in apoptosis. *Mol Biol Cell*. 15:5001-5011.

Legros, F., A. Lombes, P. Frachon, and M. Rojo. 2002. Mitochondrial fusion in human cells is efficient, requires the inner membrane potential, and is mediated by mitofusins. *Mol Biol Cell*. 13:4343-4354.

Lewerenz, J., P. Albrecht, M.L. Tien, N. Henke, S. Karumbayaram, H.I. Kornblum, M. Wiedau-Pazos, D. Schubert, P. Maher, and A. Methner. 2009. Induction of Nrf2 and xCT are involved in the action of the neuroprotective antibiotic ceftriaxone in vitro. *J Neurochem*. 111:332-343.

Lewerenz, J., M. Klein, and A. Methner. 2006. Cooperative action of glutamate transporters and cystine/glutamate antiporter system Xc- protects from oxidative glutamate toxicity. *J Neurochem*. 98:916-925.

Lewerenz, J., J. Letz, and A. Methner. 2003. Activation of stimulatory heterotrimeric G proteins increases glutathione and protects neuronal cells against oxidative stress. *J Neurochem*. 87:522-531.

Lewerenz, J., and A. Methner. 2006. Mechanismen und Bedeutung der oxidativen Glutamattoxizität. *Neuroforum*. 3:222-226.

Li, H., Y. Chen, A.F. Jones, R.H. Sanger, L.P. Collis, R. Flannery, E.C. McNay, T. Yu, R. Schwarzenbacher, B. Bossy, E. Bossy-Wetzel, M.V. Bennett, M. Pypaert, J.A. Hickman, P.J. Smith, J.M. Hardwick, and E.A. Jonas. 2008. Bcl-xL induces Drp1-dependent synapse formation in cultured hippocampal neurons. *Proc Natl Acad Sci U S A*. 105:2169-2174.

Li, Y., P. Maher, and D. Schubert. 1997a. Requirement for cGMP in nerve cell death caused by glutathione depletion. *J Cell Biol*. 139:1317-1324.

Li, Y., P. Maher, and D. Schubert. 1997b. A role for 12-lipoxygenase in nerve cell death caused by glutathione depletion. *Neuron*. 19:453-463.

Liu, H., T. Nakagawa, T. Kanematsu, T. Uchida, and S. Tsuji. 1999. Isolation of 10 differentially expressed cDNAs in differentiated Neuro2a cells induced through controlled expression of the GD3 synthase gene. *J Neurochem*. 72:1781-1790.

Lo, M., V. Ling, Y.Z. Wang, and P.W. Gout. 2008a. The xc- cystine/glutamate antiporter: a mediator of pancreatic cancer growth with a role in drug resistance. *Br J Cancer*. 99:464-472.

Lo, M., Y.Z. Wang, and P.W. Gout. 2008b. The x(c)- cystine/glutamate antiporter: a potential target for therapy of cancer and other diseases. *J Cell Physiol*. 215:593-602.

Loiseau, D., A. Chevrollier, C. Verny, V. Guillet, N. Gueguen, M.A. Pou de Crescenzo, M. Ferre, M.C. Malinge, A. Guichet, G. Nicolas, P. Amati-Bonneau, Y. Malthiery, D. Bonneau, and P. Reynier. 2007. Mitochondrial coupling defect in Charcot-Marie-Tooth type 2A disease. *Ann Neurol*. 61:315-323.

MacKenzie, A.B., A. Surprenant, and R.A. North. 1999. Functional and molecular diversity of purinergic ion channel receptors. *Ann N Y Acad Sci*. 868:716-729.

Maher, P. 2005. The effects of stress and aging on glutathione metabolism. *Ageing Res Rev*. 4:288-314.

Majewski, N., V. Nogueira, P. Bhaskar, P.E. Coy, J.E. Skeen, K. Gottlob, N.S. Chandel, C.B. Thompson, R.B. Robey, and N. Hay. 2004a. Hexokinase-mitochondria interaction mediated by Akt is required to inhibit apoptosis in the presence or absence of Bax and Bak. *Mol Cell*. 16:819-830.

Majewski, N., V. Nogueira, R.B. Robey, and N. Hay. 2004b. Akt inhibits apoptosis downstream of BID cleavage via a glucose-dependent mechanism involving mitochondrial hexokinases. *Mol Cell Biol*. 24:730-740.

Marco, A., A. Cuesta, L. Pedrola, F. Palau, and I. Marin. 2004. Evolutionary and structural analyses of GDAP1, involved in Charcot-Marie-Tooth disease, characterize a novel class of glutathione transferase-related genes. *Mol Biol Evol*. 21:176-187.

Mariani, E., M.C. Polidori, A. Cherubini, and P. Mecocci. 2005. Oxidative stress in brain aging, neurodegenerative and vascular diseases: an overview. *J Chromatogr B Analyt Technol Biomed Life Sci*. 827:65-75.

Martin, B., M. Paesmans, T. Berghmans, F. Branle, L. Ghisdal, C. Mascaux, A.P. Meert, E. Steels, F. Vallot, J.M. Verdebout, J.J. Lafitte, and J.P. Sculier. 2003. Role of Bcl-2 as a prognostic factor for survival in lung cancer: a systematic review of the literature with meta-analysis. *Br J Cancer*. 89:55-64.

Mattson, M.P. 2004. Pathways towards and away from Alzheimer's disease. *Nature*. 430:631-639.

Mordrelle, A., E. Jullian, C. Costa, E. Cormet-Boyaka, R. Benamouzig, D. Tome, and J.F. Huneau. 2000. EAAT1 is involved in transport of L-glutamate during differentiation of the Caco-2 cell line. *Am J Physiol Gastrointest Liver Physiol*. 279:G366-373.

Moroni, I., M. Morbin, M. Milani, C. Ciano, M. Bugiani, E. Pagliano, T. Cavallaro, D. Pareyson, and F. Taroni. 2009. Novel mutations in the GDAP1 gene in patients affected with early-onset axonal Charcot-Marie-Tooth type 4A. *Neuromuscul Disord*. 19:476-480.

Nelis, E., S. Erdem, P.Y. Van Den Bergh, M.C. Belpaire-Dethiou, C. Ceuterick, V. Van Gerwen, A. Cuesta, L. Pedrola, F. Palau, A.A. Gabreels-Festen, C. Verellen, E. Tan, M. Demirci, C. Van Broeckhoven, P. De Jonghe, H. Topaloglu, and V. Timmerman. 2002. Mutations in GDAP1: autosomal recessive CMT with demyelination and axonopathy. *Neurology*. 59:1865-1872.

Neuspiel, M., R. Zunino, S. Gangaraju, P. Rippstein, and H. McBride. 2005. Activated mitofusin 2 signals mitochondrial fusion, interferes with Bax activation, and reduces susceptibility to radical induced depolarization. *J Biol Chem*. 280:25060-25070.

Niemann, A., M. Ruegg, V. La Padula, A. Schenone, and U. Suter. 2005. Ganglioside-induced differentiation associated protein 1 is a regulator of the mitochondrial network: new implications for Charcot-Marie-Tooth disease. *J Cell Biol*. 170:1067-1078.

Niemann, A., K.M. Wagner, M. Ruegg, and U. Suter. 2009. GDAP1 mutations differ in their effects on mitochondrial dynamics and apoptosis depending on the mode of inheritance. *Neurobiol Dis*. 36:509-520.

North, R.A. 2002. Molecular physiology of P2X receptors. *Physiol Rev*. 82:1013-1067.

North, R.A. 2004. P2X3 receptors and peripheral pain mechanisms. *J Physiol*. 554:301-308.

Ohgoh, M., T. Hanada, T. Smith, T. Hashimoto, M. Ueno, Y. Yamanishi, M. Watanabe, and Y. Nishizawa. 2002. Altered expression of glutamate transporters in experimental autoimmune encephalomyelitis. *J Neuroimmunol*. 125:170-178.

Olanow, C.W. 1990. Oxidation reactions in Parkinson's disease. *Neurology*. 40:suppl 32-37; discussion 37-39.

Pallast, S., K. Arai, X. Wang, E.H. Lo, and K. van Leyen. 2009. 12/15-Lipoxygenase targets neuronal mitochondria under oxidative stress. *J Neurochem*. 111:882-889.

Parman, Y., E. Battaloglu, I. Baris, B. Bilir, M. Poyraz, N. Bissar-Tadmouri, A. Williams, N. Ammar, E. Nelis, V. Timmerman, P. De Jonghe, A. Najafov, F. Deymeer, P. Serdaroglu, P.J. Brophy, and G. Said. 2004. Clinicopathological and genetic study of early-onset demyelinating neuropathy. *Brain*. 127:2540-2550.

Pastorino, J.G., N. Shulga, and J.B. Hoek. 2002. Mitochondrial binding of hexokinase II inhibits Bax-induced cytochrome c release and apoptosis. *J Biol Chem*. 277:7610-7618.

Patel, S.A., B.A. Warren, J.F. Rhoderick, and R.J. Bridges. 2004. Differentiation of substrate and non-substrate inhibitors of transport system xc(-): an obligate exchanger of L-glutamate and L-cystine. *Neuropharmacology*. 46:273-284.

Patzko, A., and M.E. Shy. 2010. Update on Charcot-Marie-Tooth Disease. *Curr Neurol Neurosci Rep*.

Pearce, I.A., M.A. Cambray-Deakin, and R.D. Burgoyne. 1987. Glutamate acting on NMDA receptors stimulates neurite outgrowth from cerebellar granule cells. *FEBS Lett*. 223:143-147.

Pedersen, P.L. 2007. Warburg, me and Hexokinase 2: Multiple discoveries of key molecular events underlying one of cancers' most common phenotypes, the "Warburg Effect", i.e., elevated glycolysis in the presence of oxygen. *J Bioenerg Biomembr*. 39:211-222.

Pedrola, L., A. Espert, T. Valdes-Sanchez, M. Sanchez-Piris, E.E. Sirkowski, S.S. Scherer, I. Farinas, and F. Palau. 2008. Cell expression of GDAP1 in the nervous system and pathogenesis of Charcot-Marie-Tooth type 4A disease. *J Cell Mol Med*. 12:679-689.

Pedrola, L., A. Espert, X. Wu, R. Claramunt, M.E. Shy, and F. Palau. 2005. GDAP1, the protein causing Charcot-Marie-Tooth disease type 4A, is expressed in neurons and is associated with mitochondria. *Hum Mol Genet*. 14:1087-1094.

Piani, D., and A. Fontana. 1994. Involvement of the cystine transport system xc- in the macrophage-induced glutamate-dependent cytotoxicity to neurons. *J Immunol*. 152:3578-3585.

Pich, S., D. Bach, P. Briones, M. Liesa, M. Camps, X. Testar, M. Palacin, and A. Zorzano. 2005. The Charcot-Marie-Tooth type 2A gene product, Mfn2, up-regulates fuel oxidation through expression of OXPHOS system. *Hum Mol Genet*. 14:1405-1415.

Pignataro, L., C. Condello, and V. Sarthy. 2003. Glutamate transporter expression in differentiated retinoblastoma cells. *Invest Ophth Vis Sci*. 44:U723-U723.

Qin, S., C. Colin, I. Hinners, A. Gervais, C. Cheret, and M. Mallat. 2006. System Xc- and apolipoprotein E expressed by microglia have opposite effects on the neurotoxicity of amyloid-beta peptide 1-40. *J Neurosci*. 26:3345-3356.

Ratajewski, M., and L. Pulaski. 2009. YY1-dependent transcriptional regulation of the human GDAP1 gene. *Genomics*. 94:407-413.

Rossignol, R., R. Gilkerson, R. Aggeler, K. Yamagata, S.J. Remington, and R.A. Capaldi. 2004. Energy substrate modulates mitochondrial structure and oxidative capacity in cancer cells. *Cancer Res*. 64:985-993.

Sahin-Calapoglu, N., M. Tan, M. Soyoz, M. Calapoglu, and N. Ozcelik. 2009. Novel GDAP1 mutation in a Turkish family with CMT2K (CMT2K with novel GDAP1 mutation). *Neuromolecular Med*. 11:106-113.

Sahin, M., A. Saxena, P. Joost, J. Lewerenz, and A. Methner. 2006. Induction of Bcl-2 by functional regulation of G-protein coupled receptors protects from oxidative glutamate toxicity by increasing glutathione. *Free Radic Res*. 40:1113-1123.

Santel, A., and S. Frank. 2008. Shaping mitochondria: The complex posttranslational regulation of the mitochondrial fission protein DRP1. *IUBMB Life*. 60:448-455.

Sato, H., K. Fujiwara, J. Sagara, and S. Bannai. 1995. Induction of cystine transport activity in mouse peritoneal macrophages by bacterial lipopolysaccharide. *Biochem J*. 310 (Pt 2):547-551.

Sato, H., K. Kuriyama-Matsumura, T. Hashimoto, H. Sasaki, H. Wang, T. Ishii, G.E. Mann, and S. Bannai. 2001. Effect of oxygen on induction of the cystine transporter by bacterial lipopolysaccharide in mouse peritoneal macrophages. *J Biol Chem*. 276:10407-10412.

Sato, H., M. Tamba, T. Ishii, and S. Bannai. 1999. Cloning and expression of a plasma membrane cystine/glutamate exchange transporter composed of two distinct proteins. *J Biol Chem*. 274:11455-11458.

Sato, H., M. Tamba, K. Kuriyama-Matsumura, S. Okuno, and S. Bannai. 2000. Molecular cloning and expression of human xCT, the light chain of amino acid transport system xc. *Antioxid Redox Signal*. 2:665-671.

Savaskan, N.E., A. Heckel, E. Hahnen, T. Engelhorn, A. Doerfler, O. Ganslandt, C. Nimsky, M. Buchfelder, and I.Y. Eyupoglu. 2008. Small interfering RNA-mediated xCT silencing in gliomas inhibits neurodegeneration and alleviates brain edema. *Nat Med*. 14:629-632.

Senderek, J., C. Bergmann, V.T. Ramaekers, E. Nelis, G. Bernert, A. Makowski, S. Zuchner, P. De Jonghe, S. Rudnik-Schoneborn, K. Zerres, and J.M. Schroder. 2003. Mutations in the ganglioside-induced differentiation-associated protein-1 (GDAP1) gene in intermediate type autosomal recessive Charcot-Marie-Tooth neuropathy. *Brain*. 126:642-649.

Shadrina, M.I., P.A. Slominsky, and S.A. Limborska. 2010. Molecular mechanisms of pathogenesis of Parkinson's disease. *Int Rev Cell Mol Biol*. 281:229-266.

Shield, A.J., T.P. Murray, and P.G. Board. 2006. Functional characterisation of ganglioside-induced differentiation-associated protein 1 as a glutathione transferase. *Biochem Biophys Res Commun*. 347:859-866.

Shih, A.Y., H. Erb, X. Sun, S. Toda, P.W. Kalivas, and T.H. Murphy. 2006. Cystine/glutamate exchange modulates glutathione supply for neuroprotection from oxidative stress and cell proliferation. *J Neurosci*. 26:10514-10523.

Shih, A.Y., D.A. Johnson, G. Wong, A.D. Kraft, L. Jiang, H. Erb, J.A. Johnson, and T.H. Murphy. 2003. Coordinate regulation of glutathione biosynthesis and release by Nrf2-expressing glia potently protects neurons from oxidative stress. *J Neurosci*. 23:3394-3406.

Su, B., X. Wang, A. Nunomura, P.I. Moreira, H.G. Lee, G. Perry, M.A. Smith, and X. Zhu. 2008. Oxidative stress signaling in Alzheimer's disease. *Curr Alzheimer Res*. 5:525-532.

Tan, S., Y. Sagara, Y. Liu, P. Maher, and D. Schubert. 1998. The regulation of reactive oxygen species production during programmed cell death. *J Cell Biol*. 141:1423-1432.

Tan, S., D. Schubert, and P. Maher. 2001. Oxytosis: A novel form of programmed cell death. *Curr Top Med Chem*. 1:497-506.

Tawfik, V.L., M.L. Lacroix-Fralish, K.K. Bercury, N. Nutile-McMenemy, B.T. Harris, and J.A. Deleo. 2006. Induction of astrocyte differentiation by propentofylline increases glutamate transporter expression in vitro: heterogeneity of the quiescent phenotype. *Glia*. 54:193-203.

Torres, G.E., T.M. Egan, and M.M. Voigt. 1999. Hetero-oligomeric assembly of P2X receptor subunits. Specificities exist with regard to possible partners. *J Biol Chem*. 274:6653-6659.

Toutzaris, D., J. Lewerenz, P. Albrecht, L.T. Jensen, J. Letz, A. Geerts, S. Golz, and A. Methner. 2010. A novel giant peroxisomal superoxide dismutase motif-containing protein. *Free Radic Biol Med*. 48:811-820.

Tsujimoto, Y., and S. Shimizu. 2000. VDAC regulation by the Bcl-2 family of proteins. *Cell Death Differ*. 7:1174-1181.

Vahsen, N., C. Cande, J.J. Briere, P. Benit, N. Joza, N. Larochette, P.G. Mastroberardino, M.O. Pequignot, N. Casares, V. Lazar, O. Feraud, N. Debili, S. Wissing, S. Engelhardt, F. Madeo, M. Piacentini, J.M. Penninger, H. Schagger, P. Rustin, and G. Kroemer. 2004. AIF deficiency compromises oxidative phosphorylation. *EMBO J*. 23:4679-4689.

van Leyen, K., K. Arai, G. Jin, V. Kenyon, B. Gerstner, P.A. Rosenberg, T.R. Holman, and E.H. Lo. 2008. Novel lipoxygenase inhibitors as neuroprotective reagents. *J Neurosci Res*. 86:904-909.

van Leyen, K., R.M. Duvoisin, H. Engelhardt, and M. Wiedmann. 1998. A function for lipoxygenase in programmed organelle degradation. *Nature*. 395:392-395.

van Leyen, K., H.Y. Kim, S.R. Lee, G. Jin, K. Arai, and E.H. Lo. 2006. Baicalein and 12/15-lipoxygenase in the ischemic brain. *Stroke*. 37:3014-3018.

van Leyen, K., A. Siddiq, R.R. Ratan, and E.H. Lo. 2005. Proteasome inhibition protects HT22 neuronal cells from oxidative glutamate toxicity. *J Neurochem*. 92:824-830.

van Muiswinkel, F.L., and H.B. Kuiperij. 2005. The Nrf2-ARE Signalling pathway: promising drug target to combat oxidative stress in neurodegenerative disorders. *Curr Drug Targets CNS Neurol Disord*. 4:267-281.

Wagner, K.M. 2009. Structural and functional analysis of the neuronal mitochondrial fission factor GDAP1 and its homolog GDAP1L1. *Dissertation*.

Wagner, K.M., M. Ruegg, A. Niemann, and U. Suter. 2009. Targeting and function of the mitochondrial fission factor GDAP1 are dependent on its tail-anchor. *PLoS One*. 4:e5160.

Wang, H., M. Tamba, M. Kimata, K. Sakamoto, S. Bannai, and H. Sato. 2003. Expression of the activity of cystine/glutamate exchange transporter, system x(c)(-), by xCT and rBAT. *Biochem Biophys Res Commun*. 305:611-618.

Wasiak, S., R. Zunino, and H.M. McBride. 2007. Bax/Bak promote sumoylation of DRP1 and its stable association with mitochondria during apoptotic cell death. *J Cell Biol*. 177:439-450.

Watanabe, H., and S. Bannai. 1987. Induction of cystine transport activity in mouse peritoneal macrophages. *J Exp Med*. 165:628-640.

Waterham, H.R., J. Koster, C.W. van Roermund, P.A. Mooyer, R.J. Wanders, and J.V. Leonard. 2007. A lethal defect of mitochondrial and peroxisomal fission. *N Engl J Med*. 356:1736-1741.

Westermann, B. 2008. Molecular machinery of mitochondrial fusion and fission. *J Biol Chem*. 283:13501-13505.

Xie, F., H. Liu, Y.H. Zhu, Y.R. Qin, Y. Dai, T. Zeng, L. Chen, C. Nie, H. Tang, Y. Li, L. Fu, and X.Y. Guan. 2011. Overexpression of GPR39 contributes to malignant development of human esophageal squamous cell carcinoma. *BMC Cancer*. 11:86.

Xin, B., E. Puffenberger, L. Nye, M. Wiznitzer, and H. Wang. 2008. A novel mutation in the GDAP1 gene is associated with autosomal recessive Charcot-Marie-Tooth disease in an Amish family. *Clin Genet*. 74:274-278.

Ye, Z.C., J.D. Rothstein, and H. Sontheimer. 1999. Compromised glutamate transport in human glioma cells: reduction-mislocalization of sodium-dependent glutamate transporters and enhanced activity of cystine-glutamate exchange. *J Neurosci*. 19:10767-10777.

Zhu, X., A.K. Raina, G. Perry, and M.A. Smith. 2004. Alzheimer's disease: the two-hit hypothesis. *Lancet Neurol*. 3:219-226.

Acknowledgements

Curriculum vitae

Name	Rebecca Noack
Date/Place of birth	06.08.1981 / Mühlhausen/Thür.
Citizenship	German

Education

since 10|2006	**Heinrich-Heine University Düsseldorf** PhD thesis in the Department of Neurology, University Clinic Düsseldorf Title: 'Resistance against oxidative glutamate toxicity: Functional characterization of amino acid antiporter subunit xCT, purinergic ATP receptor P2X3 and mitochondrial fission factor GDAP1' Supervisor: Prof. Dr. Axel Methner
10|2000 – 09|2006	**Technical University Braunschweig** Diploma in Biotechnology
08|2005 – 03|2006	**University of Cologne** Diploma thesis in Bioinformatics at the Institute for Biochemistry Title: 'Comparison of different gene prediction and genome annotation methods for prokaryotes' Supervisor: Prof. Dr. Dietmar Schomburg
09|2003 – 08|2004	**University of Waterloo, Canada** Graduate studies and study thesis Title: 'Induction of Antifreeze Proteins in Winter Rye leaves by Methyl Jasmonate' Supervisor: Prof. Dr. Marilyn Griffith
09|1988 – 06|2000	**Albert-Schweitzer-Gymnasium Erfurt** School specialized in Mathematics and Natural Sciences, Abitur

Work experience

11|2004 – 03|2005	**Helmholtz Centre for Infection Research, Stöckheim** Student assistant in the Proteomics Group of the Division of Cell Biology
12|2002 – 06|2003	**Technical University Braunschweig** Student assistant at the Institute for Biochemical Engineering

Skills / Competences

Languages   German (native), Englisch (fluent), Spanish (basics), Russian (basics)
Computer skills   Microsoft applications, Programming (Perl, Python, HTML)

Congresses und Workshops

09|2010   FEBS Workshop 7th MiPmeeting Mitochondrial Physiology – The many functions of the organisms in our cell, Obergurgl, Austria
Talk: '*GDAP1, a protein mutated in hereditary polyneuropathy Charcot-Marie-Tooth disease 4A, protects from oxidative stress and is involved in mitochondrial shape and function'*
10|2009   Novartis workshop „Health Care Vision 2020", Nürnberg
09|2009   Science Retreat of the Department of Neurology of the University Clinic Düsseldorf, Schloss Mickeln, Düsseldorf
Talk: '*Reduced resistance against oxidative stress as a key to neuronal damage in Charcot-Marie-Tooth disease 4A'*
08|2009   4th Annual meeting of the BMFZ (‚Biologisch-Medizinischen Forschungszentrum') of the Heinrich-Heine University Düsseldorf, Bergisch-Gladbach
06|2009   PENS Summer School – Metabolic aspects of chronic brain disease, Günzburg
03|2009   8th GBM meeting, Göttingen

Memberships in Scientific Organizations

'Gesellschaft für Biochemie und Molekularbiologie' (GBM)
'Neurowissenschaftliche Gesellschaft' (NWG)
Mitochondrial Physiology Society (MiP)

Scholarships

FEBS Youth Travel stipend for the participation at the 7th MiPmeeting
Participation at the Selma Meyer Mentoring program of the Heinrich-Heine University Düsseldorf
DAAD scholarship for studies at the University of Waterloo, Canada

Publications

Albrecht, P., J. Lewerenz, S. Dittmer, R. Noack, P. Maher, and A. Methner. 2010. Mechanisms of oxidative glutamate toxicity: the glutamate/cystine antiporter system xc- as a neuroprotective drug target. *CNS Neurol Disord Drug Targets*. 9:373-382.

Noack, R., P. Albrecht, T. Dehmel, S. Frede, H. Summer, S. Golz, B. Kieseier, A. Kochanski, J. Lewerenz, G. Maier zur Hörste, A. Pfeiffer, M. Stettner, M. Wiedau-Pazos, and A. Methner. The mitochondrial fission factor GDAP1 protects from oxidative stress by increasing glutathione content and stabilizing the mitochondrial membrane potential. *Human Molecular Genetics.* 21(1): 150-162.

Lewerenz, J., H. Sato, P. Albrecht, N. Henke, R. Noack, A. Methner, and P. Maher. 2012. Mutation of ATF4 mediates resistance of neuronal cell lines against oxidative stress by inducing xCT expression. *Cell death & Differentiation*. 19(5): 847-858.